ENHANCEMENT OF IMPACT FORCE DETERMINATION WITH MODAL TRANSFORMATION METHOD BY USING INTEGRATION AND DATA FILTERING

KHOO SHIN YEE

FACULTY OF ENGINEERING
UNIVERSITY OF MALAYA
KUALA LUMPUR

2013

ENHANCEMENT OF IMPACT FORCE DETERMINATION WITH MODAL TRANSFORMATION METHOD BY USING INTEGRATION AND DATA FILTERING

KHOO SHIN YEE

THESIS SUBMITTED IN FULFILLMENT
OF THE REQUIREMENTS
FOR THE DEGREE OF DOCTOR OF PHILOSOPHY

FACULTY OF ENGINEERING
UNIVERSITY OF MALAYA
KUALA LUMPUR

2013

UNIVERSITI MALAYA

ORIGINAL LITERARY WORK DECLARATION

Name of Candidate: KHOO SHIN YEE

Registration/Matric No: KHA100069

Name of Degree: Doctor of Philosophy (PhD.)

Title of Project Paper/Research Report/Dissertation/Thesis ("this Work"):
Enhancement of Impact Force Determination with Modal Transformation Method by Using Integration and Data Filtering

Field of Study: Vibration

I do solemnly and sincerely declare that:

(1) I am the sole author/writer of this Work;
(2) This Work is original;
(3) Any use of any work in which copyright exists was done by way of fair dealing and for permitted purposes and any excerpt or extract from, or reference to or reproduction of any copyright work has been disclosed expressly and sufficiently and the title of the Work and its authorship have been acknowledged in this Work;
(4) I do not have any actual knowledge nor do I ought reasonably to know that the making of this work constitutes an infringement of any copyright work;
(5) I hereby assign all and every rights in the copyright to this Work to the University of Malaya ("UM"), who henceforth shall be owner of the copyright in this Work and that any reproduction or use in any form or by any means whatsoever is prohibited without the written consent of UM having been first had and obtained;
(6) I am fully aware that if in the course of making this Work I have infringed any copyright whether intentionally or otherwise, I may be subject to legal action or any other action as may be determined by UM.

Candidate's Signature Date:

Subscribed and solemnly declared before,

Witness's Signature Date:

Name:

Designation:

Abstract

Discovering the in-service dynamic forces, their location and their line of action regarding the structure are necessary during its design, development and modification stages. Additional information about the loads experienced by the structure will aid the development iterations resulting in a better outcome. However, direct measurement by using force transducer is not practical in some cases due to some difficulties in force sensor configuration. As an alternative, it would be more convenient to just measure the response and dynamic characteristic of a structure by using Operating Deflection Shape (ODS) analysis and Frequency Response Function (FRF) measurement. Hence, the analysis involved backtracking to determine the force causing the problem can be done. It is known that this inverse problem is ill-conditioned in most practical cases. In this study, a Perspex plate with 4 ground supports was used as test rig. Recovery of unknown impact force using Modal Transformation Method (MTM) is experimentally demonstrated. The transformation from high condition number of synthesised FRF matrix to a well-conditioned case is demonstrated by adding additional information of force location. The low quality of fitting a modal model by using modal parameters obtained from the polynomial curve fitting algorithm is highlighted. In this study, impact force determination with MTM is enhanced by using integration and data filtering approaches. The effectiveness of various types of responses (i.e. measured acceleration responses from sensors; velocity and displacement responses obtained from integration result) is studied, and the results of the impact force determination are examined in under-estimated, even-estimated and over-estimated cases of fixed analysis frequency range. The outcomes show the importance of selecting a suitable response unit and an appropriate analysis frequency range in impact force determination. When the excitation frequency of an impact force is unknown and time-variant, selection of an appropriate analysis frequency range by using Power Spectral Density (PSD) tool is

proposed. The PSD tool consists of the residual analysis, acceleration PSD and normalised total power of response PSD. Residual analysis is used to find the cut-off frequency which inherently possesses the information of mean noise of raw acceleration data. Hence, the acceleration PSD is utilized to set a low pass frequency which discriminates the high power contribute signal and unwanted noise signal. Normalised total power of PSD is used to detect the intrinsic problem that may occur in integrated signals such as velocity and displacement data. This study demonstrates a successful removal of intrinsic problem by using an appropriate high pass frequency. Then, a band pass filter is set for the impact force determination based on the results obtained from PSD tool. Results showed that the impact force determination with MTM by using the displacement response and PSD tool selected analysis frequency range has the best estimation accuracy, and then it is further examined in the collocated and non-collocated cases. The proposed method enhances the force determination result by an average increment of 34.28% and 17.62% of the correlation coefficients for the collocated and the non-collocated cases respectively compared to the result of the conventional method.

Abstrak

Penentuan daya dinamik, kedudukan daya, dan garis tindakan daya adalah penting di dalam kerja-kerja mereka bentuk, pembangunan dan pengubahsuaian. Maklumat yang tepat mengenai beban yang dikenakan ke atas struktur dapat membantu dalam mendapatkan lelaran yang lebih tepat. Walaubagaimanapun, kaedah menggunakan transduser daya secara terus tidak praktikal dalam kes-kes tertentu disebabkan oleh konfigurasi sensor daya yang rumit. Alternatif lain yang lebih mudah bagi menyelesaikan masalah ini adalah dengan mengkaji tindak balas dan karakteristik dinamik struktur tersebut dengan menggunakan kaedah "ODS" dan "FRF". Dengan itu, analisis melibatkan "backtracking" dalam menentukan daya yang menjadi punca kepada masalah dapat dilakukan. Sedia maklum, menyelesaikan masalah dengan kaedah penentuan secara songsang dikenali sebagai "ill-conditioned" dalam kebanyakan kes. Bagi ujikaji ini, kepingan ringan dengan empat penyokong digunakan sebagai bahan ujikaji. Pemulihan daya impak yang tidak diketahui dengan mengunakan "MTM" telah ditunjukkan melalui eksperimen. Transformasi daripada nombor syarat bagi disintesis FRF matriks yang tinggi kepada kes nombor syarat yang baik dengan mengetahui kedudukan daya telah ditunjukkan. Kualiti penyuaian model modal yang rendah menggunakan parameter modal yang diperolehi daripada "polynomial curve fitting algorithm" dapat dibuktikan. Dalam kajian ini, pengiraan daya impak dengan menggunakan MTM telah dipertingkatkan dengan menggunakan cara integrasi dan penapisan data. Keberkesanan pelbagai jenis tindak balas (iaitu, tindak balas pecutan diukur daripada sensor; tindak balas halaju dan sesaran yang diperolehi daripada hasil integrasi) pada keputusan pengiraan daya impak telah diuji dalam kes-kes "under-estimated", "even-estimated" dan "over-estimated" takat frequensi analisis. Hasil keputusan menunjukkan kepentingan pemilihan unit tindak balas yang sesuai dan takat frequensi analisis yang baik dalam analisis daya songsong. Apabila frequensi daya

impak adalan tidak diketahui dan tidak tetap dari semasa ke semasa, pemilihan takat frekuensi analisis yang sesuai dengan mengunnakan alat “PSD” telah dicadangkan. Alat PSD adalah terdiri daripada “residual analysis”, PSD pecutan dan jumlah kuasa PSD tindak balas yang dinormalkan. “Residual analysis” digunnakan untuk menentukan “cut-off frequency” di mana ia mempunyai matlumat tersembunyi tentang min data pecutan asal. Seterusnya, PSD pecutan digunakan untuk menetapkan “low pass frequency” yang membezakan isyarat yang mempunyai kuasa yang tinggi dan isyarat “noise” yang tidak diingini. Jumlah kuasa PSD tindak balas telah digunakan untuk mengesan “intrinsic problem” yang terdapat di isyarat yang telah diintegrasi seperti data halaju and sesaran. Kajian ini menunjukkan penyingkiran “intrinsic problem” yang berkesan dengan mengunakan "high pass frequency" yang sesuai. Seterusnya, “band pass filter” telah dipasang untuk analisis daya songsang dengan menggunakan keputusan yang diperolehi oleh alat PSD. Keputusan menunjukkan pengiraan daya hentaman oleh MTM dengan menggunakan tindak balas sesaran and takat frekuensi analisis yang dipilih oleh alat PSD mempunyai ketepatan anggaran yang terbaik, oleh itu ia diuji seterusnya dalam kes-kes “collocated” dan “non-collocated”. Kaedah yang dicadangkan dapat meningkat keputusan pengiraan daya sebanyak 34.28% dan 17.62% bagi kes “collocated” dan kes “non-collocated” masing-masing berbanding dengan hasil kaedah konvensional.

Acknowledgements

First of all, the author would like to express his deepest gratitude to his supervisors: Prof. Dr. Ghaffar Abdul Rahman, Assoc. Prof. Dr. Zubaidah Ismail and Dr. Chong for offering him an opportunity to conduct this research project and experiment. Under their guidance and supervision, the author managed to overcome all the obstacles that he faced during this project. Special thanks go to Prof. Dr. Siamak Noroozi for his useful comments and ideas given to the author. Without him, the project would not have gone this far.

Furthermore, the author would also like to express his gratefulness to the lab mates of vibration laboratory, Dr. Ong, Mr. Kong and Mr. Ali. Their constructive advice and suggestions have certainly helped the author in improving this project. In addition to that appreciation is expressed to the lab assistant of vibration lab, Mr. Amir who has assisted the author to set-up the experiments. Besides, the author would like to express his gratefulness to Quadrant2 Sdn.Bhd. for providing industrial exploration. The author would like to thank the vibration engineers in the oil and gas industry especially Mr. Eng, Mr. Syed Mahathir and Mr. Burn for sharing their experiences and knowledge in solving vibration problems especially in structural dynamic issue.

Moreover, the author wishes to acknowledge the advice given by all the members from Advanced Shock and Vibration Research (ASVR) Group of University of Malaya and Advanced Structural Integrity and Vibration Research (ASIVR) Group of University of Malaysia Pahang. The author gratefully acknowledges the financial assistance provided by the Postgraduate Research Fund (PV086-2011A) from University of Malaya. Apart from that, the author also thanks his family members and friends who have been very supportive all this while. Last but not least, I would like to express my sincere

appreciation to every party that had given support and shared their priceless knowledge with me.

Table of Contents

List of Figures

List of Tables

List of Symbols and Abbreviations

Symbols

∞	Infinity
α	Constant
β	Constant
ω	Excitation Frequency ($rads^{-1}$); Coefficient of frequency domain
ω_0	Natural frequency ($rads^{-1}$)
ω_d	Damped natural frequency ($rads^{-1}$)
ω_c	Cut-Off frequency
ζ	Damping ratio
σ	Decay rate ($rads^{-1}$)
λ	Pole location; $\lambda = -\sigma + i\omega_d$
γ^2	Coefficient of coherence
$\gamma^2_{I:J}$	Coherence between input force and output response
Δt	Time resolution; Time increment (s)
Δf	Frequency resolution (Hz)
$\bullet^*$	Complex conjugate function of a matrix
$\bullet^h$	Complex conjugate transpose function of a matrix (Hermitian matrix)
$\bullet^T$	Transpose function of a matrix
$\bullet_I$	Response DOF; I = 1, 2, ..., total number of response DOF, n
$\bullet_J$	Force DOF; J = 1, 2, ..., total number of force DOF, fz
$\bullet_k$	Variable of mode; k = 1, 2, ..., total number of mode, m
$\bullet_N$	Normal coordinate

$\bullet_p$	Principal coordinate
$\bullet_r$	Integer; r = 0, 1, ..., BS-1
$[\boldsymbol{\Phi}]$	n by m mode shape matrix in principal coordinate
$[\boldsymbol{\Phi}_{\mathbf{N}}]$	n by m mode shape matrix in normal coordinate; It is also known as UMM mode shape matrix
$[\boldsymbol{\Phi}_{\mathbf{N},acc}]$	Accelerance UMM mode shape matrix
$[\boldsymbol{\Phi}_{\mathbf{N},disp}]$	Admittance UMM mode shape matrix
$[\boldsymbol{\Phi}_{\mathbf{N},vel}]$	Mobility UMM mode shape matrix
$\{\boldsymbol{\Phi}\}$	n by 1 mode shape vector in principal coordinate
$\{\boldsymbol{\Phi}_N\}$	n by 1 mode shape vector in normal coordinate
A	Scaling constant
AS	Auto spectrum
$AS_{I:I}$	Auto spectrum of the output response
$AS_{J:J}$	Auto spectrum of the input force
BS	Block size or the total number of sample per block with unit of samples
C	Damping element (Nsm^{-1})
C_N	Modal damping element in normal coordinate
C_p	Modal damping element in principal coordinate
CN	Condition number
$Corr$	Correlation
$CorrCoef$	Correlation coefficient
CS	Cross spectrum
$CS_{I:J}$	Cross spectrum between input force and output acceleration response

$[\mathbf{C}]$	n by n damping symmetric matrix (Nsm^{-1})
$[\mathbf{C_N}]$	m by m modal damping matrix in normal coordinate
$[\mathbf{C_p}]$	m by m modal damping matrix in principal coordinate
dB	Decibel unit
fz	Total number of force DOF
$F[r]$	Sampled sequences of frequency trace that have finite length at r^{th} sample where $r = 0, 1, ..., BS-1$
g	Unit of mass; Grams
G	Synthesised FRF element
[G]	Synthesised FRF matrix; Unit depending on motion type: Acceleration (ms^{-2}/N); Velocity (ms^{-1}/N); Displacement (m/N)
$\mathbf{[G_{acc}]}$	Synthesised accelerance FRF (ms^{-2}/N)
$\mathbf{[G_{vel}]}$	Synthesised mobility FRF (ms^{-1}/N)
$\mathbf{[G_{disp}]}$	Synthesised admittance FRF (m/N)
H	Measured FRF element
$H_{I:J}$	Measured FRF element due to response DOF I and force DOF J
$[\mathbf{H}]$	Raw FRF matrix; Unit depending on motion type: Acceleration (ms^{-2}/N) ; Velocity (ms^{-1}/N) ; Displacement (m/N)
$\mathbf{[H_N]}$	Transfer function between mass normalised modal displacement and mass normalised modal force
i	Imaginary part; $i = \sqrt{-1}$
inv	Direct inverse method
I	Response DOF; I =1,2, ... , total number of response DOF, n
J	Force DOF; J =1,2, ... , total number of force DOF, fz

k	Variable of mode; k =1,2, ... ,total number of mode, m
k	Kilo which is equal to 10^3
m	Total number of mode
m	Unit of length; Metre
M	Mass element (kg)
M_N	Modal mass element in normal coordinate
M_p	Modal mass element in principal coordinate
M_PSD	Mean of PSD
$[\mathbf{M}]$	n by n mass symmetric matrix (kg)
$[\mathbf{M_N}]$	m by m modal mass matrix in normal coordinate
$[\mathbf{M_p}]$	m by m modal mass matrix in principal coordinate
n	Total number of response DOF
$norm2$	Largest singular value of a matrix
N	Unit of force; Newton
$pinv$	Pseudo-inverse method
PSD	Coefficient of PSD
Q	Identified input force element (N)
$\tilde{Q}$	Measured input force element (N)
Q_N	Modal input force element in normal coordinate
Q_p	Modal input force element in principal coordinate
$\{\boldsymbol{Q}\}$	n by 1 identified force vector (N)
$\{\boldsymbol{Q}_{acc}\}$	Identified force vector by using acceleration response (N)
$\{\boldsymbol{Q}_{vel}\}$	Identified force vector by using velocity response (N)

$\{Q_{disp}\}$	Identified force vector by using displacement response (N)
$\{Q_N\}$	*m* by 1 mass normalised modal force vector in normal coordinate
r	Residue mode shape element; integer (i.e. *r* = 0, 1, ..., *BS*-1)
RS	Residual
[r]	*n* by *n* residue matrix; Unit depending on motion type: Acceleration ((ms^{-2})/Ns); Velocity ((ms^{-1})/Ns) ; Displacement (m/Ns)
s	Laplace domain coefficient
s	Unit of time; Second
S	Stiffness element (Nm^{-1})
S	Unit of block size; Samples
S_N	Modal element in normal coordinate
S_p	Modal element in principal coordinate
SD_PSD	Standard deviation of PSD
SR	Sampling rate with unit of samples per second (S/s)
[S]	*n* by *n* stiffness symmetric matrix (Nm^{-1})
$[\mathbf{S_N}]$	*m* by *m* modal stiffness matrix in normal coordinate
$[\mathbf{S_p}]$	*m* by *m* modal stiffness matrix in principal coordinate
t	Coefficient of time domain (s)
T[*u*]	Sampled sequences of time trace that have finite length at u^{th} sample where *u* =0,1,..., *BS*-1
TC	Threshold constant
TV_new	Threshold value of the new PSD sample
TV_RA	Threshold value obtained from residual analysis
u	Integer; *r* = 0, 1, ..., *BS*-1

V	Unit of voltage or electric potential; Volt
$w(t)$	Window function
X	Displacement element (m)
X_N	Modal displacement element in normal coordinate
X_p	Modal displacement element in principal coordinate
$\dot{X}$	Velocity element (ms^{-1})
$\ddot{X}$	Acceleration element (ms^{-2})
$\{\boldsymbol{X}\}$	*n* by 1 displacement vector (m)
$\{\boldsymbol{X_N}\}$	*m* by 1 mass normalised modal displacement vector in normal coordinate
$\{\dot{\boldsymbol{X}}\}$	*n* by 1 velocity vector (ms^{-1})
$\{\ddot{\boldsymbol{X}}\}$	*n* by 1 acceleration vector (ms^{-2})
$y'(t)$	Modified time history
$y(t)$	Original time signal
Y_{filter}	Filtering data
Y_{raw}	Raw data

Note: Braces of bold serif italic **{*r*}** for vectors; Brackets of upright bold serif [**r**] for matrices; italic *r* for scalar variables.

Abbreviations

2D	Two Dimensions
3D	Three Dimensions
ADC	Analogue-To-Digital Converter
ANN	Artificial Neural Network
ASIVR	Advanced Structural Integrity and Vibration Research
ASVR	Advanced Shock and Vibration Research
cDAQ	Compact Data Acquisition
CAE	Computer-Aided Engineering
CMIF	Complex Mode Indicator Function
CFRP	Carbon Fibre Reinforced Plastic
COH	Coherence
DAQ	Data Acquisition
DC	Direct Current
DFT	Discrete Fourier Transform
DMISF	Delayed, Multi-Step Inverse Structural Filter
DOF	Degree of Freedom
DP	Dynamic Programming
DSP	Digital Signal Processing
FEA	Finite Element Analysis
FEM	Finite Element Method
FFT	Fast Fourier Transform
FRF	Frequency Response Function
ICP	Integrated Circuit Piezoelectric
IFFT	Inverse Fast Fourier Transform
IRF	Impulse Response Function

ISF	Inverse Structural Filter
LS	Least Square
MAC	Modal Assurance Criterion
MATLAB	Matrix Laboratory
MDOF	Multiple Degree of Freedom
MIMO	Multiple Input Multiple Output
MMIF	Multivariate Mode Indicator Function
MTM	Modal Transformation Method
NI	National Instrument
NI-DAQmx	National Instrument Measurement and Automation
ODS	Operating Deflection Shape
PC	Personal Computer
PSD	Power Spectral Density
PTIM-MP	Precise Time-Step Integration Method for Markov Parameters
SDOF	Single Degree of Freedom
SISO	Single Input Single Output
SIMO	Single Input Multiple Output
SVD	Singular Value Decomposition
SWAT	Sum of Weighted Accelerations Technique
UM	University of Malaya
UMM	Unit Modal Mass
USB	Universal Serial Bus
VES	Virtual Engineering Series

Chapter 1: Introduction

1.1: Background

Identification of dynamic force excitation on a system is important for performance evaluation, design optimisation, noise suppression, vibration control as well as condition monitoring. In the early stage of the system development, numerous virtual testings can be carried out before validation of the prototype in order to reduce cost of material and labour. Virtual testing such as stress analysis would require knowledge of the excitation forces in the case of structural modification (Mao et al., 2010). Once the vibration force can be modelled with practical accuracy, the result can be used as a database for Computer-Aided Engineering (CAE) simulations of trouble shooting and design improvement analysis for noise and vibration (Otsuka et al., 2007). Such studies can be utilized for eliminating the unwanted vibration mode of a structure by considering both force and structural dynamic characteristic (Ryu et al., 2010).

However, direct measurement of the excitation force acting on a structure is not possible in many cases. This is because installation of force sensor at the structure's junctions could change its dynamic characteristic due to altering of boundary conditions (Yoon & Singh, 2011). There are many situations where the direct measurement of the excitation forces is not possible or feasible. For example: Engine torque pulses or the motor rotation forces (Jang et al., 2010); Forces transmitted from machinery, such as compressors, to the foundations (Yoon & Singh, 2010); Fluid structure interaction force in a piping or pump system (DeVis et al., 1992); Shock or impact loads on vehicles parts such as ship hulls or tires forces due to roadway unevenness (Pesterev et al., 2005).

For the case where direct measurement of force is not feasible and the force information is important for the design, development or health monitoring purpose, other force identification approach must be developed. Many indirect force measurements called "force determination method", "force reconstruction method", "force identification method" or "force recovery method" have been developed widely to estimate the unknown dynamic force. Studies to recover different dynamics forces such as wind load (Hwang et al., 2011), cutting force (Huang et al., 2009), moving force (Yu, 2003), contact force (Uhl, 2006), pressure (Sewell et al., 2010), machine rotation force (Lee & Chen, 2011; Ma et al., 1999), engine torque pulses (Starkey & Merrill, 1989) and impact force (Allen & Carne, 2008; Hundhausen et al., 2005; Yan & Zhou, 2009). Besides, Ong et al. (2011) utilized estimated cyclic loads from Operating Deflection Shape (ODS) of a T-plate structure to determine a suitable excitation level used in Impact-Synchronous Modal Analysis (Rahman et al., 2011a, 2011b).

1.1.1: Determination of Unknown Impact Force

Among these dynamic forces, impact force excitation is of primary importance for lightweight structural design. In fact, impulsive load can cause damage easily to a lightweight structure because they are more susceptible to damage compared to heavyweight structure. Impact force is defined as a high magnitude force that acts on structure for a short duration of time. It causes broadband excitation in frequency domain and excites several natural frequencies of the structure simultaneously as shown in Figure 1.1 (b). The excitation frequency of the impact force depends on the impact duration, contact stiffness between the impact force and material and the shape of impact force (Halvorsen & Brown, 1977). In general, smaller impact duration or larger contact stiffness will eventually have a broader excitation frequency range.

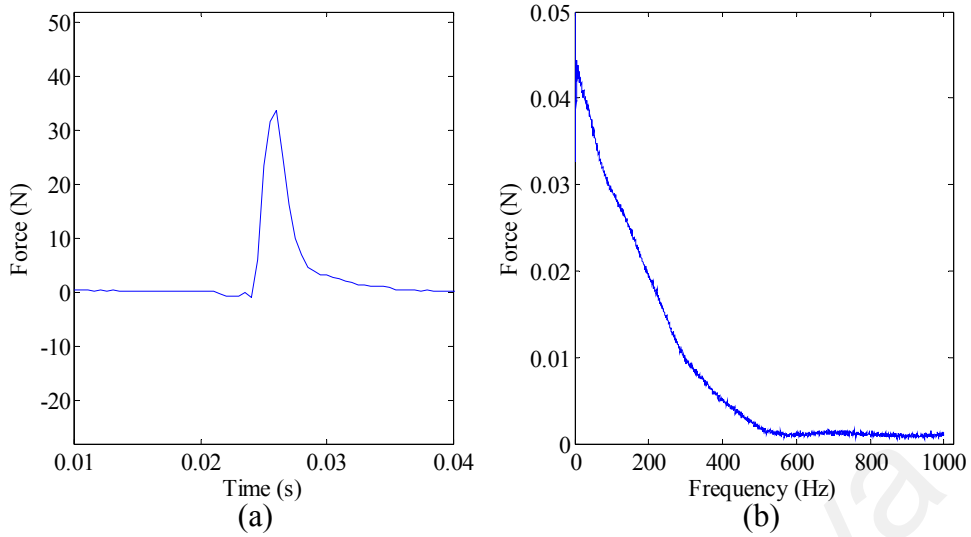

Figure 1.1:
Impact Force Function: (a) Time Domain, (b) Frequency Domain

In the automobile industry, impact force is the main cause of vibration problem in frequency range of 20-100Hz and is the main reason for material fatigue in lightweight vehicles (Gu et al., 2008; Lee & Kim, 2008). At the design, development and modification stage of a lightweight structure development, additional information about the loads experienced by the structure will aid the development iterations resulting in a better outcome. In fact, determination of the input forces and their locations are helpful in identifying areas that are more susceptible to damage. The amplitude of force reflects the structure vibration condition so that any requirements for stiffening or structure modification are identified to preserve a better structural integrity. A lightweight structure with good damage tolerance creates advantage to the competitive manufacturing field. Thus, impact force determination on a lightweight structure is the main subject of this research.

There are many real-time applications where force location is known in advance while the magnitude of force remains unknown. For example, impact on a vehicle structure due to a bump, cleat or roadway unevenness where force location is near the tyre where

direct force measurement is not allowed. In this case, an accurate determination of dynamic force's amplitude helps the engineer to monitor the automobile's vibration condition. Hence, actions such as stiffening or structural modification can be taken to preserve a better structural integrity based on the diagnosis results.

1.1.2: Force Identification Method

Many dynamic force identification methods have been developed and majority of them can be categorized into the optimisation method and the direct inverse method (Wang, 2002). The optimisation method uses optimisation loop to compute iteratively the response of a system due to an estimated force. The estimated force is assumed to be equal to original excitation when the estimated response matches the measured response. Various optimisation methods such as Gauss-Newton method (Guillaume et al., 2002) and genetic algorithm (Martin & Doyle, 1996b; Yan & Zhou, 2009) are used in the force identification procedure. Liu and Han (2009) conducted a computational inverse procedure to determine the transient loads. In additional to that, Sewell et al. (2010) presented a development of the Artificial Neural Network (ANN) method to improve the accuracy of the Inverse Problem Engine's output.

In this study direct inverse method is chosen to solve the dynamic inverse problem because optimisation method and ANN method needs higher computational and training time. In fact, direct inverse method calculates excitation force directly by multiplying the system's inverse measured or synthesised Frequency Response Function (FRF) with the measured responses at each frequency point of interest. It can be typically classified into 2 types: FRF based direct inverse method (Blau, 1999; Hundhausen et al., 2005) and modal model method (Desanghere & Snoeys, 1985). Note that the modal model method is also called Modal Transformation Method (MTM) (Briggs & Tse, 1992; Kim

& Lee, 1986) and modal coordinate transformation method (Kriel, 2000; Shih et al., 1989).

The former method would be superior to the latter method in terms of force accuracy, however it requires a huge amount of raw FRF data. In fact by curve fitting a single column or row of FRF matrix, the modal parameters called the damped natural frequencies, modal damping and residue mode shapes can be obtained. These modal parameters can be used to synthesise a FRF matrix by using reciprocity theorem with the assumption of a linear system. This method is very useful especially when the input location is inaccessible as the MTM is able to estimate the FRF between inaccessible input and the selected output location as well. This shows that the latter method would be superior to the former method in terms of the measurement and computational efficiencies plus the ability to synthesise FRFs with inaccessible force Degree of Freedom (DOF). Considering the application of MTM is being practiced more in reality, thus it is valuable to estimate the unknown force by using this method in this research.

1.1.3: Ill-Posed Problem

Direct inverse method is more labour intensive as it needs extra care and attention from users since the procedures to discover force can be ill-conditioned. A problem is called well-posed problem if the following conditions are fulfilled (Hadamard, 1923): the solution is exist, unique and depends continuously on the data (stability condition). On the other hand, dynamic force obtained from the inverse problem is always unstable because there are only a finite number of measured responses used to represent actual responses of a structure which is a continuum (i.e. a continuous vector function in the spatial coordinate). The solution is sensitive to the measurement noise and hence it is

unstable (Chen & Yuan, 2010). In other words it is an ill-conditioned problem, where small variation in response will result in large changes of identified force.

An ill-posed problem may happen when there is a lack of information. For example, such an ill-posed problem can surface when a problem of load identification is not collocated (Uhl, 2006). Uhl stated that a non-collocated problem would occur if at least one of the loads does not have a distinguishable influence on any of the sensors (i.e. the remote sensors are far away from the impact location and none of them are located at the impact location) (Uhl, 2006).

In an impact force determination problem, the solution is the time history of impact force which consists of loading and unloading parts (Goldsmith, 1960). The loading part is a part where the force is initially zero, increase to its maximum, and then decreases to zero; the unloading part is where the force remains zero after loading (Gunawan et al., 2008). According to Gunawan, the solution for impact force determination problem usually exists but the uniqueness and stability of the solutions are often violated. Various types of regularisation are suggested to overcome the ill-posed problem (Gunawan et al., 2008). The regularisation method can be formulated based on the following approaches: Tikhonov regularisation (Choi et al., 2006); Singular Value Decomposition (SVD) (Kim & Lee, 2009).

Tikhonov regularisation states that the best solution for the ill-posed problem is the one that minimizes the least-square criterion and also minimizes the noise effect in the solution (Gunawan et al., 2008). The idea has been widely implemented for solving various force reconstruction problems. For example: Boukria used the Tikhonov regularisation method to estimate impact force acting on a circular plate (Boukria et al.,

2011). However, it is difficult to select an appropriate regularisation parameter for Tikhonov regularisation and it often requires a L-curves graph to assist users to choose the regularisation parameter (Hansen, 2001; Hansen et al., 2006).

The SVD method is more user-friendly compared to Tikhonov regularisation. It improves the condition of FRF matrix by eliminating FRF matrix that is related to a very small singular value or singular vector. This way, SVD helps to improve the uniqueness of the solution. Besides, Kim and Lee found that the system matrix may be singular or near-singular and have small singular values in a non-minimum phase system, they showed that the SVD inverse technique works well for a non-minimum phase system (Kim & Lee, 2009). There are 2 major limitations of implementing SVD. Firstly, it is difficult for SVD to approximate the unloading part of impact force because high frequency components of the singular values are affected by noise. Apart from that, SVD also requires a high computation cost which is the highest among the direct solution methods and thus only suitable for small scale inverse problem (Golub & Loan, 1996). Regularisation methods such as cubic spline (Gunawan et al., 2006) and quadratic spline (Gunawan et al., 2008) are proposed to approximate the impact force for the large scale inverse problem,. Furthermore, iterative Tikhonov regularisation method and Levenberg-Marquardt iterative regularisation (Gunawan, 2012) are adopted for the impact force reconstruction. A more accurate force determination result can be obtained by using iterative regularisation compared to the non-iterative method.

Moreover, Moore-Penrose pseudo-inverse method adopts a Least Square (LS) solution of the predicted force by forming an over-determined problem, which uses more equations than number of applied forces to solve problem. This improves the condition number of the inverse problem which reduces the error of identified force to a certain

extent. By using the LS criterion only, it is able to provide satisfactory solution for some impact-force inverse problems (i.e. the impact force acting on a ceramic body armor (Cardi et al., 2006a, 2006b) and impact force acting on a standoff metallic thermal protection system panel (Hundhausen et al., 2007)). Previous studies show that it is possible to incorporate pseudo-inverse with SVD for a better force determination result in moving force problem (Yu, 2003).

1.1.4: Priori Data for Well-Posed Problem

Instead of using the regularisation methods, priori data such as information that characterizes the impact-force profile can be utilized to form a well-posed problem. There are plenty of studies that show force determination problem can become well-posed once the force location is known in advance (Liu & Han, 2003). In recent years, various model-based force reconstruction methods have been proposed, especially within the context of accurate models (modal model, Impulse Response Function (IRF) or FRF) (Zhang et al., 2012). In fact, these models can be estimated from experimental modal analysis (Schwarz & Richardson, 1999) or predicted by a finite element model where the quality of the model affecting the accuracy of estimated force.

In this study, the MTM is used in conjunction with the Moore-Penrose pseudo-inverse method to generate an over-determined problem to calculate a LS solution of unknown impact force, where the force location is known in advance. Theoretically this method will produce an accurate force determination result without the concern of the ill-posed problem. However, there are several error sources for this method which reduce the force's accuracy.

1.2: Problem Statement

There are several error sources for force identification by using MTM, such as the accuracy of modal model and the measurement noise of response data. In this study, data filtering approach and integration method are proposed to enhance the accuracy of impact force determination result.

1.2.1: Accuracy of Modal Model

There are several error sources that make the MTM infeasible. This method relies heavily on the quality of measured raw FRF data and the quality of the curve fitting result for modal parameters extraction purpose. When modal model is used, there is an unavoidable error due to the effects of mode outside the selected frequency bandwidth. Current curve fitting algorithm such as polynomial curve fitting method compensates the outside band mode contribution by using extra polynomial terms (Vibrant Technology, 2001). However, the fitting function of modal model does not account for the effects of the outside mode. As a result, the accuracy of the modal model or the synthesised FRF is affected.

1.2.2: Measurement Noise of Response Data

Besides the error source from the FRF data, the measurement noise from the measured structural response contributes to the poor estimation of the unknown force as well. Although these noises and error are small, they can still be amplified through the inversion process. The effect of the amplified noise would propagate to the final estimated force and may diminish the force accuracy.

1.2.3: Data Filtering Approach

To enhance the impact force determination result, data filtering approach such as band pass filtering can be applied to eliminate or reduce the noise effect. In fact, filtering of measured structural response can limit the possibility of the ill-posed problem (Uhl, 2006). However, there are several difficulties in using the data filtering approach in the impact force determination. First of all, it is very hard to decide the cut-off frequency, which precisely differentiates between the useful signal and unwanted noise. If the cut-off frequency is too low, the distortion of signal will happen. If it is too high, the noise effect on the force determination will be significant. The difficulty of applying the data filtering approach increases for a time-variant excitation frequency case. In fact, the broadband excitation frequency of an impact force may change from time to time that mainly depends on the impact duration and contact materials.

In general, residual analysis is a well-known graphical tool which utilizes curve fitting method to determine the cut-off frequency from the measured raw data (Biewener & Full, 1992). However this method is time consuming as it needs extensive care and attention on the curve fitting for every new raw data. It is impractical to apply this technique in the case where the actual excitation frequency is time-variant and not consistent. This is because the excitation frequency region will change from time to time, so is the required cut-off frequency. For this reason, engineers would rather choose a higher fixed analysis frequency range which includes the entire possible excitation frequency region although it may contain unwanted noise region. Liu stated that it is often difficult to make the decision on cutting off the frequencies, which should be related somehow to the information on the noise. Engineering experience and judgement and trial and error are needed to make a proper decision (Liu & Han, 2003).

This motivates the author to find a suitable tool to determine the optimum cut-off frequency for impact force determination purpose in time-variant case.

1.2.3.1: Power Spectral Density Tool

A frequency range determinator named the Power Spectral Density (PSD) tool has been developed throughout this study. It assists user to select an appropriate analysis frequency range of FRF and response for impact force determination purpose. PSD tool consists of 3 components: residual analysis, acceleration PSD and normalised total power of response PSDs. Once low pass frequency and high pass frequency are determined by using PSD tool, a band pass filtering is applied to select the analysis frequency range.

1.2.4: Integration Method

Apart from using the normal filter such as the band pass filter of the data filtering approach, it is also possible to filter both the system and response data by using integration method. In fact, the integration process determines the mean value of a signal by adding the positive and negative "area" together. Integration is able to reduce the noise variance and thus narrowing the noise and signal plus noise probability density function (McDonough & Whalen, 1995). In the case of a random noise signal, the positive and negative "area" is equally distributed. In order words, integration of a random noise signal will give a zero mean. Therefore, noise elements that exist in a signal can be eliminated by using the integration process. In addition, forming a mean value through integration method apparently eliminates noise better than a normal filter (Karrenberg, 2002).

There are 2 unavoidable problems when an integration process is adopted: unknown constant of integration; amplification of low frequency noise and causing a spurious trend (i.e. intrinsic problem or intrinsic error). The first problem can be commonly eliminated by suppressing the Direct Current (DC) frequency (i.e. 0Hz). To solve the intrinsic problem, a high pass filtering must be adopted. Unfortunately, it is hard to discriminate between the intrinsic problem low frequency data and real low frequency data (Audenino & Belingardi, 1996; Karrenberg, 2002). In fact filtering data by using the integration method is very useful, however it has its own limitations. In order to make the integration method successful, an appropriate high pass frequency must be obtained to solve the intrinsic problem.

1.2.4.1: Effectiveness of Various Types of Responses in Impact Force Determination

An experimental study by Hwang et al. (2011) showed that the modal wind load identification from acceleration response obtained by numerically differentiating displacement, using Kalman filter yielded more accurate results than measured displacement response. There is no study on the effectiveness of different types of responses in impact force determination via MTM so far in the knowledge of the author. Thus motivation to fill this literature gap is created.

To study the effectiveness of various types of responses in impact force determination, acceleration, velocity and displacement responses must be obtained in advance. However, it is impractical to measure these responses simultaneously by using various sensors at a single DOF. Typically acceleration is the most common unit dealing with inverse force problem. Uhl (2006)stated that the most practical and cheapest system responses are acceleration measurements, which gives a more accurate and stable result, against displacement measurement. Hence, acceleration measurement is suggested to be

used in this study and the other 2 types of responses are estimated from the measured acceleration by the means of integration. In fact, it is always preferable to integrate rather than to differentiate because differentiation process will amplify the noise content in a signal especially in high frequency region (Audenino & Belingardi, 1996).

1.3: Objectives of the Research

Over the years, in the effort to improve the estimation accuracy in force determination, the focus is mainly in the complicated technical problems in mathematics, especially in the ill-posedness and regularisation method (Jiang & Hu, 2009). However, relatively less effort is made on the Digital Signal Processing (DSP) aspects, especially by using data filtering approach and integration method. In this study, impact force determination with MTM by using data filtering and integration methods are proposed to further enhance the conventional method. The impact location is known in advance and the only left unknown force history to be reconstructed is through the impact force determination. The following are objectives that have been made:

i. To study the accuracy of impact force determination via MTM by using fixed analysis frequency range in various types of responses. Note that the first study is done for known excitation frequency range case. Hence, the fixed analysis frequency range can be divided into under-estimated, even-estimated and over-estimated cases which have much lower, similar and much higher analysis frequency range respectively, compared to the excitation frequency range.

ii. To study the accuracy of impact force determination via MTM by using PSD tool selected analysis frequency range in various types of responses. Note that the second study is performed for the case of unknown excitation frequency

range. An appropriate analysis frequency range is determined by using self-developed PSD tool.

iii. To propose the most suitable analysis frequency range and type of response in impact force determination via MTM. Note that the results of the first and second studies are compared and analysed in the third study. Therefore, the most suitable analysis frequency range and type of response can be proposed.

iv. To study the effectiveness of the proposed force determination method in both collocated and non-collocated cases, in comparison to the conventional method. Note that the studies so far are performed under collocated case for 1 point analysis only. The fourth study extends the previous studies to a 15 points analysis under both collocated and non-collocated cases.

1.4: Research Flow and Scope

Based on the objectives, the research flow chart has been constructed as shown in Figure 1.2. First of all, the impact force determination via MTM will be examined in one point analysis where the force determination is conducted at point 1 only. The force determination will be examined in fixed and PSD tool selected analysis frequency ranges. There are 3 cases of fixed analysis frequency ranges, which are under-estimated (i.e. 0.5-100.1Hz), even-estimated (i.e. 0.5-500.0Hz) and over-estimated (i.e. 0.5-999.5Hz) respectively compared to the actual excitation frequency range (i.e. 0.5-500.0Hz). On the other hand, PSD tool is utilized to set a band pass filter that differentiates between highly contributed signal and unwanted noise signal in this study. As a result, PSD tool selected frequency range can be obtained.

In each case of fixed and PSD tool selected analysis frequency ranges, the impact force determination will be conducted by using various types of responses such as acceleration, velocity and displacement responses. A total of 15 measured responses data are used for the impact force determination. The effectiveness of the different types of analysis frequency range on the impact force determination is examined as well as the effectiveness of the various types of responses. By comparing the results for fixed and PSD tool selected analysis frequency ranges in various types of responses, the most suitable analysis frequency range and the most suitable type of response or the best vibration unit can be proposed for the impact force determination via MTM.

Hence, this proposed method will be applied to estimate 15 sets of single unknown force at 15 discrete locations for a complete analysis. The impact force determination via MTM using the proposed method will be conducted in the collocated and non-collocated cases. Note that in the collocated case, the impact location is close to one of the response sensors (i.e. total 15 response sensors including the impact location), while the impact location is far away from the entire response sensors for non-collocated cases (i.e. total 14 response sensors excluding the impact location). Next the effectiveness of the proposed method will be compared to the force determination result by using a conventional method (i.e. use an over-determined fixed analysis frequency range and acceleration response in the impact force determination).

1.5: Outline of the Thesis

The thesis is subdivided into 5 parts: introduction, theoretical background, research methodology, result and discussion, and the conclusions. Introduction part is presented in the chapter 1. Next, theoretical background will be described in chapter 2. Chapter 3 provides the research methodology including the materials and methods used in the

experiment. Chapter 4 discusses and elaborates the experimental results. Chapter 5 concludes the outcomes and findings of this research.

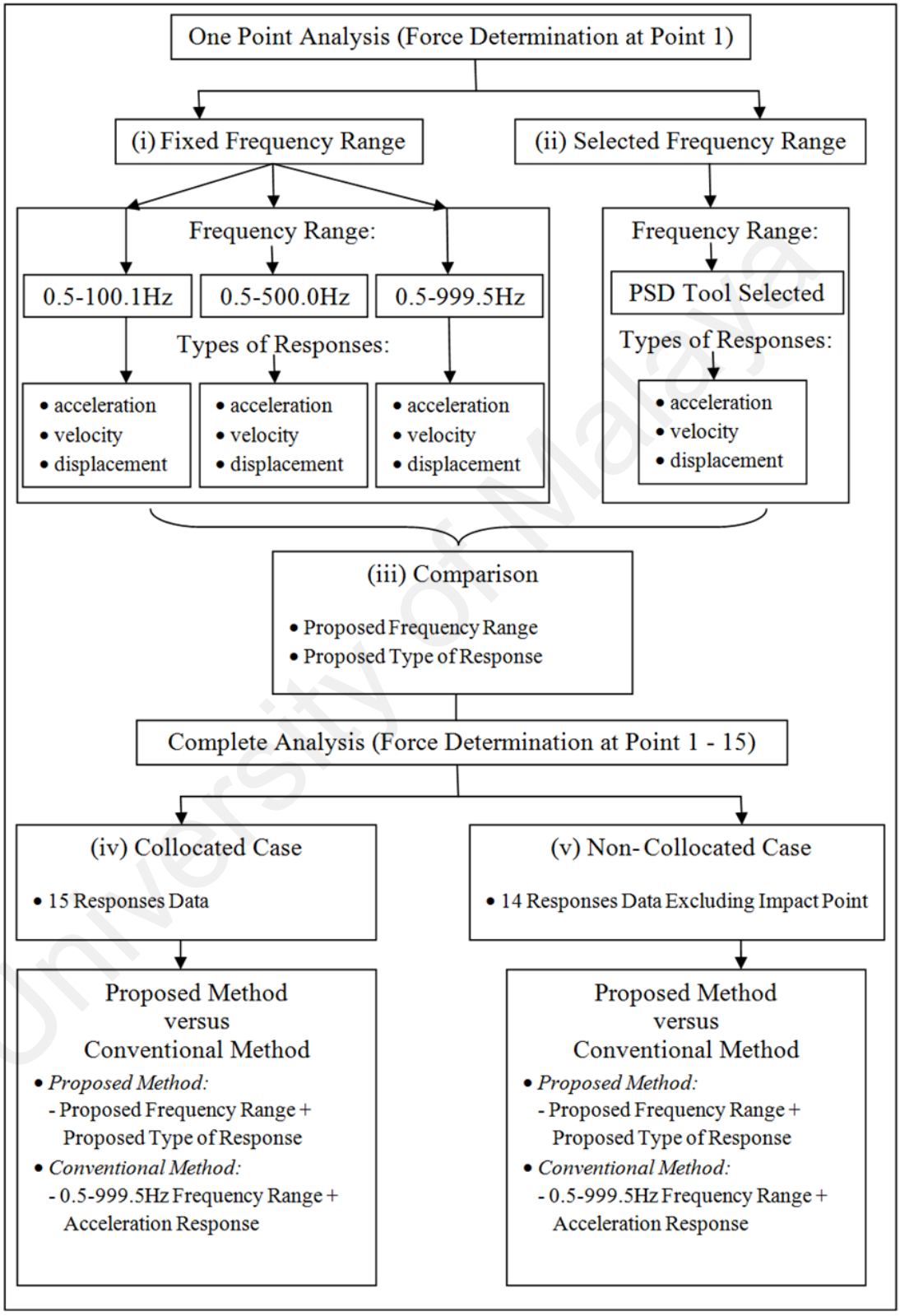

Figure 1.2:
Research Flow Chart

Chapter 2: Theoretical Background

2.1: Introduction

In this chapter, comprehensive literature reviews concerning impact force determination by using an inverse problem have been summarised and compiled. Next, the formulation and theoretical background for the impact force determination with MTM by using various types of responses are explained in Section 2.3. Besides, signal processing techniques used in this research are also provided in Section 2.4 including the FRF, Coherence (COH) function and integration function. Lastly, the data filtering approach by using PSD tool is introduced in the Section 2.5.

2.2: Literature Review

Plate is commonly used in power plant, industrial plant, automotive and aerospace, thus it is essential for engineers to understand the behaviour of such structures through the study of theory and analysis. The major concern on the reliability of such a structure is the damage due to impact loads (Lee, 2008). In this case, a dynamic analysis is required to study the behaviour of the plate as an impact force is a time varying load. In fact a dynamic analysis is more complex than a static analysis. A linear static analysis will produce only one solution, but a dynamic analysis can result in a series of solutions that corresponds to the time that is chosen to be studied. In a dynamic analysis, not only internal forces are present but also inertia forces resulting from the accelerations of the structure. At the same time the response of the structure varies in time when affected to a dynamic load.

In general, dynamic analysis of a structure can be divided into 2 categories: (a) direct problem (b) inverse problem. Direct problem is the case where the input and system parameters are given to determine the output. Inverse problem is the case where the input and output are given to estimate the system parameters or the system parameters and output are given to reconstruct the input. Apparently, impact force determination is an inverse problem which currently interest researchers and engineers in various fields. Several reviews on the force determination based on inverse problem have been made for last 2 decades (Chella et al., 2012; Dobson & Rider, 1990; Inoue et al., 2001; Ouyang, 2011; Stevens, 1987). Goodier et al. (1959) initiates an early attempt to recover an unknown impact force from the remote response by solving an integral equation.

In fact, time domain and frequency domain force identification have been developed widely. Time domain force reconstruction algorithm is primarily important in the case where the available data may be of such short duration that leakage renders FRF processing to be inaccurate (Allen & Carne, 2008). One common time domain approach is the deconvolution technique by using Inverse Structural Filter (ISF) (Chang & Sun, 1989; Jacquelin et al., 2003; Steltzner & Kammer, 1999). The ISF is enhanced to the Delayed, Multi-Step Inverse Structural Filter (DMISF) via the way it is computed. The ISF was obtained directly from inverting the measured impulse response, whereas DMISF was derived from a state space model of the forward dynamic system. Another common method is based on modal filtering, dubbed the Sum of Weighted Accelerations Technique (SWAT), which estimates the unknown force by isolating the rigid body modal accelerations (Allen & Carne, 2006; Carne et al., 1992). DMISF was found to give excellent results relative to other force algorithms (i.e. ISF and SWAT methods) while the SWAT algorithm is much more computationally efficient than any of the other methods (Allen & Carne, 2008).

Ödeen and Lundberg (1991) established a impulse response method to predict the impact force history by using velocity response. Good agreement was obtained between the recovered force histories and those measured with the aid of strain gauges on the long cylindrical rod. O'Callahan and Piergentili (1996) found that unknown force location and its magnitude can be adequately determined when the assumed forces are located at where the actual forces act.

A real time approach to estimate the unknown impact force based on Finite Element Analysis (FEA) has been proposed by Shin (2000) in his paper entitled "Real-Time Recovery of Impact Force Based on FEA". For both concurrent control of dynamic behaviour and on-line detection of impact damage, real-time impact force must be obtained in advance. The real-time inverse scheme is based on modal model method and the force recovery equations are formulated based on over-determining condition. FEA is used for modal parameters extraction and hence SVD is used to solve the equation of force recovery. Time averaging is applied to filter out noise of the response data to further improve the force accuracy (Shin, 2000).

In a paper entitled "Identification of Impact Force on Composite Structures Using an Inverse Approach" by Hu (2007), the effectiveness of impact force determination is examined in the case where impact damage occurs in structures. In this research, a 4-corner clamped Carbon Fibre Reinforced Plastic (CFRP) plate specimen is used as the test rig. The transfer matrix that relates the forces and strain responses is constructed from Finite Element Method (FEM). Then, the optimisation method is used to obtain the time history of unknown impact force by using accelerometers and strain sensors. The accelerometers feedback gives a better force determination result compared to the strain sensors feedback.

Besides, the result shows that the proposed method is still effective for estimating acceptable time history of impact force (Hu et al., 2007). Based on the information of identified impact forces, real-time health monitoring of a structure is possible. For example, Hu and Fukunaga (2005) developed a FEM model based on the identified force to estimate the possible internal various damages caused by the impact force. Furthermore, the associated damage caused by the impact and the residual strength of the structures can be predicted by quantifying the impact source (Chen & Yuan, 2010). Moreover, study found that the use of the arrival times of flexural waves will effectively reduce the impact force determination time (Atobe et al., 2011).

Ma and Ho (2004) proposed an inverse method to identify input forces of non-linear structural systems. This method is composed of the extended Kalman filter and a recursive least-squares estimator. By using the inverse method, input forces acting on non-linear structural systems can be estimated from measured dynamic responses. Numerical results demonstrated that the application of the input force estimation method to non-linear structural systems is successful. Lourens et al. (2012) developed an augmented Kalman filter for the reconstruction of the impact force and sine-sweep force. This method modelled the noise that is present on the measurement and state variables to be a stochastic process. Experiment was carried out in collocated and non-collocated cases, and the result was compared to the Dynamic Programming (DP) algorithm, which is a commonly used recursive least-squares method. Result showed that Kalman filter has a better force accuracy in collocated case as it accounted for the modelling errors. The condition number increased significantly in the non-collocated case, which indicated an increment in ill-conditioning. In this case, DP algorithm produced a better solution (Lourens et al., 2012).

Sekula and Holnicki-Szulc (2007) in their paper entitled "Comparison of Real Time Impact Load Identification Procedures" presented a solution maps heuristic approach to estimate dropped mass impact force by using structural response. The solution map stores the output response due to difference types of excitation forces in its database. An optimisation problem is formed between the measured response due to the unknown impact force and the impact parameter such as the mass and velocity of the impacting body. Once the structural response is measured, the best solution can be found from the existing solution map.

Gu et al. (2008) has developed direct integration method for calculating dynamic impact load. Besides, he investigates the correlation between dynamic impact load, vehicle speed and axle load. While, Mao et al. (2010) utilized the Precise Time-Step Integration Method for Markov Parameters (PTIM-MP) with the aid of Tikhonov regularisation technique to solve this ill-posed problem of force reconstruction.

Huang et al. (1997) described an inverse technique for the prediction of impact forces from acceleration measurements on a vibratory ball mill. A time based-optimisation problem is formed based on the measured response and estimated response from the superposition of the modal responses. The predicted and measured impact forces are in good agreement. Wang (2003) in his paper with topic of "Determination of Unknown Impact Force Acing on a Simply Supported Beam" formulated both time-based and frequency-based optimisation methods for impact force determination on a simply supported beam. The objective of the optimisation problem is to find the solution for force amplitude and force location by minimizing the objective function such as the sum of square errors between the measured response and estimated response. This paper adopts the Modal Assurance Criterion (MAC) to predict the impact location.

In fact, a lot of time-based force algorithms have been widely developed for the impact force determination because the time domain methods have the ability of exploring the transient behaviour of impulsive force (Kriel, 2000). Compared to the time domain approach, there is a relatively small amount of research works on the frequency-based algorithm for the impact force determination. The challenges in the inverse problem are manifested differently in the frequency domain. It is expected to avoid some common time-based force determination problems as the frequency domain approach is more straightforward and simple. For example, convolution in time domain requires a higher computational time compared to multiplication in frequency domain, while both give a similar result. Thus, it is valuable to estimate transient signals such as the impact force in frequency domain.

Previously, the frequency domain approach often suffers from the leakage problem which reduces the quality of signal when it transforms into frequency domain. The leakage of FRF indeed can be avoided by using an appropriate sampling rate and block size during the measurement. However, if the leakage problem is unavoidable, it can be corrected by using window function for the signal processing and some analytical approaches (Dishan, 1995; Kang et al., 2000).

Several literatures on the force determination by using a frequency-based force algorithm are reviewed subsequently. Martin and Doyle (1996a) used a frequency domain deconvolution method to estimate force history from the experimentally measured acceleration responses. In his study, some of the fundamental difficulties and issues involved in this problem have been clarified. The proposed method was examined on 4 example structures. Doyle (1997) had proposed wavelet deconvolution method as one of the ways to overcome the limitation of frequency domain

deconvolution method. It was found that reasonable force determination result can be obtained although there were multiple reflections.

McCarthy and Lyon (1995) proposed an inverse-filtering method which incorporates with cepstral-smoothing and minimum-phase processing to estimate valve impact force in reciprocating compressor. It is proposed to use the force information for valve health monitoring purpose. Besides, the recovery of double impacts by using a cepstral comb window is demonstrated (McCarthy & Lyon, 1995). Furthermore, tuned COH function is introduced to separate the coherent and incoherent components of a measured response signal. The diagnostic signature recovery results of valve impact forces showed significant improvement by using the coherent vibration signal (McCarthy, 1997).

The FRF based LS approach (Stevens, 1987) is the most widely used approach because it can be applied to a variety of force identification problems. Wang explained the theoretical background of the FRF based direct inverse method for impact force determination in detail (Wang, 2002). Hundhausen et al. (2005, 2007) applied this method to estimate impulsive loads acting on a standoff metallic thermal protection system panel. In this study, 4 tri-axis accelerometers are used to estimate unknown forces at 9 locations. The FRF based impact force determination measures both impact location and force history simultaneously. Results showed that force determination through FRF method is accurate in terms of impact location and force magnitude. The percentage of errors between amplitude of measured forces and identified forces is less than 5% only. Liu and Shepardjr (2005) discussed the application and limitation of LS scheme. Besides, several existing methods for overcoming some of these limitations are reviewed. According to Liu and Shepardjr (2005), the total LS scheme is able to give a

much better result when both the transfer function matrix and the response data contain errors.

Cardi et al. (2006a) used the FRF to solve the impact force acting on a ceramic body armor using a Newtonian analytical model. In this study, it was found that the estimation of the impact force becomes less accurate at certain locations which have more energy at higher frequencies. This is because the measured FRF was not well defined for that particular high frequency region. In fact, the input force excitation frequency range is unknown and the decision of the range of analysis frequency range is always subjective. Future work is necessary to find an appropriate analysis frequency range prior to impact force determination (Cardi et al., 2006a).

According to Thite and Thompson (2006), reducing both measurement error and condition number will improve the force determination result. This study demonstrated that the selection of responses measurement locations with low condition number can be an alternative way to improve force determination instead of applying the regularisation method (Thite & Thompson, 2006). Zheng et al. (2011) further improves the optimum response selection method by taking into account the COH factor of the transfer function matrix. A significant increment in computational effective is observed by implementing this method (Zheng et al., 2011).

Instead of applying the optimum response method, Zhang et al. (2012) proposed a Bayesian approach for impact force determination which accounts for all error sources that contribute to the estimated force in a probabilistic framework. This study describes that the measurement noise and model uncertainty are the major sources of errors. The model uncertainty found in the FRFs level and modal parameters level will eventually

diminish the force determination result. By quantifying the measurement noise and model uncertainty through Monte Carlo Markov chain method, an unknown impact force is reconstructed based on the Bayesian force reconstruction methodology. The measured force and estimated force match very well in the time domain through this approach (Zhang et al., 2012).

MTM has more advantages than the FRF based direct inverse method, especially when points of operational inputs are inaccessible for artificial excitation but accessible for response measurement (Kim & Kim, 1999). Besides, it has higher computation speed compared to the deconvolution, inverse filtering, and FRF based direct inverse methods. Okubo (1985) stated that the force determination with MTM relies on the extraction of the modal parameters from the measured FRF. The limitation of curve fitting algorithms may causes error in modal parameters estimation especially at resonances and anti-resonances. Most of the researchers failed to estimate the unknown force by using MTM. For example, Hollandsworth and Busby (1989) used the MTM to predict the impact force which resulted in a beam response. Measured acceleration responses were used for the force determination purpose. The force identification quality was poor. The result showed 50% of error between the actual and estimated value.

Apart from the direct calculation of unknown force through MTM, Bridggs and Tse (1992) estimated impact force on a read/write head of a computer hard disk drive by using MTM and pattern matching technique. An acceptable force determination result was obtained in this study. Furthermore, Kim and Kim (1999) studied how the mechanisms of the errors from modal parameters, especially the poles and mode shape vectors affect the force determination result. In order to counteract the error propagation, traditional MTM is extended into discrete modal filter approach. Result showed that the

modal filtering approach was able to calculate both force location and magnitude within acceptable accuracy. Mendrok and Uhl (2010) improved the modal filtering method by incorporating it with Ritz vectors. In fact, Ritz vectors have the property to consider the static load and have high resistance on the truncation error. This modified modal filter technique led to an enhancement of force accuracy.

Previous development of force determination via MTM was focused on improving the force reconstruction algorithm. Less attention was paid to the physical nature of the force determination problem although there is a possibility that the ill-posedness was a result of physical issues instead of mathematical issues. For this reason, Jiang and Hu (2008, 2009) initiated an investigation on the effect of mode selection and consistent spatial expression toward force determination result via MTM. It was hypothesized that there is an optimum range for the force reconstruction when a particular level of noise in response is given for a specific test object. Scale factor of each mode was proposed as the tool to determine the threshold for mode selection. Hence, an optimal frequency range and optimal spatial modes can be selected based on the scale factor. Numerical simulations on the beam and plate structures were given to examine the effectiveness of the proposed method. It was found that the force accuracy was enhanced once an appropriate range was selected based on the scale factor. Besides, Jiang and Hu's studies showed that if the selected range is too broad, force accuracy will be decreased (Jiang & Hu, 2008, 2009).

The excitation frequency of the force is not initially known in the force identification process (Liu & Shepardjr, 2005). Moreover, the determination of unknown impact force excitation frequency is especially hard due to its time-variant characteristic (i.e. it may change from time to time depending on the impact condition such as the impact duration). Previous literature showed that most of the impact force determination problem used a fixed analysis frequency range and this may cause inaccurate force determination result. For example, the study of Cardi showed an inaccurate impact force determination result when significant vibration modes in high frequency were not included (Cardi et al., 2006a). For the application to a wide range of problem, studies always cover a wide frequency range, which include the low and high modal density regions (Choi et al., 2007). However, ill-posed problem may occur where the solution of impact force determination is not unique due to the high frequency contents of unfiltered signals (Uhl, 2006).

Instead of adopting a fixed analysis frequency range, previous study proposed to select the range by using mode selection method via the scale factor tool (Jiang & Hu, 2009). However, this method is limited to structures which can be modelled numerically in its current form. From a practical aspect, another tool named PSD tool is proposed to select an appropriate analysis frequency range in this study. Besides, integration method is adopted to estimate the unknown force by using various types of responses. The research gap between current study and previous study is shown in Table 2.1.

Table 2.1:
Research Gap between Current Study and Previous Study

No.	Previous Study	Research Gap	Current Study
1	Focus on mathematical issues, i.e. improving the force reconstruction algorithm (Cardi et al., 2006a; Choi et al., 2007).	Unknown useful analysis frequency range because the excitation frequency of impact force is unknown.	Focus on physical issues, i.e. selecting an appropriate range by using data filtering with PSD tool.
2	Focus on physical issues, i.e. selecting range by using mode selection method (Jiang & Hu, 2008, 2009).	Limited to simple structures, i.e. beam and plate, which can be modelled and solved numerically.	Data filtering with PSD tool is applicable to experimental work.
3	Focus on measured acceleration (Uhl, 2006).	Unknown useful type of response in impact force determination via MTM.	Consider velocity and displacement obtained from numerical integration.

2.3: Theory of Vibration

Vibration refers to mechanical oscillations about an equilibrium point. It is the result of energy being transferred back and forth between kinetic and potential energies. The structural responses or vibration of a machine structures will depend on the following factors (William & Marie, 1998): amount of modal damping; closeness of the natural frequency to the excitation frequency; and the relationship between the mode shape and the distribution of excitation forces. In fact, the modal damping, natural frequency and mode shape define completely the dynamic characteristics of a structural. A structural response is the outcome of a complex interaction between the excitation forces and the dynamic characteristics of the structure in reality.

An open loop system represents the relationship between input force, output response and dynamic characteristic of a linear system as shown in Figure 2.1. These excitation forces and dynamic characteristics are not just functions of space and time but also of

frequency. In general, the dynamic characteristic of a linear system can be expressed in frequency domain by using FRF. Depending on the unit of measured response, it can be classified into accelerance FRF, mobility FRF and admittance FRF for the acceleration, velocity and displacement responses respectively. It is worthwhile to mention that the behaviour of the excitation force does not affect the dynamic characteristic of the system. FRF only depends on geometric, material and boundary properties of a linear time-invariant system, and it is independent of the excitation types (i.e. in harmonic, impulse, random or any other forms). Theoretically, if the output response and FRF can be measured in advance, the unknown input excitation force can be evaluated next.

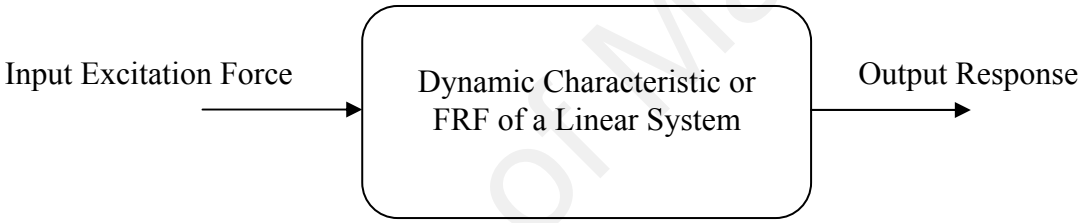

Figure 2.1:
Relationship between Excitation Force, Output Response and FRF in a Linear System

2.3.1: Multiple Degree of Freedom System

DOF of a system is the number of independent coordinates required to describe the motion of a system. A particle will have 6 DOFs, which consist of 3 DOFs translation motion and 3 DOFs rotation motion. Thus, a continuous system with infinite particle will eventually have infinite DOFs. However, a continuous system can be discretised into multiple *n* DOFs system according to the frequency of interest to be studied. For example, a higher number of DOF was chosen to describe a motion of a system which is vibrating in a high frequency compared to a low frequency case.

The spatial coordinate equation of motion for forced vibrations of Multiple Degree of Freedom (MDOF) system with viscous damping which fully describes the test rig under analysis is shown in Eq. (2.1).

$$\underset{nxn}{[\mathbf{M}]}\underset{nx1}{\{\ddot{\boldsymbol{X}}(t)\}}+\underset{nxn}{[\mathbf{C}]}\underset{nx1}{\{\dot{\boldsymbol{X}}(t)\}}+\underset{nxn}{[\mathbf{S}]}\underset{nx1}{\{\boldsymbol{X}(t)\}}=\underset{nx1}{\{\boldsymbol{Q}(t)\}}, \tag{2.1}$$

where [**M**], [**C**] and [**S**] are n by n matrices of mass, damping and stiffness respectively. $\{\ddot{\boldsymbol{X}}(t)\}$, $\{\dot{\boldsymbol{X}}(t)\}$, $\{\boldsymbol{X}(t)\}$ and $\{\boldsymbol{Q}(t)\}$ are n by 1 acceleration, velocity, displacement and force vectors respectively in the function of time. Expanding Eq. (2.1),

$$\begin{bmatrix} M_{1:1} & M_{1:2} & \cdots & M_{1:n} \\ M_{2:1} & M_{2:2} & \cdots & M_{2:n} \\ \vdots & \vdots & \ddots & \vdots \\ M_{n:1} & M_{n:2} & \cdots & M_{n:n} \end{bmatrix} \begin{Bmatrix} \ddot{X}_1 \\ \ddot{X}_2 \\ \vdots \\ \ddot{X}_n \end{Bmatrix} + \begin{bmatrix} C_{1:1} & C_{1:2} & \cdots & C_{1:n} \\ C_{2:1} & C_{2:2} & \cdots & C_{2:n} \\ \vdots & \vdots & \ddots & \vdots \\ C_{n:1} & C_{n:2} & \cdots & C_{n:n} \end{bmatrix} \begin{Bmatrix} \dot{X}_1 \\ \dot{X}_2 \\ \vdots \\ \dot{X}_n \end{Bmatrix} + \begin{bmatrix} S_{1:1} & S_{1:2} & \cdots & S_{1:n} \\ S_{2:1} & S_{2:2} & \cdots & S_{2:n} \\ \vdots & \vdots & \ddots & \vdots \\ S_{n:1} & S_{n:2} & \cdots & S_{n:n} \end{bmatrix} \begin{Bmatrix} X_1 \\ X_2 \\ \vdots \\ X_n \end{Bmatrix}$$

$$= \begin{Bmatrix} Q_1 \\ Q_2 \\ \vdots \\ Q_n \end{Bmatrix}. \tag{2.2}$$

The general solution of the linear forced vibration system above can be expressed in frequency domain as follow:

$$\underset{n\text{x}1}{\{\ddot{\boldsymbol{X}}(f)\}}=\underset{nxn}{[\mathbf{H}(f)]}\underset{n\text{x}1}{\{\boldsymbol{Q}(f)\}}, \tag{2.3}$$

where $[\mathbf{H}(f)]$ is n by n square matrix of FRF, which represents the dynamic characteristic of a system. It is a transfer function and named as accelerance FRF whereby acceleration is used as the response. $\{\ddot{\boldsymbol{X}}(f)\}$, and $\{\boldsymbol{Q}(f)\}$ are n by 1 frequency varying vectors of accelerations and forces. These functions are complex function which is transformable from Cartesian coordinate to polar coordinate and vice versa. Expanding Eq. (2.3),

$$\begin{Bmatrix} \ddot{X}_1 \\ \ddot{X}_2 \\ \vdots \\ \ddot{X}_n \end{Bmatrix} = \begin{bmatrix} H_{1:1} & H_{1:2} & \cdots & H_{1:n} \\ H_{2:1} & H_{2:2} & \cdots & H_{2:n} \\ \vdots & \vdots & \ddots & \vdots \\ H_{n:1} & H_{n:2} & \cdots & H_{n:n} \end{bmatrix} \begin{Bmatrix} Q_1 \\ Q_2 \\ \vdots \\ Q_n \end{Bmatrix}. \tag{2.4}$$

Note that the measurement of output acceleration and input force at point I and J respectively provide enough details to form the coefficient $H_{I:J}$. In fact, it is the ratio of the complex spectrum of the response to the complex spectrum of the known excitation. An experimental determination of FRF has the advantage of being applicable to all types of structures and this is useful in structures that have complex boundary conditions. If the reciprocity holds true where $H_{I:J} = H_{J:I}$, then it shows that rows and columns contain the same dynamic information. Therefore, single row or single column of FRF matrix is able to obtain the modal parameters of dynamic characteristics, namely, natural frequency, damping, and mode shape (Richardson & Schwarz, 2003).

2.3.2: Modal Transformation Method

Systems subjected to arbitrary excitations became extremely difficult to analyse and visualise in the original spatial coordinates, especially in the presence of damping. These difficulties can be avoided by using a more suitable set of coordinate such as principal coordinate. It is used to uncouple the equation of motion in spatial coordinate. Furthermore, the principal coordinate of modal matrix can be normalised into normal coordinate with mass matrix to scale the mode shape. In these coordinates, each equation may be solved as if it relates to a system with only Single Degree of Freedom (SDOF) as shown in Figure 2.2. This approach is known as Normal-Mode Method of Dynamic Analysis or MTM.

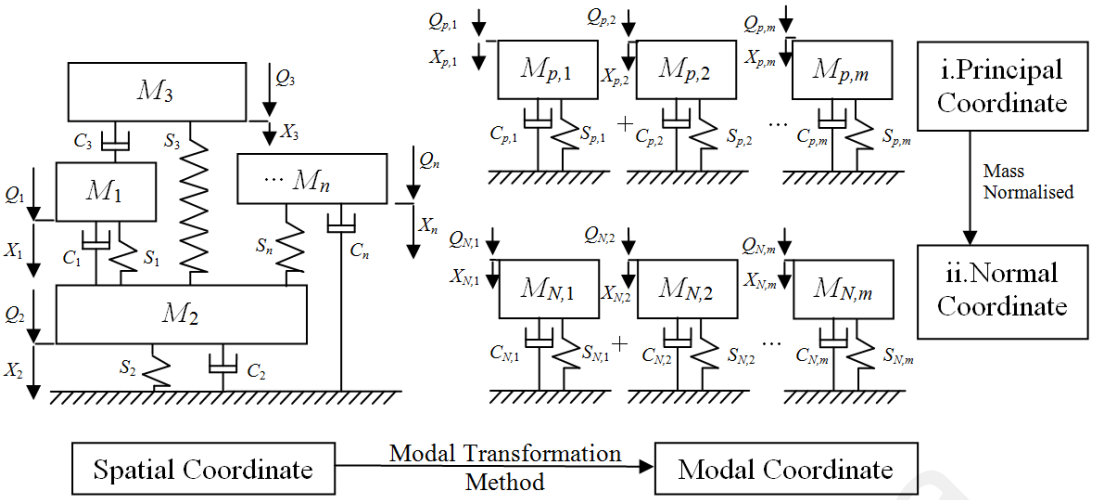

Figure 2.2:
Model in the Spatial Coordinate and Modal Coordinate

2.3.2.1: Orthogonal Behaviour among Vibration Modes

The inherent relationship among the normal modes of vibration is examined. It shows that for a system with 2 distinct modes α and β, the natural frequency must vary: $\omega_{0,\alpha} \neq \omega_{0,\beta}$. There are orthogonal relationships among the normal modes of vibration (William & Marie, 1998) as shown in Eqs. (2.5), (2.6) and (2.7).

$$[\mathbf{\Phi}]^{\mathrm{T}}_{\beta}[\mathbf{M}][\mathbf{\Phi}]_{\alpha} = [\mathbf{\Phi}]^{\mathrm{T}}_{\alpha}[\mathbf{M}][\mathbf{\Phi}]_{\beta} = 0, \tag{2.5}$$

$$[\mathbf{\Phi}]^{\mathrm{T}}_{\beta}[\mathbf{S}][\mathbf{\Phi}]_{\alpha} = [\mathbf{\Phi}]^{\mathrm{T}}_{\alpha}[\mathbf{S}][\mathbf{\Phi}]_{\beta} = 0, \tag{2.6}$$

$$[\mathbf{\Phi}]^{\mathrm{T}}_{\beta}[\mathbf{C}][\mathbf{\Phi}]_{\alpha} = [\mathbf{\Phi}]^{\mathrm{T}}_{\alpha}[\mathbf{C}][\mathbf{\Phi}]_{\beta} = 0, \tag{2.7}$$

where $[\mathbf{\Phi}]$ is the n DOFs by m modes mode shape matrix. $\bullet^{\mathrm{T}}$ is a transpose of a matrix.

2.3.2.2: Modal Mass, Stiffness and Damping Matrices in Principal Coordinate

Using orthogonal relationships of modal matrix, the spatial mass, stiffness and damping matrices can be uncoupled in the form of modal mass, modal stiffness and modal

damping matrices as shown in Eqs. (2.8), (2.9) and (2.10) respectively. The result of post-multiplied spatial mass, stiffness and damping matrix with principal mode shape matrix and pre-multiplied by its transpose is a diagonal matrix.

$$\underset{mxm}{[\mathbf{M_p}]}=\underset{mxn}{[\mathbf{\Phi}]^{\mathrm{T}}}\underset{nxn}{[\mathbf{M}]}\underset{nxm}{[\mathbf{\Phi}]}=\underset{mxm}{[\ddots M_{p,k} \ddots]}, \tag{2.8}$$

$$\underset{mxm}{[\mathbf{S_p}]}=\underset{mxn}{[\mathbf{\Phi}]^{\mathrm{T}}}\underset{nxn}{[\mathbf{S}]}\underset{nxm}{[\mathbf{\Phi}]}=\underset{mxm}{[\ddots S_{p,k} \ddots]}, \tag{2.9}$$

$$\underset{mxm}{[\mathbf{C_p}]}=\underset{mxn}{[\mathbf{\Phi}]^{\mathrm{T}}}\underset{nxn}{[\mathbf{C}]}\underset{nxm}{[\mathbf{\Phi}]}=\underset{mxm}{[\ddots C_{p,k} \ddots]}, \tag{2.10}$$

where $[\mathbf{M_p}]$, $[\mathbf{S_p}]$ and $[\mathbf{C_p}]$ are *m* by *m* matrices of modal mass, modal stiffness and modal damping respectively in principal coordinate. $[\mathbf{\Phi}]$ is the *n* DOFs by *m* modes mode shape matrix and expand it in Eq. (2.11) shows that each column of $[\mathbf{\Phi}]$ is a mode shape vector for a specific mode. The mode shape vector of the k^{th} mode, $\{\boldsymbol{\Phi}_k\}$ does not have unique values and it can be arbitrarily scaled to any set of values (Schwarz & Richardson, 2006). *k* is the variable of mode defined as $k = 1, 2, ..., m$.

Caughey's method shows that when $[\ddots M_{p,k} \ddots]$ is a diagonalised modal mass matrix, it implies that $[\ddots C_{p,k} \ddots]$ is also diagonalised into modal damping matrix (Rahman & Iwankiewicz, 2005). The diagonal element of modal mass, $M_{p,k}$, modal stiffness , $S_{p,k}$ and modal damping, $C_{p,k}$ in principal coordinate are given in Eqs. (2.12), (2.13) and (2.14).

$$\underset{nxm}{[\mathbf{\Phi}]}=[\underset{nx1}{\{\boldsymbol{\Phi}_1\}}\underset{nx1}{\{\boldsymbol{\Phi}_2\}}...\underset{nx1}{\{\boldsymbol{\Phi}_m\}}], \tag{2.11}$$

$$M_{p,k} = 1 \Big/ A_k \omega_{d,k}, \tag{2.12}$$

$$S_{p,k} = (\sigma_k^2 + \omega_{d,k}^2) \Big/ A_k \omega_{d,k}, \tag{2.13}$$

$$C_{p,k} = 2\sigma_k \Big/ A_k \omega_{d,k}, \tag{2.14}$$

where A_k is a scaling constant for the k^{th} mode. This constant can arbitrarily scale the modal matrix such as modal mass, modal damping and modal stiffness. This implies that these modal matrices are related to mode shape where the relationship of one shape component to any other is unique but its value is not unique (Schwarz & Richardson, 2006). $\omega_{d,k}$ is the k^{th} mode damped natural frequency. σ_k is the k^{th} mode decay rate.

2.3.2.3: Modal Mass, Stiffness and Damping Matrices in Normal Coordinate

One method to scale mode shape matrix in principal coordinate is by transforming it into normal coordinate. Theoretically, this is done simply by setting the triple product $[\mathbf{\Phi}]^{\text{T}}[\mathbf{M}][\mathbf{\Phi}]$, to result in the modal mass to be equal to an identity matrix. However there is no mass matrix available when modal parameters are obtained from FRF measurements. Hence, another method called the Unit Modal Mass (UMM) scaling is developed to scale experimental mode shapes even without the information of mass matrix (Richardson & Jamestown, 2000). This is accomplished by choosing the scaling constant such as $A_k = 1/\omega_{d,k}$ so that the modal mass is equal to 1. Hence, modal matrices such as modal stiffness, modal damping, and mode shape matrices in principal coordinate are normalised into normal coordinate as shown in Eqs. (2.15), (2.16), (2.17) and (2.18).

$$M_{N,k}=1 \text{ ,if } A_k = {}^{1}\!/\!_{\omega_{d,k}}\text{ ,} \tag{2.15}$$

$$S_{N,k}=(\sigma_k^2+\omega_{d,k}^2)=\omega_{0,k}^2\text{ ,} \tag{2.16}$$

$$C_{N,k}=2\sigma_k=2\zeta_k\omega_{0,k}\text{ ,} \tag{2.17}$$

$$[\underset{nxm}{\boldsymbol{\Phi}_{\mathbf{N}}}]=[\underset{nx1}{\{\boldsymbol{\Phi}_{N,1}\}}\underset{nx1}{\{\boldsymbol{\Phi}_{N,2}\}}\ldots\underset{nx1}{\{\boldsymbol{\Phi}_{N,m}\}}]\text{ ,} \tag{2.18}$$

where $M_{N,k}$, $S_{N,k}$ and $C_{N,k}$ are the diagonal elements of k^{th} mode modal mass, modal stiffness and modal damping in normal coordinate. $\omega_{0,k}$ is the k^{th} mode natural frequency. ζ_k is the k^{th} mode damping ratio. $[\boldsymbol{\Phi}_{\mathbf{N}}]$ is the mass normalised mode shape matrix or UMM mode shape matrix. $\{\boldsymbol{\Phi}_{N,k}\}$ is the k^{th} mode mass normalised mode shape vector where k = 1, 2, ..., m.

2.3.2.4: Relationship between Residue Mode Shape and UMM Mode Shape

Fitting the measured FRFs to a modal model according to the following standard definition (Allemang & Brown, 1998) as shown in Eq. (2.19) is a common approach for identifying dynamic characteristics for a linear time-invariant system. Residues are the constant numerators of the transfer function matrix in partial fraction expansion form as shown in Eq. (2.19). Section 2.3.2.3 shows that the mode shape needs to be scaled and one of the common methods to scale it is UMM scaling. This is accomplished by using the relationship between residues and mode shapes as shown in Eq. (2.20). The residue matrix is formed by an outer product of the mode shape vector with itself. Eq. (2.20) shows every row and column of the residue matrix contains the mode shape. Thus only one row or column of the FRF matrix needs to be measured. In addition, it must follow the assumption of linearity, Maxwell's reciprocity and distinct pole locations (Richardson & Schwarz, 2003). Besides, reference sensors shall not be chosen in nodal

point where zero mode shape will be obtained.

$$[\underset{nxn}{\mathbf{H}_{I:J}}(s)] = \sum_{k=1}^{m} \frac{[\mathbf{r}_{I:J,k}]}{2i(s-\lambda_k)} - \frac{[\mathbf{r}_{I:J,k}]^*}{2i(s-\lambda_k^*)}\Bigg|_{s=i\omega}, \tag{2.19}$$

$$[\underset{nxn}{\mathbf{r}_{I:J,k}}] = A_k \{\underset{nx1}{\boldsymbol{\Phi}_{\mathbf{N},I,k}}\} \{\underset{1xn}{\boldsymbol{\Phi}_{\mathbf{N},J,k}}\}^{\mathrm{T}}, \tag{2.20}$$

where $i = \sqrt{-1}$. $\lambda_k = -\sigma_k + i\omega_{d,k}$ is the pole location for the k^{th} mode. s is the Laplace domain coefficient. $\bullet^*$ is the complex conjugate function. $[\mathbf{H}_{I:J}]$ is the n by n FRF matrix in which row and column are indicated by response DOF, I and force DOF, J respectively. Note that the experimental FRF data is only defined along the imaginary axis in the S-plane and thus s is equal to $i\omega$. $[\mathbf{r}_{I:J,k}]$ is the k^{th} mode n by n residue matrix in which row and column are indicated by response DOF, I and force DOF, J respectively. $\{\boldsymbol{\Phi}_{\mathbf{N},I,k}\}$ = k^{th} mode mass normalised mode shape vector due to response DOF, I. $\{\boldsymbol{\Phi}_{\mathbf{N},J,k}\}^{\mathrm{T}}$ = transpose of k^{th} mode mass normalised mode shape vector due to force DOF, J.

For the J^{th} column measurement of FRF matrix, $[\mathbf{H}(\omega)]$, Eq. (2.20) can be simplified into Eq. (2.21).

$$\underset{n\text{x}1}{\begin{Bmatrix} r_{I=1:J,k} \\ r_{I=2:J,k} \\ \vdots \\ r_{I=J:J,k} \\ \vdots \\ r_{I=n:J,k} \end{Bmatrix}} = A_k \boldsymbol{\Phi}_{N,J,k} \underset{n\text{x}1}{\begin{Bmatrix} \boldsymbol{\Phi}_{N,I=1,k} \\ \boldsymbol{\Phi}_{N,I=2,k} \\ \vdots \\ \boldsymbol{\Phi}_{N,I=J,k} \\ \vdots \\ \boldsymbol{\Phi}_{N,I=n,k} \end{Bmatrix}}. \tag{2.21}$$

Hence by performing a J^{th} column driving point measurement of FRF, the residue at driving point for k^{th} mode, $r_{J:J,k}$ is obtained, as shown in Eq. (2.22).

$$r_{J:J,k} = A_k \ (\Phi_{N,J,k})^2, \tag{2.22}$$

where response DOF I is equal to force DOF J at driving point.

By using Eqs. (2.15), (2.21) and (2.22), the residue mode shape can be transformed into UMM mass normalised mode shape as shown in Eq. (2.23).

$$\underset{n\text{x}1}{\begin{Bmatrix} \Phi_{N,I=1,k} \\ \Phi_{N,I=2,k} \\ \vdots \\ \Phi_{N,I=J,k} \\ \vdots \\ \Phi_{N,I=n,k} \end{Bmatrix}} = \frac{1}{A_k \Phi_{N,J,k}} \underset{n\text{x}1}{\begin{Bmatrix} r_{I=1:J,k} \\ r_{I=2:J,k} \\ \vdots \\ r_{I=J:J,k} \\ \vdots \\ r_{I=n:J,k} \end{Bmatrix}} = \sqrt{\frac{\omega_{d,k}}{r_{J:J,k}}} \underset{n\text{x}1}{\begin{Bmatrix} r_{I=1:J,k} \\ r_{I=2:J,k} \\ \vdots \\ r_{I=J:J,k} \\ \vdots \\ r_{I=n:J,k} \end{Bmatrix}}. \tag{2.23}$$

Since reciprocity theorem is assumed in this linear system, both results of UMM mode shape obtained from I^{th} row and J^{th} column measurements of FRF matrix are the same as shown in Eq. (2.24).

$$\begin{aligned} \underset{nxm}{[\boldsymbol{\Phi}_{\mathbf{N}}]} &= \left[\begin{Bmatrix} \Phi_{N,I=1,k=1} \\ \Phi_{N,I=2,k=1} \\ \vdots \\ \Phi_{N,I=J,k=1} \\ \vdots \\ \Phi_{N,I=n,k=1} \end{Bmatrix} \begin{Bmatrix} \Phi_{N,I=1,k=2} \\ \Phi_{N,I=2,k=2} \\ \vdots \\ \Phi_{N,I=J,k=2} \\ \vdots \\ \Phi_{N,I=n,k=2} \end{Bmatrix} \cdots \begin{Bmatrix} \Phi_{N,I=1,k=m} \\ \Phi_{N,I=2,k=m} \\ \vdots \\ \Phi_{N,I=J,k=m} \\ \vdots \\ \Phi_{N,I=n,k=m} \end{Bmatrix} \right] \\ &= \left[\begin{Bmatrix} \Phi_{N,J=1,k=1} \\ \Phi_{N,J=2,k=1} \\ \vdots \\ \Phi_{N,J=I,k=1} \\ \vdots \\ \Phi_{N,J=n,k=1} \end{Bmatrix} \begin{Bmatrix} \Phi_{N,J=1,k=2} \\ \Phi_{N,J=2,k=2} \\ \vdots \\ \Phi_{N,J=I,k=2} \\ \vdots \\ \Phi_{N,J=n,k=2} \end{Bmatrix} \cdots \begin{Bmatrix} \Phi_{N,J=1,k=m} \\ \Phi_{N,J=2,k=m} \\ \vdots \\ \Phi_{N,J=I,k=m} \\ \vdots \\ \Phi_{N,J=n,k=m} \end{Bmatrix} \right]. \end{aligned} \tag{2.24}$$

2.3.2.5: Synthesis of FRF by Using MTM

Coordinate transformation of response and force from spatial coordinate into normal coordinate are shown in Eqs. (2.25) and (2.26). The spatial equation of motion in Eq. (2.1) can be transformed into normal coordinate as shown in Eqs. (2.27) and (2.28). This can be done by post-multiplying the equation with the transpose of the mass normalised mode shape matrix and replacing the spatial response matrix with the coordinate transformation.

$$\underset{nx1}{\{\ddot{\boldsymbol{X}}(t)\}}=\underset{nxm}{[\boldsymbol{\Phi}_{\mathbf{N}}]}\underset{mx1}{\{\ddot{\boldsymbol{X}}_{\boldsymbol{N}}(t)\}};\underset{nx1}{\{\dot{\boldsymbol{X}}(t)\}}=\underset{nxm}{[\boldsymbol{\Phi}_{\mathbf{N}}]}\underset{mx1}{\{\dot{\boldsymbol{X}}_{\boldsymbol{N}}(t)\}};\underset{nx1}{\{\boldsymbol{X}(t)\}}=\underset{nxm}{[\boldsymbol{\Phi}_{\mathbf{N}}]}\underset{mx1}{\{\boldsymbol{X}_{\boldsymbol{N}}(t)\}}, \tag{2.25}$$

$$\underset{mx1}{\{\boldsymbol{Q}_{\boldsymbol{N}}(t)\}}=\underset{mxn}{[\boldsymbol{\Phi}_{\mathbf{N}}]^{\mathrm{T}}}\underset{nx1}{\{\boldsymbol{Q}(t)\}}, \tag{2.26}$$

$$\underset{mxn}{[\boldsymbol{\Phi}_{\mathbf{N}}]^{\mathrm{T}}}\underset{nxn}{[\mathbf{M}]}\underset{nxm}{[\boldsymbol{\Phi}_{\mathbf{N}}]}\underset{mx1}{\{\ddot{\boldsymbol{X}}_{\boldsymbol{N}}(t)\}}+\underset{mxn}{[\boldsymbol{\Phi}_{\mathbf{N}}]^{\mathrm{T}}}\underset{nxn}{[\mathbf{C}]}\underset{nxm}{[\boldsymbol{\Phi}_{\mathbf{N}}]}\underset{mx1}{\{\dot{\boldsymbol{X}}_{\boldsymbol{N}}(t)\}}+\underset{mxn}{[\boldsymbol{\Phi}_{\mathbf{N}}]^{\mathrm{T}}}\underset{nxn}{[\mathbf{S}]}\underset{nxm}{[\boldsymbol{\Phi}_{\mathbf{N}}]}\underset{mx1}{\{\boldsymbol{X}_{\boldsymbol{N}}(t)\}}=\underset{mxn}{[\boldsymbol{\Phi}_{\mathbf{N}}]^{\mathrm{T}}}\underset{nx1}{\{\boldsymbol{Q}(t)\}}, \tag{2.27}$$

$$\underset{mxm}{[\mathbf{M}_{\mathbf{N}}]}\underset{mx1}{\{\ddot{\boldsymbol{X}}_{\boldsymbol{N}}(t)\}}+\underset{mxm}{[\mathbf{C}_{\mathbf{N}}]}\underset{mx1}{\{\dot{\boldsymbol{X}}_{\boldsymbol{N}}(t)\}}+\underset{mxm}{[\mathbf{S}_{\mathbf{N}}]}\underset{mx1}{\{\boldsymbol{X}_{\boldsymbol{N}}(t)\}}=\underset{mx1}{\{\boldsymbol{Q}_{\boldsymbol{N}}(t)\}}, \tag{2.28}$$

where $\{\boldsymbol{Q}_{\boldsymbol{N}}(t)\}$, $\{\ddot{\boldsymbol{X}}_{\boldsymbol{N}}(t)\}$, $\{\dot{\boldsymbol{X}}_{\boldsymbol{N}}(t)\}$ and $\{\boldsymbol{X}_{\boldsymbol{N}}(t)\}$ are corresponding mass normalised modal force and modal response matrix. By expanding Eq. (2.28) into Eq. (2.29), it shows that the equation is diagonalised and uncoupled into *m* modal sets of SDOF system.

$$\begin{bmatrix} M_{N,1} & 0 & \cdots & 0 \\ 0 & M_{N,2} & \cdots & 0 \\ \vdots & \vdots & \ddots & \vdots \\ 0 & 0 & \cdots & M_{N,m} \end{bmatrix}\begin{Bmatrix} \ddot{X}_{N,1}(t) \\ \ddot{X}_{N,2}(t) \\ \vdots \\ \ddot{X}_{N,m}(t) \end{Bmatrix}+\begin{bmatrix} C_{N,1} & 0 & \cdots & 0 \\ 0 & C_{N,2} & \cdots & 0 \\ \vdots & \vdots & \ddots & \vdots \\ 0 & 0 & \cdots & C_{N,m} \end{bmatrix}\begin{Bmatrix} \dot{X}_{N,1}(t) \\ \dot{X}_{N,2}(t) \\ \vdots \\ \dot{X}_{N,m}(t) \end{Bmatrix}+\begin{bmatrix} S_{N,1} & 0 & \cdots & 0 \\ 0 & S_{N,2} & \cdots & 0 \\ \vdots & \vdots & \ddots & \vdots \\ 0 & 0 & \cdots & S_{N,m} \end{bmatrix}\begin{Bmatrix} X_{N,1}(t) \\ X_{N,2}(t) \\ \vdots \\ X_{N,m}(t) \end{Bmatrix}$$

$$=\begin{Bmatrix} Q_{N,1}(t) \\ Q_{N,2}(t) \\ \vdots \\ Q_{N,m}(t) \end{Bmatrix}. \tag{2.29}$$

Transforming Eq. (2.29) into frequency domain by using Fourier Transform and integration method in Eq. (2.30) follows a steady state condition as shown in Eq. (2.31).

$$X_{N,k}(\omega) = \int_{-\infty}^{\infty} X_{N,k}(t) e^{i\omega t} dt; \dot{X}_{N,k}(\omega) = i\omega X_{N,k}(\omega); \ddot{X}_{N,k}(\omega) = -\omega^2 X_{N,k}(\omega), \tag{2.30}$$

$$\left[-\omega^2 \begin{bmatrix} 1 & 0 & \cdots & 0 \\ 0 & 1 & \cdots & 0 \\ \vdots & \vdots & \ddots & \vdots \\ 0 & 0 & \cdots & 1 \end{bmatrix} + i\omega \begin{bmatrix} 2\sigma_1 & 0 & \cdots & 0 \\ 0 & 2\sigma_2 & \cdots & 0 \\ \vdots & \vdots & \ddots & \vdots \\ 0 & 0 & \cdots & 2\sigma_m \end{bmatrix} + \begin{bmatrix} \omega_{0,1}^2 & 0 & \cdots & 0 \\ 0 & \omega_{0,2}^2 & \cdots & 0 \\ \vdots & \vdots & \ddots & \vdots \\ 0 & 0 & \cdots & \omega_{0,m}^2 \end{bmatrix} \right] \begin{Bmatrix} X_{N,1}(\omega) \\ X_{N,2}(\omega) \\ \vdots \\ X_{N,m}(\omega) \end{Bmatrix}$$

$$= \begin{Bmatrix} Q_{N,1}(\omega) \\ Q_{N,2}(\omega) \\ \vdots \\ Q_{N,m}(\omega) \end{Bmatrix}. \tag{2.31}$$

Simplify Eq. (2.31) and rearrange the matrix to show the transfer function between mass normalised modal displacement and mass normalised modal force in frequency domain as described in Eqs. (2.32) and (2.33).

$$[\mathbf{H_N}(\omega)] = \frac{\{\boldsymbol{X_N}(\omega)\}}{\{\boldsymbol{Q_N}(\omega)\}} = \frac{1}{[-\omega^2[\mathbf{M_N}] + i\omega[\mathbf{C_N}] + [\mathbf{S_N}]]} = [\underset{m \times m}{\ddots} H_{N,k} \ddots], \tag{2.32}$$

$$H_{N,k} = \frac{1}{(\omega_{0,k}^2 - \omega^2) + i(2\zeta_k \omega_{0,k} \omega)}, \tag{2.33}$$

where $H_{N,k}(\omega)$ is the k^{th} mode transfer function between mass normalised modal displacement and mass normalised modal force in frequency domain. $[\ddots]$ is a diagonal matrix. $i = \sqrt{-1}$. $\omega_{0,k}$ is the k^{th} mode natural frequency. ζ_k is the k^{th} mode damping ratio. $H_{N,k}$ is the k^{th} mode transfer function. k = 1, 2, ..., m mode.

Substitute mass normalised modal displacement obtained from Eq. (2.32) into Fourier Transform of spatial response from Eq. (2.25) to obtain Eq. (2.34).

$$\underset{nx1}{\{\boldsymbol{X}(\omega)\}}=\underset{nxm}{[\boldsymbol{\Phi}_{\mathbf{N}}]}\underset{mxm}{[\mathbf{H}_{\mathbf{N}}(\omega)]}\underset{mx1}{\{\boldsymbol{Q}_{N}(\omega)\}}. \tag{2.34}$$

Substitute Eq. (2.34) into Fourier transform of Eq. (2.26) to acquire Eqs. (2.35) and (2.36). Given that the total number of response, mode and force measurement are *n*, *m* and *fz* respectively.

$$\underset{nx1}{\{\boldsymbol{X}(\omega)\}}=\underset{nxm}{[\boldsymbol{\Phi}_{\mathbf{N}}]}\underset{mxm}{[\mathbf{H}_{\mathbf{N}}(\omega)]}\underset{mxfz}{[\boldsymbol{\Phi}_{\mathbf{N}}]^{\mathrm{T}}}\underset{fzx1}{\{\boldsymbol{Q}(\omega)\}}, \tag{2.35}$$

$$\underset{nxfz}{[\mathbf{G}(\omega)]}=\underset{nxm}{[\boldsymbol{\Phi}_{\mathbf{N}}]}\underset{mxm}{[\mathbf{H}_{\mathbf{N}}(\omega)]}\underset{mxfz}{[\boldsymbol{\Phi}_{\mathbf{N}}]^{\mathrm{T}}}, \tag{2.36}$$

where $[\mathbf{G}(\omega)]$ is the synthesised FRF. Note that MTM is applied to synthesise the entire FRF matrix.

2.3.2.6: Relationship between Measured Response Motion and Residue Unit

Unit of residue is equal to unit of motion divided by unit of force in Newton multiply with unit of frequency in rads^{-1} as shown in Eq. (2.19). This shows that the residue unit will depend on the measured response types such as acceleration, velocity or displacement. The unit of residue is equal to $\mathrm{ms}^{-2}/\mathrm{Ns}$, $\mathrm{ms}^{-1}/\mathrm{Ns}$, and m/Ns for measured acceleration, velocity and displacement respectively. The residue unit can be converted to other motion type (Richardson & Jamestown, 2000) by using the relation as shown in Table 2.2.

Note that the residue for a particular k^{th} mode is proportional to the product of the UMM mode shape at the response DOF, $\Phi_{N,Ik}$ and force DOF, $\Phi_{N,Jk}$ as shown in Eq. (2.20). Therefore, selection motion type of response of residue will relate the UMM mode shape to the selected motion. Hence, calculated response type will be the same as the

selected motion as well. For example, if residue is converted to unit related to acceleration motion by using the relation as shown in Table 2.2, and then the calculated response will give acceleration motion. This is applied to velocity and displacement responses as shown in Eqs. (2.37), (2.38) and (2.39).

$$\underset{nx1}{\left\{\ddot{\boldsymbol{X}}(\omega)\right\}}=\underset{nxm}{[\boldsymbol{\Phi}_{\mathbf{N},acc}]}\underset{mxm}{[\mathbf{H}_{\mathbf{N}}(\omega)]}\underset{mxfz}{[\boldsymbol{\Phi}_{\mathbf{N},acc}]^{\mathrm{T}}}\underset{fzx1}{\left\{\boldsymbol{Q}(\omega)\right\}}, \tag{2.37}$$

$$\underset{nx1}{\left\{\dot{\boldsymbol{X}}(\omega)\right\}}=\underset{nxm}{[\boldsymbol{\Phi}_{\mathbf{N},vel}]}\underset{mxm}{[\mathbf{H}_{\mathbf{N}}(\omega)]}\underset{mxfz}{[\boldsymbol{\Phi}_{\mathbf{N},vel}]^{\mathrm{T}}}\underset{fzx1}{\left\{\boldsymbol{Q}(\omega)\right\}}, \tag{2.38}$$

$$\underset{nx1}{\left\{\boldsymbol{X}(\omega)\right\}}=\underset{nxm}{[\boldsymbol{\Phi}_{\mathbf{N},disp}]}\underset{mxm}{[\mathbf{H}_{\mathbf{N}}(\omega)]}\underset{mxfz}{[\boldsymbol{\Phi}_{\mathbf{N},disp}]^{\mathrm{T}}}\underset{fzx1}{\left\{\boldsymbol{Q}(\omega)\right\}}, \tag{2.39}$$

where $[\boldsymbol{\Phi}_{\mathbf{N},disp}]$,$[\boldsymbol{\Phi}_{\mathbf{N},vel}]$, $[\boldsymbol{\Phi}_{\mathbf{N},acc}]$ are the admittance, mobility and accelerance UMM mode shapes matrices, which were determined from admittance residue, mobility residue, and accelerance residue mode shapes that has unit motion related to displacement, velocity and acceleration.

Table 2.2:
Conversion of Residue's Motion Type

Measured Residue's Motion Type \ **Convert To Other Motion**	**Displacement**	**Velocity**	**Acceleration**
Displacement		Divide residue by $1/\lambda_k$	Divide residue by $1/\lambda_k^2$
Velocity	Multiply residue by $1/\lambda_k$		Divide residue by $1/\lambda_k$
Acceleration	Multiply residue by $1/\lambda_k^2$	Multiply residue by $1/\lambda_k$	

where $\lambda_k = -\sigma_k + i\omega_{d,k}$ = pole location for the k^{th} mode. $i = \sqrt{-1}$. $\omega_{d,k}$ is the k^{th} mode damped natural frequency. σ_k is the k^{th} mode decay rate. k = 1, 2, ..., m mode.

2.3.2.7: Force Determination by Using Different Types of Responses

In this study, 3 types of synthesised FRFs named accelerance, mobility and admittance FRFs are obtained from acceleration, velocity and displacement responses respectively. These synthesised FRFs are computed by using Eqs. (2.40), (2.41) and (2.42).

$$\underset{nxfz}{[\mathbf{G}_{acc}(\omega)]} = \underset{nxm}{[\mathbf{\Phi}_{\mathbf{N},acc}]}\underset{mxm}{[\mathbf{H}_{\mathbf{N}}(\omega)]}\underset{mxfz}{[\mathbf{\Phi}_{\mathbf{N},acc}]^{\mathrm{T}}}, \tag{2.40}$$

$$\underset{nxfz}{[\mathbf{G}_{vel}(\omega)]} = \underset{nxm}{[\mathbf{\Phi}_{\mathbf{N},vel}]}\underset{mxm}{[\mathbf{H}_{\mathbf{N}}(\omega)]}\underset{mxfz}{[\mathbf{\Phi}_{\mathbf{N},vel}]^{\mathrm{T}}}, \tag{2.41}$$

$$\underset{nxfz}{[\mathbf{G}_{disp}(\omega)]} = \underset{nxm}{[\mathbf{\Phi}_{\mathbf{N},disp}]}\underset{mxm}{[\mathbf{H}_{\mathbf{N}}(\omega)]}\underset{mxfz}{[\mathbf{\Phi}_{\mathbf{N},disp}]^{\mathrm{T}}}, \tag{2.42}$$

where ω is angular frequency. $[\mathbf{G}_{acc}(\omega)]$, $[\mathbf{G}_{vel}(\omega)]$ and $[\mathbf{G}_{disp}(\omega)]$ are the synthesis of accelerance, mobility and admittance matrices, which are generated by using MTM. $[\mathbf{\Phi}_{\mathbf{N},acc}]$, $[\mathbf{\Phi}_{\mathbf{N},vel}]$, $[\mathbf{\Phi}_{\mathbf{N},disp}]$ are accelerance, mobility and admittance UMM mode shape matrices, which are determined from residue mode shape. They have units related to acceleration, velocity and displacement respectively. $\bullet^{\mathrm{T}}$ is a transpose function of a matrix. $[\mathbf{H}_{\mathbf{N}}(\omega)]$ is the transfer function matrix between mass normalised modal displacement, $\{\boldsymbol{X}_{\boldsymbol{N}}(\omega)\}$ and mass normalised modal force, $\{\boldsymbol{Q}_{\boldsymbol{N}}(\omega)\}$ in frequency domain as shown in Eq. (2.32).

By using MTM, force identification can be done by using acceleration, velocity and displacement responses as shown in Eqs. (2.43), (2.44) and (2.45) respectively. Given that the total number of response, mode and force measurement are n, m and fz

respectively. It was shown that by multiplying pseudo-inverse of non-square synthesised FRF matrices with measured response, LS solution of force determination can be obtained if it satisfies $n \geq m \geq fz$ (Richardson & Schwarz, 2003).

$$\underset{fz\text{x}1}{\{\boldsymbol{Q}_{acc}(\omega)\}} = pinv\{\underset{nxfz}{[\mathbf{G}_{acc}]}\}\underset{n\text{x}1}{\{\ddot{\boldsymbol{X}}(\omega)\}}, \tag{2.43}$$

$$\underset{fz\text{x}1}{\{\boldsymbol{Q}_{vel}(\omega)\}} = pinv\{\underset{nxfz}{[\mathbf{G}_{vel}]}\}\underset{n\text{x}1}{\{\dot{\boldsymbol{X}}(\omega)\}}, \tag{2.44}$$

$$\underset{fz\text{x}1}{\{\boldsymbol{Q}_{disp}(\omega)\}} = pinv\{\underset{nxfz}{[\mathbf{G}_{disp}]}\}\underset{n\text{x}1}{\{\boldsymbol{X}(\omega)\}}, \tag{2.45}$$

where $\{\boldsymbol{Q}_{acc}(\omega)\}, \{\boldsymbol{Q}_{vel}(\omega)\}$ and $\{\boldsymbol{Q}_{disp}(\omega)\}$ are corresponding force vectors, which are determined by using acceleration vector, $\{\ddot{\boldsymbol{X}}(\omega)\}$, velocity vector, $\{\dot{\boldsymbol{X}}(\omega)\}$ and displacement response vector, $\{\boldsymbol{X}(\omega)\}$. The symbol of *pinv* means pseudo-inverse method. It can be defined by Eq. (2.46) as follows:

$$pinv\{[\mathbf{G}]\} = inv\{[\mathbf{G}]^{\text{h}}[\mathbf{G}]\}[\mathbf{G}]^{\text{h}}, \tag{2.46}$$

where *inv* is the direct inverse method. $\bullet^{\text{h}}$ is the complex conjugate transpose function of a matrix (Hermitian matrix). $[\mathbf{G}]$ is the synthesised FRF matrix.

By using pseudo-inverse method, non-collocated (i.e. force and response locations are different) responses are sufficient to estimate the force. This means that force determination can be done by using remote responses that are far away from the impact location. This is illustrated in Eq. (2.47). Note that force at point 1 can be identified from responses other than point 1.

$$\begin{Bmatrix} Q_{acc,1} \\ Q_{acc,2} \\ \vdots \\ Q_{acc,n} \end{Bmatrix} = pinv \begin{bmatrix} G_{acc,2:1} & G_{acc,2:2} & \cdots & G_{acc,2:fz} \\ G_{acc,3:1} & G_{acc,3:2} & \cdots & G_{acc,3:fz} \\ \vdots & \vdots & \ddots & \vdots \\ G_{acc,n:1} & G_{acc,n:2} & \cdots & G_{acc,n:fz} \end{bmatrix} \begin{Bmatrix} \ddot{X}_2 \\ \ddot{X}_3 \\ \vdots \\ \ddot{X}_n \end{Bmatrix}. \quad (2.47)$$

2.3.2.8: Limitation of MTM

Typically, the number of responses, n exceeds number of modes, m (i.e. $n>m$) will lead to an under-posed case (i.e. more unknowns than data). This is because n DOF system will generate n modes and this will produce a n by n square synthesised FRF matrix whose row is linearly dependent, in which this will lead to a singular problem. In fact, it is recommended to use priori data such as impact location to have a well-posed problem. If the number and positions of the force are known in advance, LS solution of force determination can be obtained if it satisfies $n \geq m \geq fz$.

2.4: Digital Signal Processing

DSP converts signals from an analogue form to a digital form by sampling it using an Analogue-To-Digital Converter (ADC), turning the analogue signals into a stream of number. The aim of DSP is to measure, filter, modify and improve the information signals. DSP characterises these signals by a sequence of numbers or symbols. Subsequently processing of these signals can be done in different type of domain such as time, frequency, state space and modal domain. The choice of domain depends on its ability to represent the essential characteristics of the signal.

2.4.1: Sampling Rate and Block Size

Sampling rate and block size are 2 main parameters in acquiring a signal. The time and frequency resolution of a signal are based on these 2 parameters as shown in Eqs. (2.48) and (2.49). By considering the required frequency resolution and time resolution for a

specific signal, an appropriate sampling rate and block size can be selected. In general, if block size is too high, it will sacrifice the measurement time. If the sampling rate is too high, the frequency resolution will be affected.

$$\Delta f = \frac{SR}{BS}, \tag{2.48}$$

$$\Delta t = \frac{1}{SR}, \tag{2.49}$$

where Δf and Δt are frequency resolution and time resolution respectively. SR is the sampling rate with unit of samples per second (S/s). BS is the block size or the total number of sample per block with unit of samples (S).

Besides the concern on the frequency and time resolutions, an appropriate sampling rate was chosen based on the knowledge of the frequency content of a signal. The Nyquist theorem sets the rule for acquiring, digitizing and sampling a signal. It states that the sampling rate must exceed the Nyquist rate (i.e. equal to twice the maximum frequency present in the signal). Or else, it will result in aliasing of higher frequency component, meaning that these high frequency components will shift to a lower frequency and hence produce an inaccurate representation of data. Thus, for a signal that has the highest frequency component up to 1000Hz, the data needs to be sampled at least 2000S/s. In general, it is preferable to acquire signal at a high sampling rate if the signal of interest is unknown. However, this will include the unwanted noise at high frequency region as well. Therefore it is required to undergo some spectral analysis to identify the frequencies that contribute the most to the signal power, subsequently the frequency range of unwanted noise signal can be removed prior to data analysis.

2.4.2: Windowing Function

Fast Fourier Transform (FFT) is a well-known algorithm to transform time traces into frequency domain. It assumes that a signal is periodic in each data block. If a signal is non-periodic (i.e. the number of periods in an acquisition is not an integer and the endpoints are discontinuous), FFT of such a signal will cause a leakage problem, that is, a phenomenon where signal energy smears out over a wide frequency range. In this case, choosing a suitable windowing function can reduce the effect of leakage. By multiplying a non-periodic signal with a suitable window function, the signal can become periodic. The window function is expressed in Eq. (2.50).

$$y'(t) = w(t)y(t), \tag{2.50}$$

where $y'(t)$ is the modified time history. $w(t)$ is the selected window function. $y(t)$ is the original signal.

There are a lot of window functions such as rectangular window, exponential window, hanning window and flattop window. They are chosen based on the types and characteristics of the signals. For example: Rectangular window is suitable for periodic signal or signal that starts and ends at zero; Exponential window is suitable for decaying signal which has a non-zero end; Hanning and flattop windows are suitable for non-periodic sinusoidal signal. Based on this criterion, rectangular window is used in the FRF measurement and ODS analysis for both impulse force and impulse response signals in this study. For rectangular window, the window function, $w(t)$ is equal to 1.

2.4.3: The Discrete Fourier Transform and the Fast Fourier Transform

Measured traces in time domain can be transformed into frequency domain or vice versa by using forward and backward Discrete Fourier Transform (DFT) as shown in Eqs.

(2.51) and (2.52) as follows (Soon et al., 2001).

$$F[r] = \frac{1}{BS} \sum_{u=0}^{BS\text{-}1} T[u] e^{-2\pi iru/BS} \Big|_{r=0,1,2,\ldots,BS\text{-}1}, \tag{2.51}$$

$$T[u] = \sum_{r=0}^{BS\text{-}1} F[r] e^{2\pi iru/BS} \Big|_{u=0,1,2,\ldots,BS\text{-}1}, \tag{2.52}$$

where $F[r]$ and $T[u]$ are sampled sequences of frequency trace and time trace that have finite length (i.e. non-zero for a finite number of values) at r^{th} sample and u^{th} sample respectively. Block size, *BS,* is the total number of collected sample. The mathematic operations are evaluated at $r = 0, 1, ..., BS\text{-}1$ and $u = 0, 1, ..., BS\text{-}1$.

In general, FFT is an efficient algorithm for the computation of the DFT (Cooley & Tukey, 1965). It applies only if *BS* is a power of two. Their computation speed is obvious when their total number of multiply and add operations are compared, known as $(BS)^2$ for DFT and $(BS)*\log_2(BS)$ for FFT. For example, FFT is 341 times faster than DFT for *BS* is equal to 4096S. *i* is equal to $\sqrt{-1}$. In terms of accuracy, both of them produce the same result. Thus, FFT and Inverse Fast Fourier Transform (IFFT) are preferably to be used in the transformation between frequency domain and time domain.

2.4.4: Frequency Response Function

FRF is a transfer function that describes the complex relationship between input and output in frequency domain. It contains the dynamic characteristic of a system and it is a complex function which is transformable from Cartesian coordinate to polar coordinate and vice versa. FRF only remains a geometric, material and boundary properties of a linear time-invariant system and it is independent from the excitation

types. The raw FRF is estimated by using Eq. (2.53), which is known as FRF measurement as follows (Halvorsen & Brown, 1977):

$$H_{I:J}(\omega)=\frac{CS_{I:J}(\omega)}{AS_{J:J}(\omega)}=\frac{\ddot{X}(\omega)\tilde{Q}^{*}(\omega)}{\tilde{Q}(\omega)\tilde{Q}^{*}(\omega)}, \tag{2.53}$$

where coefficients *I* and *J* are output response DOF and input force DOF respectively. FRF coefficient, $H_{I:J}$ is the ratio of the cross spectrum, $CS_{I:J}$ between input force, $\tilde{Q}$ and output acceleration response, $\ddot{X}$ to the auto spectrum, $AS_{J:J}$ of the input. Variable ω is the angular frequency which has unit rads^{-1}. $\bullet^{*}$ is a complex conjugate function. Note that all the excitation forces must be measured simultaneously with the resulting responses.

2.4.5: Coherence

COH is a measure of the linearity between measured input data and output data. It shows the ratio of the maximum energy in a combined output signal due to its various components, and the total amount of energy in the output signal. It is widely used in assessing the accuracy of FRF measurement. COH near to 1 indicates that the FRF measurement is reliable. Poor COH is indicative of measurement errors, poor signal to noise ratio, nonlinear or time-invariant behaviour of the structure, or a combination of them (Fu & He, 2001). It is defined in Eq. (2.54).

$$\gamma^{2}_{I:J}(\omega)=\frac{\left|CS_{I:J}(\omega)\right|^{2}}{AS_{J:J}(\omega)AS_{I:I}(\omega)}=\frac{\left|\ddot{X}(\omega)\tilde{Q}^{*}(\omega)\right|^{2}}{\left(\tilde{Q}(\omega)\tilde{Q}^{*}(\omega)\right)\left(\ddot{X}(\omega)\ddot{X}^{*}(\omega)\right)}, \tag{2.54}$$

where coefficients *I* and *J* are output response DOF and input force DOF respectively. COH, $\gamma^{2}_{I:J}$ is the ratio of the square of the absolute cross spectrum, $CS_{I:J}$ between input force, $\tilde{Q}$ and output acceleration response, $\ddot{X}$ to the product of the auto spectrum,

$AS_{J:J}$ and $AS_{I:I}$ of the input and output signal respectively. Variable ω is the angular frequency. $\bullet^*$ is a complex conjugate function. Note that $\left|CS_{I:J}(\omega)\right|^2 \leq AS_{J:J}(\omega)AS_{I:I}(\omega)$ and $0 \leq \gamma^2_{I:J} \leq 1$.

2.4.6: Operating Deflection Shape

ODS can be defined as any forced motion of 2 or more DOFs (points & directions) on a machine or structure (Vold et al., 2000). An ODS analysis can animate the vibration pattern of a structure as a function of time or for a specific frequency. For a non-stationary signal such as a transient signal, time-based ODS is extremely useful in giving an overall ODS compared to frequency-based ODS. Note that stationary is known as steady state as well.

In general, 2 methods of measurement are used to acquire the ODS (Vold et al., 2000): simultaneous method; and measurement set method. In this study, the former method is used where all channels of data are acquired simultaneously by using a multi-channel acquisition system. This method is suitable for a small scale test object and it is time efficient. However, for a large scale test object, it is not able to acquire a few channels of data at a time. In this case, the measurement set method is used. The most common measurement set method is the ODS FRF. It is formed by the magnitude of auto spectrum of a roving response and the phase of the cross spectrum between the roving response and the fixed reference response. The measurement set method works well for stationary signal and it works well for non-stationary signal only if a structure or machine is undergoing a repeatable operation. Note that the magnitude and phase of the response signal remain the same and repeatable for every Data Acquisition (DAQ) in a repeatable operation. In addition, an external trigger is often used for such measurement.

2.4.7: Integration of Acceleration Response in Frequency Domain

Measured acceleration response in frequency domain can be integrated into velocity and displacement responses by using Eqs. (2.55) and (2.56) as follows (Rainer, 1986).

$$\dot{X}_r(\omega_r) = \ddot{X}_r(\omega_r) / i\omega_r \Big|_{r=0,1,2,\ldots,BS\text{-}1}, \tag{2.55}$$

$$X_r(\omega_r) = \text{-}\ddot{X}_r(\omega_r) / \omega_r^2 \Big|_{r=0,1,2,\ldots,BS\text{-}1}, \tag{2.56}$$

where $\{\ddot{X}_r(\omega_r)\}$, $\{\dot{X}_r(\omega_r)\}$ and $\{X_r(\omega_r)\}$ are corresponding acceleration, velocity and displacement responses in frequency domain for the r^{th} sample. ω_r is the r^{th} sample angular frequency (rads^{-1}). Block size, *BS* is the total number of collected sample. *i* is equal to $\sqrt{\text{-}1}$. The integration is a smothering operation, so it helps to remove some noise that may be included in the measurement of velocity or acceleration (Liu & Han, 2003).

Note that the acceleration signal is divided by ω and ω^2 respectively for velocity and displacement signals. Hence, the gains of signal at the higher frequencies are smaller and they are disproportionately reduced in size. In this way, the noise effect in high frequency region can be reduced largely for an integrated signal. This implies that integrated signal possesses a low pass characteristic in nature (Karrenberg, 2002).

2.4.8: Correlation

In order to access the accuracy of curve fitting, correlation between the measured FRF and synthesised FRF can be calculated. The correlation is the normalised complex product of the synthesised and measured values (LMS International, 2000). It can be calculated as shown in Eq. (2.57).

$$Corr = \frac{\left|\sum_{r=0}^{BS\text{-}1}(G_r H_r^*)\right|^2}{\left(\sum_{r=0}^{BS\text{-}1}(G_r G_r^*)\right)\left(\sum_{r=0}^{BS\text{-}1}(H_r H_r^*)\right)}, \tag{2.57}$$

where *Corr* is the correlation. G_r and H_r are the r^{th} sample of synthesised FRF and measured FRF respectively. $\bullet^*$ is the complex conjugate function. Block size, *BS,* is the total number of collected sample. Note that the correlation value greater than 0.9 indicates a high quality of synthesised data.

2.4.9: Condition Number

Condition number of a matrix measures the sensitivity of the solution of a system of linear equations to errors in the data and gives an indication of the ill-conditioning of the matrix (Feng & Chen, 2010). Note that condition number nears 1 is said to be well-conditioned; condition number far away from 1 is said to be ill-conditioned.

The condition number of square and non-square matrixes can be calculated as follows:

$$CN(\omega) = norm2\{[\underset{nxfz}{\mathbf{H}}(\omega)]\} * norm2\{pinv\{[\underset{nxfz}{\mathbf{H}}(\omega)]\}\}, \tag{2.58}$$

where *CN* is the condition number of a FRF matrix. *norm2* is the largest singular value of a matrix.

2.4.10: Correlation Coefficient

Correlation coefficient represents the normalised measure of the strength and the direction of a linear relationship between 2 variables. It is widely used in comparing the identified and actual data especially for a force correlogram in time domain (Hwang et al., 2011). The mathematical formula for computing the correlation coefficient is shown in Eq. 2.59.

$$CorrCoef = \frac{BS\sum_{r=0}^{BS-1}(Q_r\tilde{Q}_r) - (\sum_{r=0}^{BS-1}(Q_r))(\sum_{r=0}^{BS-1}(\tilde{Q}_r))}{\sqrt{BS(\sum_{r=0}^{BS-1}(Q_r^2)) - (\sum_{r=0}^{BS-1}(Q_r))^2}\sqrt{BS(\sum_{r=0}^{BS-1}(\tilde{Q}_r^2)) - (\sum_{r=0}^{BS-1}(\tilde{Q}_r))^2}}, \quad (2.59)$$

where *CorrCoef* is the correlation coefficient. Q_r and $\tilde{Q}_r$ are r^{th} sample of identified force and measured force in time domain respectively. *BS* is total number of samples.

The correlation coefficient has a range within ±1. The identified and measured data have a strong positive linear correlation if it has a value close to +1. If they have no linear or weak correlation, the correlation coefficient is close to zero. For a negative correlation, the correlation coefficient between the calculated and measured data is close to -1. In the case of impact force determination, only a correlation greater than 0.9 is described as good in terms of force accuracy.

2.5: Data Filtering Approach

Data filtering can be done by using a digital filter. Filter can be used to attenuate different parts of the frequency spectrum. One or 2 cut-off frequencies are commonly used to define the boundary attenuated region and un-attenuated region. Typically, there are 3 common digital filters: high pass filter, low pass filter and band pass filter. For the high pass filter, the cut-off frequency is selected so that higher frequencies data are remained while lower frequencies data are attenuated. It is used to remove low-frequency movement artifacts from low-voltage signals in wires (Derrick, 2004). For the low pass filter, the cut-off frequency is selected so that lower frequencies data are remained while higher frequencies data are attenuated. It is often used for anti-aliasing purpose (Derrick, 2004). Note that the high pass filtering approach can effectively minimizes the intrinsic problem caused by integration process (Ribeiro et al., 2001). For the band pass filter, a high pass and low pass frequencies are selected so that the data

between these 2 cut-off frequencies are remained un-attenuated only while the data beyond these cut-off frequencies are attenuated. For the impact force analysis via MTM, a band pass filter that has the same frequency range as the excited modes with insignificant amount of noise is required.

2.5.1: Residual Analysis

It is very important to select an appropriate cut-off frequency for the data filtering purpose. The selection is subjective based on the user's knowledge of the signal and noise (Derrick, 2004). In fact, signal distortion will occur if the cut-off frequency is too low with respect to the signal frequency range of interest. If it is too high, unwanted noise will pollute the signal. Residual analysis provides an objective method to determine an appropriate cut-off frequency (Biewener & Full, 1992). The residual can be calculated as shown in Eq. (2.60).

$$RS(\omega_c) = [\frac{1}{BS} \sum_{r=0}^{BS\text{-}1} (Y_{raw,r} - Y_{filter,r})^2]^{1/2}, \quad (2.60)$$

where $RS(\omega_c)$ is the residual at a given cut-off frequency. $Y_{raw,r}$ is the r^{th} sample of raw data. $Y_{filter,r}$ is the rth sample of the filtering data. BS is the sample size or also known as block size.

The residual graph is plotted as shown in Figure 2.3. From the Figure 2.3, the user can select an appropriate cut-off frequency which will balance the problem related to signal distortion and amount of noise. There are basically 3 curve fitting steps to find the cut-off frequency. First, a straight line "de" is extended to "da". The intercept at y-axis of the segment "da" represents the mean noise for the raw data. Secondly, a horizontal intercept line is plotted from interception at point "a" and cross over the residual

function. Lastly, the intercept between the horizontal line and the residual function (i.e. point "b") is referred as the optimum selection of the cut-off frequency. At this point, the amount of noise and signal distortion is equal.

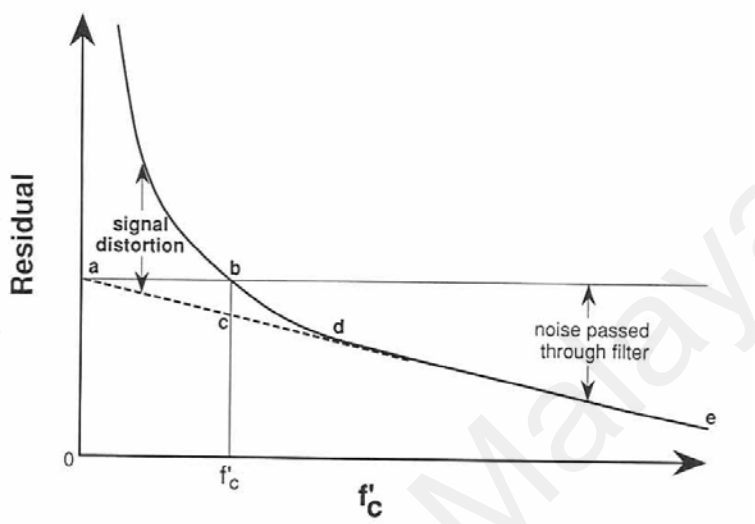

Figure 2.3:
Residual Analysis for the Determination of an Appropriate Filter Cut-Off Frequency (Biewener & Full, 1992)

In the case of time-variant excitation frequency, the excitation frequency region keeps on changing. This often happens in the case of impact force excitation which is depended on the impact condition (i.e. impact duration). In this case, the cut-off frequency will change as well depending on the excitation frequency. In such situation, it is time consuming to use the residual analysis to find the cut-off frequency as it requires extensive care in curve fitting (Derrick, 2004). There is a need to develop a new tool that is useful in finding an appropriate cut-off frequency especially in the time-variant impact force determination case.

2.5.2: Power Spectral Density

PSD is an Auto Spectrum that has been normalised by the frequency resolution of the Auto Spectrum (Vibrant Technology, 2012). So basically, PSD describes how the average power of a signal is distributed with frequency as shown in Eq. (2.61).

$$PSD=\frac{AS_{I:I}(\omega)}{\Delta f}=\frac{\left(\ddot{X}(\omega)\ddot{X}^{*}(\omega)\right)}{\Delta f}, \tag{2.61}$$

where PSD is the coefficient of PSD. Coefficients I is the output response DOF. Acceleration PSD is the ratio of the Auto Spectrum, $AS_{I:I}$ of the output acceleration response, $\ddot{X}$ to the frequency resolution, Δf and it has unit of $(ms^{-2})^2$/Hz. By using velocity and displacement responses as the output, velocity and displacement PSDs can be obtained, with unit of $(ms^{-1})^2$/Hz and $(m)^2$/Hz respectively. Δf is equal to sampling rate divided by block size. Variable ω is the angular frequency. $\bullet^{*}$ is a complex conjugate function.

To display the magnitude of PSD in decibel unit (dB), Eq. (2.62) is used.

$$\text{Magnitude of PSD in dB}=10\log_{10}(PSD). \tag{2.62}$$

The mean and standard deviation of PSD can be calculated by using Eqs. (2.63) and (2.64).

$$M\_PSD=\frac{1}{BS}\sum_{r=0}^{BS\text{-}1}10\log_{10}(PSD_r), \tag{2.63}$$

$$SD\_PSD=\sqrt{\frac{1}{BS\text{-}1}\sum_{r=0}^{BS\text{-}1}(10\log_{10}(PSD_r)\text{-}M\_PSD)^2}, \tag{2.64}$$

where PSD_r is the r^{th} sample of the PSD data. BS is the block size. M_PSD and SD_PSD are the mean and standard deviation of PSD in decibel unit. The mean of PSD is used to estimate the central value contained within the PSD data. Standard deviation is defined as the square root of the variance. In a PSD sample, PSD data greater than the "mean plus standard deviation threshold" is considered as very high power contributed data (i.e. PSD data at frequencies that contribute the most to the signal power). On the contrary, PSD data less than the "mean minus standard deviation threshold" is considered as very low power contributed data.

In fact, threshold line can be set in PSD graph to discriminate between the power contribution of useful data and unwanted noise. Previously in Section 2.5.1, from the residual analysis, the mean noise for raw data and the cut-off frequency can be identified. This cut-off frequency is used in PSD graph to find the threshold value. Assuming that the power contribution of random noise remains constant, a threshold constant relate the threshold value, mean and standard deviation of PSD can be established as shown in Eq. (2.65).

$$TC = \frac{(TV\_RA - M\_PSD)}{(SD\_PSD)} \quad , \tag{2.65}$$

where TC is the threshold constant. TV_RA is the threshold value obtained from the intersect point between PSD data and cut-off frequency acquired from residual analysis. M_PSD is the mean of the PSD data. SD_PSD is the standard deviation of the PSD data.

Thus for every new sample of acceleration PSD, this threshold constant can be used to calculate the cut-off frequency for low pass filter. This is shown in Eq. (2.66).

$$TV\_new = M\_PSD + (TC \text{ x } SD\_PSD) \ , \tag{2.66}$$

where *M_PSD* is the mean of the PSD data. *TC* is the threshold constant and it contains the statistical value of noise data. *SD_PSD* is the standard deviation of the PSD data. *TV_new* is the threshold value of the new PSD sample. Based on this threshold value, a threshold line can be set to discriminate between useful data and unwanted noise. Hence, cut-off frequency can be selected from PSD graph. This method can select an appropriate cut-off frequency in a faster way and it is more consistent instead of using the residual analysis in time-variant excitation case.

The area under a PSD curve has units of $(ms^{-2})^2$ which is proportional to power (Norton & Karczub, 2003). The total power in a specific frequency band can be calculated by integration of PSD data or simply summation over the frequency band with trapezium rule. By using trapezium rule, the area under the curve can be calculated as shown in Eq. (2.67). Hence, the normalised total power in decibel unit can be obtained by dividing the total power at a specific frequency band to the total power in whole frequency band.

$$\text{Total Power} = \sum_{r=0}^{BS-2} \frac{10\log_{10}(PSD_r) + 10\log_{10}(PSD_{r+1})}{2} \Delta t \ , \tag{2.67}$$

where Δt is equal to the time increment. It can be obtained by one divided the sampling rate.

Chapter 3: Research Methodology

3.1: Introduction

In this study the methodology of the impact force determination via MTM has been improved in 2 ways. Firstly, integration method is implemented so that the effectiveness of different types of responses on the impact force determination can be studied. In this way, the most suitable type of response can be selected. Secondly, it is proposed to select an appropriate analysis frequency range prior to impact force determination. PSD tool is used to select a suitable low pass frequency based on the power contribution of useful data and unwanted noise. Besides, the PSD tool is used to solve the intrinsic problem by selecting an appropriate high pass frequency. Based on the selected low pass frequency and high pass frequency, a band pass filter can be set-upped to eliminate the entire unwanted noise frequency region. It helps to improve the conventional force determination methodology that tends to fix the analysis frequency range.

3.2: Apparatus and Equipment Set-Up

This section will introduce the apparatus and equipment set-up used in the impact force determination. First of all, a Perspex plate test rig is needed for analysis and study. The equipments needed are an impact hammer, 15 accelerometers, multi-channel DAQ hardware, DAQ software (i.e. DASYLab), curve fitting software (i.e. ME'Scope), and matrix calculation software (i.e. Matrix Laboratory (MATLAB) software). The equipment set-up is shown in Figure 3.1. From Figure 3.1, it shows that all of these input and output sensors are connected to a multi-channel DAQ system which consists of 4-channel DAQ hardware and a compact DAQ (cDAQ) chassis. These DAQs are connected to a laptop which is equipped with DAQ software and other post-processing software. Detailed instrumentation characteristics are displayed in Table 3.1.

Table 3.1:
List of Instrumentations

Instrument	Description
Automobile test rig	A rectangular plate with 4 supports to ground which is used to simulate motion of vehicle's body. 15 points are labelled on the test rig to discrete the system Dimension: 20cm x 48cm x 0.9cm
PCB Impact Hammer , Model 086C03	Sensitivity: 2.09mV/N Tip type: Medium tip with vinyl cover Hammer mass: 0.16kg Frequency range: 2.5 kHz Amplitude range: ± 2200 N peak
Wilcoxon SNAP Model S100C accelerometer	Sensitivity: 100mV/g Frequency range: 0.5-10,000Hz Amplitude range: ±80g peak
NI USB Dynamic Signal Acquisition Module, Model NI-USB 9233	Number of channel: 4 ADC resolution:24 bits Type of ADC: delta sigma (i.e. with analogue pre-filtering)
Legacy NI Compact DAQ Chassis, Model NI cDAQ-9172	Accepts up to 8 C Series I/O modules Compact (i.e. 25cm x 9cm x 9cm) Hi-Speed USB connection to PC 11 to 30 V power supply included
DASYLab® v10.0	Sampling rate: 2000S/s (i.e. for NI 9233) Block size: 4096S Channel 1: impact hammer Channel 2 to channel 16: accelerometers at positions 1 to 15 Averaging: 100 (i.e. for FRF measurement) Averaging: 1 (i.e. for ODS analysis) Window: Rectangular window for both excitation and response signals To perform FRF measurement and ODS analysis.
MATLAB® R2010a	To post-process collected data from NI-DASYLab. To do the matrix calculation such as pseudo-inverse.
ME'scopeVES 4.0.0.99	To perform curve fitting for modal parameters extraction from FRFs data. Modal peaks function is used as mode indicator. Orthopolynomial method is used to extract damped natural frequency, modal damping and residue mode shape.

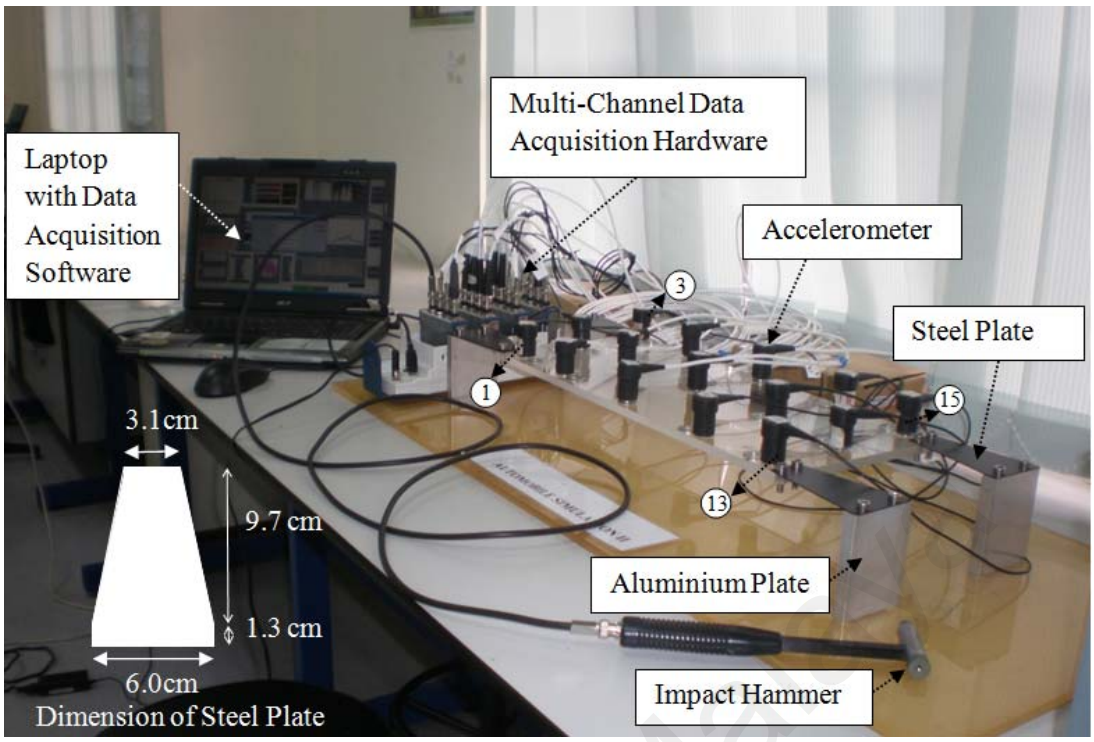

Figure 3.1:
Experimental Set-Up for Impact Force Determination Experimental Study

3.2.1: Perspex Plate Test Rig

A test rig was constructed out of a rectangular Perspex plate measuring 20cm in width, 48cm in length, and 0.9cm thick with 4 ground supports. The plate weighs 1100g. A complex vehicle body inherently comes with infinite DOF. However, it can be simplified into a simple structure with few DOFs. In this study, the attention is confined to the motion in the vertical plane only. Motions of a vehicle body include rotational (i.e. pitching and rolling modes) and translational (i.e. heaving mode) along the centre of mass of the structure, which usually appear in the low frequency region. In this simple vehicle body simulation, the Perspex plate would produce similar dynamic behaviour as in an actual vehicle body. It contains all the mentioned vibration modes. Thus this simple plate can represent a vehicle body which is generally considered as a lightweight structure.

Each of the ground supports is a combination of an aluminium plate and a trapezium steel plate. Dimensions of the aluminium plate are 1.3cm in width, 6.4cm in length, and 8.9cm in height. Detailed dimensions of the steel plate are shown in Figure 3.1. The steel plate is made of music wire, which is a high carbon steel with very high yield strength known as spring steel. The thickness of the steel plates near point 1 and point 3 (i.e. 0.2cm) are larger than the plates near point 13 and point 15 (i.e. 0.1cm). The test rig has 15 discrete locations with number labelled on it as shown in Figure 3.2. There are 15 accelerometers attached to this test rig.

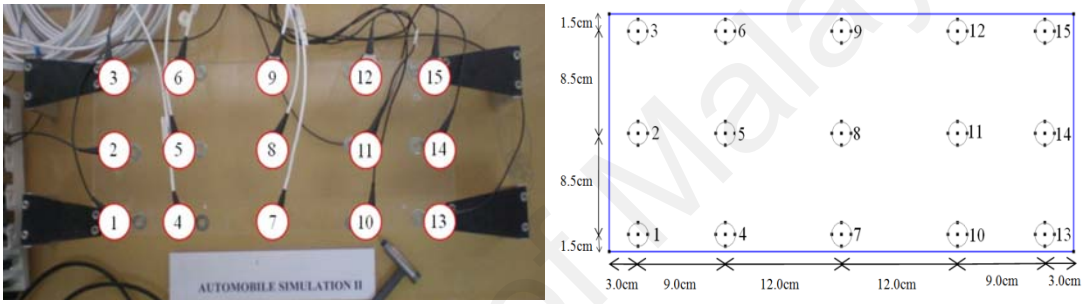

(a) (b)

Figure 3.2:
Point Numbering: (a) Vibration Test Rig, (b) Schematic Drawing

3.2.2: Accelerometer

Accelerometer is one of the most commonly used sensors in the vibration analysis. In this study, Wilcoxon Research SNAP Model S100C accelerometer is used as the response sensor. It is an Integrated Circuit Piezoelectric (ICP) accelerometer which has a built-in charge amplifier. Once there is a response, stressed piezoelectric quartz will emit charge proportional to acceleration. Hence, internal circuitry converts the charges into voltage (low impedance) and output through the sensor's casing. This sensor is able to sustain temperature within -50^{o}C to 80^{o}C. This sensor has a wide range of frequency response. It can detect signal within 0.5-10000.0Hz. Besides, it has the sensitivity of 100mV/g and can measure acceleration up to 784.8ms^{-2}.

The dimensions of this sensor are 3.73cm in height, 1.98cm in diameter and the weight of the sensor is 45g. The accelerometers are used to measure the acceleration responses due to impact force. In this study, Single Input Single Output (SISO) approach or roving accelerometers are not feasible for this test rig as it may cause mass loading effect. Mass loading effect occurs when an additional transducer mass is added to the test rig. This effect would cause data inconsistency throughout the measurement (i.e. shifted FRF). As a rule of thumb, the mass of the accelerometer should be less than one-tenth of the mass of the structure to which it is attached and it also depends on the location of the accelerometer and vibration mode (Baharin & Rahman, 2009). In this study, 15 accelerometers constitute a significant part of the structure (i.e. 61.36% of the mass of the plate which is 1100g). This affects the dynamic characteristics of the structure. However in the force identification study, Single Input Multiple Output (SIMO) approach is adopted where multiple acceleration responses are measured simultaneously using 15 accelerometers for collocated case. For non-collocated case, multiple acceleration responses are measured simultaneously using 14 accelerometers. Additional 1 accelerometer is used as dummy masses. All of these 15 accelerometers are assumed to form part of the structure. This ensures the data are collected simultaneously and consistently throughout the measurement. This avoids distortion of FRF due to mass loading effect. In short, the mass loading effect has been eliminated by using the SIMO approach and is suitable for force identification purposes.

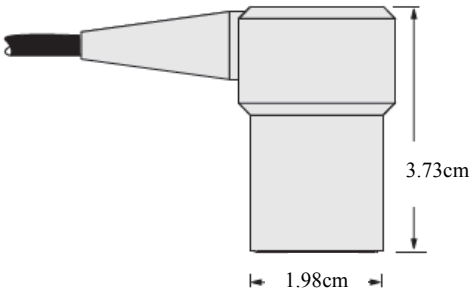

Figure 3.3:
Size of S100C Accelerometer

There are several mounting methods such as probe tip, 2-pole magnet, flat magnet, mounting pad, adhesive mount, and stud mount. The mounting method of an accelerometer to a structure affects the performance of the sensor especially on the high frequency response as shown in Figure 3.4. Considering the accessibility and flat surface of the structures, a cyanoacrylate adhesive mount with broad frequency response is chosen as the mounting method in this study so that there is no phase lag occurs during the measurement.

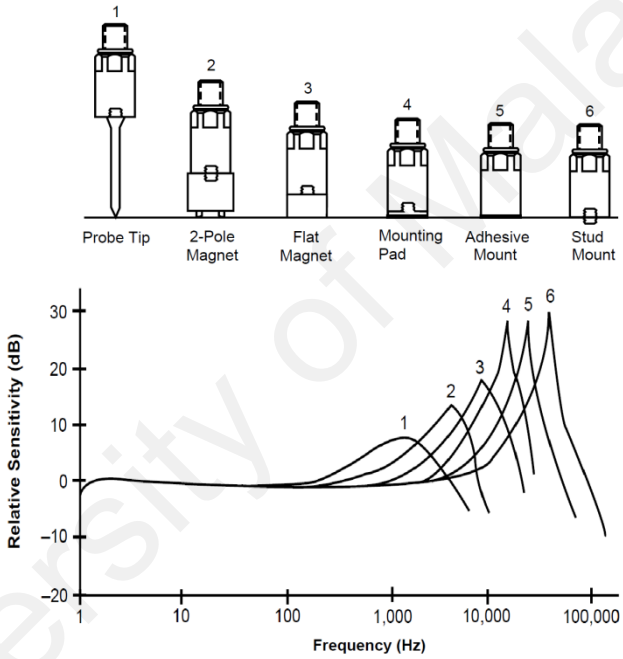

Figure 3.4:
Mounting Techniques and Their Effects on the Frequency Response
(SKF Condition Monitoring, 1999)

3.2.3: Impact Hammer

An impact hammer is commonly used for structural behaviour testing. It is used to strike the test object to produce a hammer impulse which is nearly-constant force over a broad frequency range. The impact hammer is capable to excite all the natural frequencies of the test object in that excited frequency range. The amplitude and frequency content of the force impulse depend on the hammer size, length, material, and

velocity at impact. Different types of tips will produce different frequency contents of the force. A soft tip will have a narrower frequency range compared to a stiff tip. Moreover, the size of hammer is depending on the size of the test object. It requires a mini-hammer for a small structure and sledgehammer for a large and heavy structure. In some cases, it requires a massive mechanical ram for a very large structure.

In this study, a PCB ICP ® impact hammer model 086C03 is used as the striking tool as shown in Figure 3.5. It has a sensitivity of 2.09mV/N and it is able to measure ±2200N peak. The hammer mass is 0.16kg. The tip used is the medium tip with vinyl cover and it has 2.5kHz frequency range. There is an integral, ICP® quartz force sensor mounted on the striking end of the hammer head. The impact force information will be sensed by the built-in sensing element functions consisting of rigid quartz crystals, micro-electric and unity gain amplifier. Hence, it is transferred into electric signal for further analysis. By using impact hammer, the impact force can be measured and recorded, thus provide a means of comparison against the identified impact force from the impact force determination. In this study, the direction of force is restricted to vertical direction and impact area is near to the accelerometers' location.

Figure 3.5:
Impact Hammer

3.2.4: Data Acquisition Hardware

DAQ hardware is also known as ADC which receives analogue information such as response and force signals from sensors and digitizes it. The digitized value will be sent to the computer and received by DAQ software. It acts as the interface between the computer and the outside world. It is a device used to digitize the incoming analogue signals so that the computer can interpret them.

In this study, the National Instrument-Universal Serial Bus (NI-USB) dynamic signal acquisition module, model NI-USB 9233 is used as the DAQ hardware for the force and accelerometer signals. NI-USB 9233 has the capability to power up the impact hammer and accelerometer. It consists of 4 input channels which can simultaneously acquire signals at rate from 2-50kHz. It has a 24-bit delta-sigma ADC with analogue pre-filtered (i.e. it performs digital filtering with a cut-off frequency that automatically adjusts to the selected data rate). The sampling rate of NI-USB 9233 can be chosen within 2-50kS/s. The valid sampling rates of NI-USB 9233 are as following: 2.000kS/s, 2.083kS/s, 2.174kS/s, 2.273kS/s, 2.381kS/s, 2.500kS/s, 2.632kS/s, 2.778kS/s, 2.941kS/s, 3,125kS/s, 3.333kS/s, 3.571kS/s, 3.846kS/s, 4.167kS/s, 4.545kS/s, 5.000kS/s, 5.556kS/s, 6.250kS/s, 7.143kS/s, 8.333kS/s, 10.000kS/s, 12.500kS/s, 16.667kS/s, 25.000kS/s, 33.333kS/s and 50.000kS/s. The NI-USB 9233 has a voltage range of ± 5V and a dynamic range of over 100 dB.

In this study, 4 NI-USB 9233 are required to acquire 16 signals (i.e. 15 acceleration signals and a force signal). To ensure all signals are acquired simultaneously, these 4 NI-USB 9233 are connected to a Legacy NI cDAQ Chassis, Model NI cDAQ-9172. This is recognized as a multi-channel DAQ system. This DAQ chassis is able to accept up to 8 dynamic signal acquisition modules. It is compact and small scale in size (i.e.

25.4cm x 8.8cm x 5.9 cm). The chassis weight is approximately 0.84kg. It requires 11 to 30 V power supply. The DAQ system consists of 4 signal acquisition modules and a DAQ chassis as shown in Figure 3.6. The DAQ system uses a Hi-Speed USB 2.0 connection to PC to ensure data throughput.

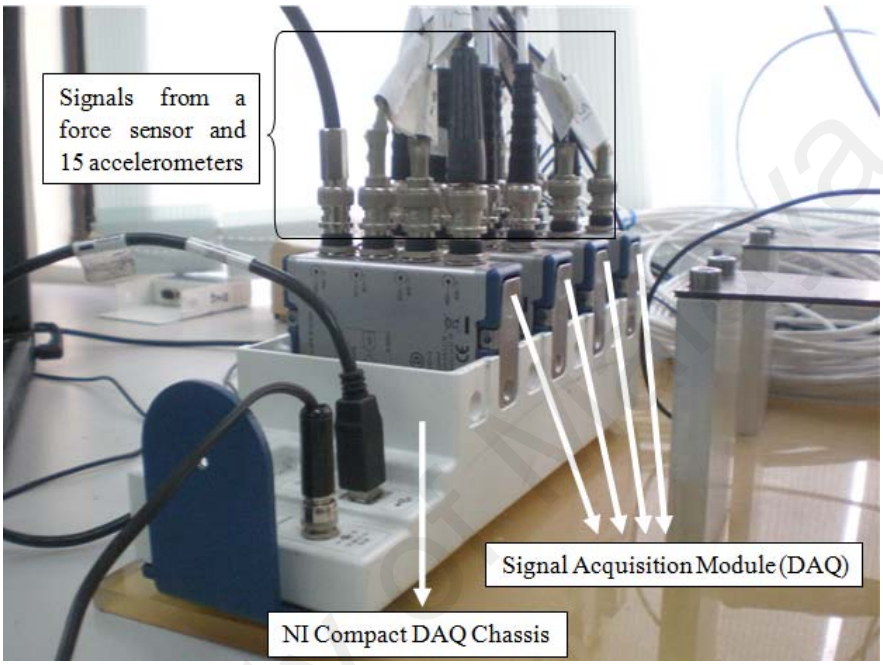

Figure 3.6:
Multi-Channel DAQ System

3.2.5: Data Acquisition Software

Software is needed to control and drive the DAQ hardware so that the DAQ system can work properly. In this study, NI Measurement & Automation (NI-DAQmx) is used as the driver software. The function of driver software is to ease the user to communicate the DAQ hardware with the DAQ software. The driver software forms the middle layer between the application software and the hardware. It enables a simple communication with no complicated programming commands to access the hardware function. Through the driver software, DAQ software such as DASYLab can be linked and conjugated to the DAQ hardware. In fact, DASYLab is a virtual instrument platform which consists of various features such as virtual oscilloscope, virtual FFT analyser and digital filter. The

flexibility in creating and modifying the instrument to fit users' needs and desires is the major advantage of virtual instrument.

With DASYLab, user can create a software application programme on the computer system for FRF measurement, COH measurement and ODS analysis based on the theories discussed in Sections 2.4.4-2.4.6.

3.2.5.1: FRF and COH Measurements Application Programme

FRF and COH are both done in frequency domain. It is known that a time trace can be transformed into frequency domain by using FFT. Note that the signal in frequency domain is a complex signal which consists of real and imaginary parts. In this study, impact force is used as the input and 15 acceleration responses are used as the outputs. After all the input and output signals were obtained simultaneously, a SIMO FRF can be established. Assuming that the impact force signal and acceleration response signal are equal to $a(\omega)+b(\omega)i$ and $c(\omega)+d(\omega)i$ respectively whereby $a(\omega)$, $b(\omega)$, $c(\omega)$ and $d(\omega)$ are the known values in real part and imaginary part in the function of frequency; $i=\sqrt{-1}$. Hence, Eqs. (2.53) and (2.54) can be rewritten as Eqs. (3.1) and (3.2).

$$H_{I:J}(\omega)=\frac{(ac+bd)}{a^2+b^2}+\frac{(ad-bc)}{a^2+b^2}i, \tag{3.1}$$

$$\gamma^2_{I:J}(\omega)=\frac{\left|(ac+bd)+(ad-bc)i\right|^2}{\left(a^2+b^2\right)\left(c^2+d^2\right)}, \tag{3.2}$$

where $H_{I:J}$ is the FRF coefficient. $\gamma^2_{I:J}$ is the COH coefficient. Coefficients *I* and *J* are output response DOF and input force DOF respectively. Note that for the calculation of COH, averaging in the numerator occurs before the absolute value is taken.

Based on Eqs (3.1) and (3.2), the FRF measurement and COH measurement application programmes can be designed as shown in Figures 3.7 and 3.8. From Figure 3.7, a 16-channel Analogue Input Module is constructed where the first channel is the signal from impact hammer and the other 15 channels are the signals from 15 accelerometers. Note that only first channel and second channel are shown here for demonstration purpose. Triggering function consists of a Pre/Post Trigger Module and Relay Module which are used to allow the response and force signals pass through only if impact force exceeds the selected threshold value. Besides, user can always adjust the pre-trigger and post-trigger values to ensure that both force and response signals have zero start and zero end. Rectangular window is used as the data window for the time traces. Then, FFT Module is used to transform the time traces into frequency domain. Each FFT module gives 2 outcomes where the first channel is the real part of signal while the second channel is the imaginary part of signal.

Frequency averaging is applied by using the Block Average Module. It helps to eliminate noise by using averaging method. In this study, 100 averages are used to clean up the noise. After that, Eq. (3.1) can be applied to the Formula Module to calculate the FRF. The FRF in Cartesian coordinate is then displayed in a chart by using Y/T Chart Module. Hence, the measured FRF is stored in database by using the Write Data Module. From Figure 3.8, COH measurement has a similar arrangement as the FRF measurement worksheet in the initial part (i.e. Analogue Input Module until the FFT Module). Refer to Eq. (3.2) , Formula Module labelled "Formula30" is used to generate 4 outputs, which consist of a numerator component (i.e. $(ac+bd)$) at first channel, a numerator component (i.e. $(ad-bc)$) at second channel, a denominator output (i.e. (a^2+b^2)) at third channel and a denominator output (i.e. (c^2+d^2)) at fourth channel. Then, frequency averaging with 100 averages is applied by using the Block Average

Module. After that, Eq. (3.2) can be applied to the Formula Module labelled "Formula31" to calculate the COH. Hence, the measured COH is displayed in a chart by using Y/T Chart Module and it is stored in database by using the Write Data Module.

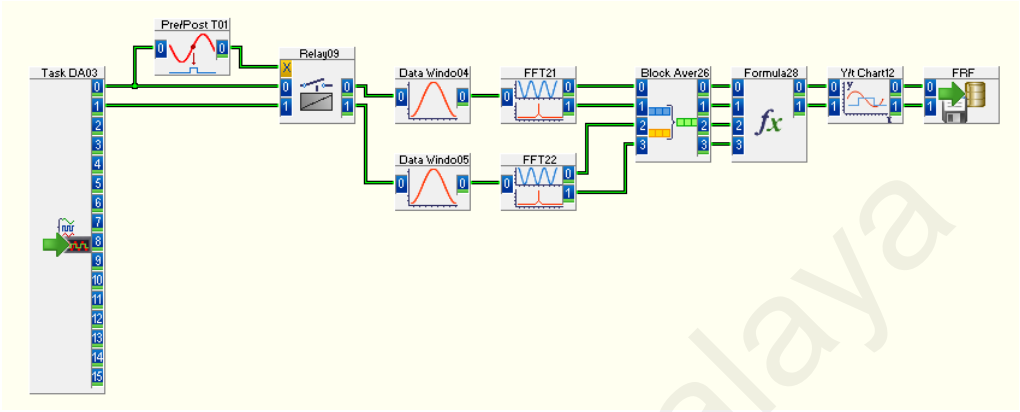

Figure 3.7:
Arrangement of FRF Measurement in DASYLab

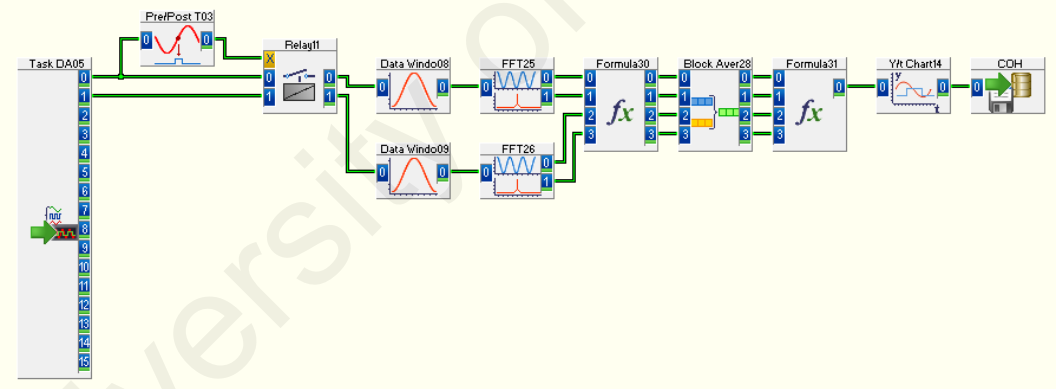

Figure 3.8:
Arrangement of COH Measurement in DASYLab

3.2.5.2: ODS Analysis Application Programme

In this study, acceleration responses due to an unknown impact force that is acting on the vibration test rig will be used for impact force determination. ODS analysis application programme is used to capture simultaneously all the 15 acceleration responses simultaneously at the defined DOF on the vibration test rig as shown in Figure 3.9. This is known as the time-based ODS analysis. From Figure 3.9, a 16-

channel Analogue Input Module is constructed where the first channel is the signal from impact hammer and the other 15 channels are the signals from 15 accelerometers. Note that the impact force is assumed unknown in the impact force determination and this measured impact force is used for verification purpose. Triggering function consists of a Pre/Post Trigger Module and Relay Module which are used to allow the raw data pass through for further signal processing once the impact force exceeds the threshold value. Besides, Scaling Module is used to convert the unit of signals. The time domain raw data are then saved in database created using the Write Data Module. This saved data can be used for further analysis in DASYLab, ME'Scope and MATLAB.

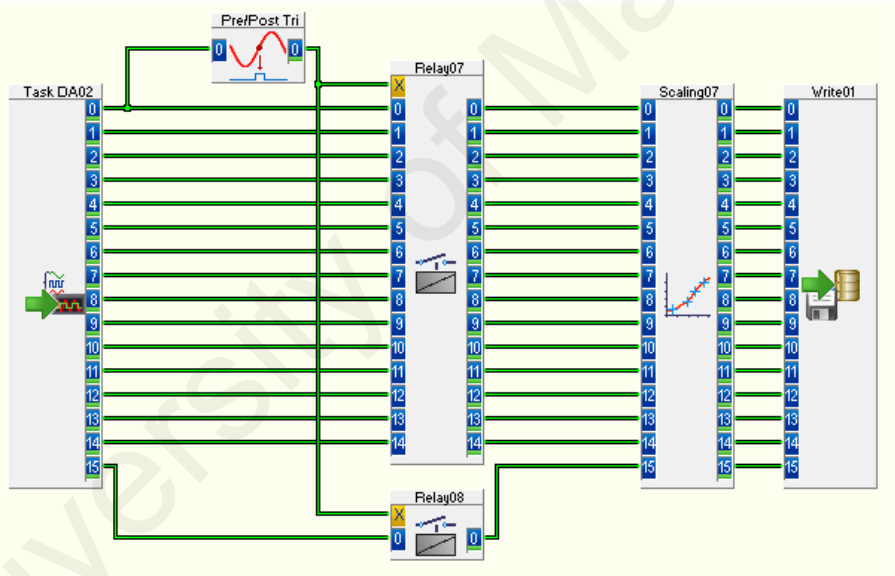

Figure 3.9:
Arrangement of Time-Based ODS Analysis in DASYLab

3.2.6: ME'scopeVES (Visual Engineering Series)

ME'ScopeVES is software used by engineer to analyze noise and vibration problems in structures and machines. By using this software, user can display and analyze the measured time or frequency traces easily. In this study, ME'Scope is used for modal parameters estimation purpose. In fact, curve fitting is a process of matching a parametric model of a FRF to a set of measurement data. Modal parameters such as

residue mode shapes, modal damping and damped natural frequencies are estimated by curve fitting a set of experimentally derived FRFs.

There are several steps for modal parameters estimation (Vibrant Technology, 2012):

i. Determine the number of modes in a selected frequency band.
ii. Estimate modal damping and modal damped frequency for each mode in the selected frequency band.
iii. Estimate the residue mode shapes for the modes with frequency and damping estimates.
iv. Save the modal parameters into a Shape Table file.

3.2.6.1: Determination of the Number of Modes

In this step, all the measured FRF traces are overlaid and then visually inspected for resonance peaks. Since modal frequency and modal damping are global properties of a structure, this shows that resonance peaks will appear at the same frequencies if multiple FRF traces are overlaid together. Then, global curve fitting algorithms can be used to estimate the dynamic characteristics by simultaneously matching redundant information (Allen & Ginsberg, 2006).

Curve fitting is done in a selected frequency band so that noise contaminated data can be excluded. Note that for accelerance and admittance FRFs, overlay the imaginary parts and look for peaks. For mobility accelerance, use the real part. Otherwise, use the magnitude. In this study, imaginary part of measured accelerance FRFs are overlaid instead of magnitude plot. The peak of the imaginary part of measured accelerance FRFs is more pronounced than the peak in the magnitude plot, particularly if two resonances are closely spaced, or highly damped (Brandt, 2011). For the case of low

damping ratio (i.e. $\zeta << 1$), the peak is located near natural frequency. There are 3 types of mode indicators available: Modal Peak Function, Complex Mode Indicator Function (CMIF) and Multivariate Mode Indicator Function (MMIF). The former method is a single reference mode indicator which sums up all the FRF traces together. The CMIF and MMIF are multiple reference mode indicators which yield multiple indicator curves from a multiple reference set of FRFs. In this study, Modal Peak Function is used for a single reference set of FRFs.

3.2.6.2: Estimation of the Modal Damping and Modal Frequency

Modal damping and modal frequency can be estimated by using SDOF or MDOF curve fitting methods. In general, SDOF method is used on lightly coupled modes while MDOF method is used on heavily coupled modes. However, SDOF methods and MDOF methods can be combined to curve fit a set of FRFs data. SDOF methods such as Co-Quad method and Peak method estimate modal frequency and modal damping one mode at a time. Co-Quad method uses line cursor to estimate modal frequency only and the FRFs value at the position of line cursor is saved as a component of the mode shape. The Peak method find the peak value in its cursor band and the FRFs value at the peaks in each FRF is saved as a component of the mode shape. The modal frequency is obtained by averaging all the peak frequencies. The SDOF methods are useful to estimate modal parameters for modes that are widely separated by treating the data in the vicinity of a peak as if it is due to a single mode.

MDOF methods such as Polynomial method and Complex Exponential Method simultaneously estimate the modal parameters of 2 or more modes from a set of FRFs. Note that MDOF methods act as a SDOF method if it only estimates modal parameters of one mode from a set of FRFs. The Polynomial method is a global frequency domain

method that curve fits a set of FRFs directly. In this method, a LS curve fit of multiple FRFs is performed. Hence, the coefficients of the FRF denominator polynomial, called the characteristic polynomial can be estimated. Then, modal frequency and damping can be estimated as the roots of the characteristic polynomial. On the other hand, the way the Complex Exponential method estimate the modal parameters is similar to the Polynomial method. The main difference is that Complex Exponential method operates on a set of IRFs and thus it is a global time domain method.

3.2.6.3: Estimation of the Residue Mode Shape

Once the modal frequency and modal damping were obtained, residue mode shapes are estimated from the coefficients of the numerator polynomial of each FRF by using a LS curve fitting process. Curve fitting a residue mode shape is inherently a local curve fitting process which estimates residue for each mode and each FRF one at a time. All the SDOF and MDOF methods can be used to estimate residue mode shapes.

The residual effects of modes that lie outside of the curve fitting band (i.e. out-of-band modes) must be compensated in order to obtain an accurate modal parameters estimation. The SDOF methods ignore the residual effects of out-of-band modes by assuming these residual effects are small. The MDOF methods employ 2 ways to compensate the residual effects: Computational Modes and Extra Numerator Polynomial Terms. The former way over-specifies the number of modes used in the curve fitting model by assuming that the extra modes or the computational modes will account for the out-of-band modes. This can be applied for both the Polynomial and Complex Exponential methods. The latter way specifies an extra numerator polynomial terms for the curve fitting model by using the Polynomial method where this higher order numerator polynomial will then compensate for the out-of-band modes.

3.2.6.4: Save Modal Parameters Data

Considering the high performance of the Polynomial method in estimating the modal parameters, it is used as the curve fitting method in this study. After the modal parameters are obtained, they can be saved into a Shape Table file and used for further analysis. Then, the obtained mode shapes can be viewed in animation on a 3D model.

3.2.7: Matrix Laboratory Software

MATLAB is software mainly used for manipulating matrix and arrays, implementing algorithm, and plotting data. There are a lot of useful built-in functions and algorithms for the mathematic calculation purpose, data analysis by using descriptive statistics and signal processing purpose can be found in the MATLAB software. For example, it has the built-in Moore-Penrose pseudo-inverse of matrix, FFT, trapezoidal numerical integration, mean and correlation coefficient with commands "*pinv*", "*fft*", "*trapz*", "*mean*" and "*corrcoef*". Besides using the built-in functions, the high end users can always define and implement their own algorithm. In addition, MATLAB provides programming environment to user as well. User can always control the flow by using programming techniques such as the conditional control (i.e. "if...else...end") and loop control (i.e. "for...end"). Moreover, user can plot the data in various formats such as bar graph, 2D graph and 3D graph.

3.3: Experiment Procedure

This section describes the experimental procedure conducted to test and establish the accuracy and applicability of the impact force determination procedure with MTM. A method which utilises the ODS, FRF, MTM, integration method and PSD tool to evaluate the unknown impact force was proposed here. The methodologies of the FRF measurement and ODS analysis were introduced first. Next, MTM was used to

synthesis FRFs by using modal parameters obtained from single column FRFs curve fitting. By using the integration method, the method for impact force determination from different types of responses using MTM was presented. After that, selection of an appropriate analysis frequency range by using PSD tool was demonstrated. The proposed force determination method was examined in both collocated and non-collocated cases, and the effectiveness of the proposed method was compared to the conventional method.

3.3.1: Methodology of FRF Measurement

In this study, a single reference or single column of FRF matrix is measured by using the FRF measurement that follows the impulsive excitation technique (Halvorsen & Brown, 1977). First of all, a total of 15 points has been selected to define the geometry of the test rig as shown in Figure 3.2. Note that the total number of measurement points is often greater than the total number of vibration modes to ensure a sufficient description of the measured vibration modes (Fu & He, 2001). Then, 15 accelerometers have been attached to these 15 locations by using a cyanoacrylate adhesive mount and they are used to measure the vertical motion of the test rig.

SIMO approach has been implemented whereby in this analysis, a known impact force function was excited 100 times vertically at a discrete point on vibration test rig and the resultant acceleration response signals at all accelerometer location were measured simultaneously for 100 averaging. Hence, FRF can be computed by dividing the output response spectrum to the input force spectrum for every frequency line. One column of FRF matrix was obtained for each SIMO approach. Advantages of using this SIMO approach instead of using the SISO approach are experimental time saving and reduction of roving mass loading effect (Avitabile, 2001). It is valuable to say that the

reference impact location must not be a node point and it must be able to excite all the modes in the frequency of interest. A set of driving point FRFs at the 15 locations were measured and they were utilized to find the appropriate reference (Schwarz et al., 2002). As a result, point 1 was selected as the reference impact location. Note that it is very hard to excite the point exactly as the response location in practical, thus force was applied at location near to the sensor.

An initial assessment of measured FRF data is implemented to ensure that the test rig satisfies the assumptions of time invariance, linearity and reciprocity (Fu & He, 2001). Theoretically, FRF data of a linear system is independent of the force amplitudes. To check the linearity of the test rig, the measured FRFs data using various excitation amplitudes are overlaid to verify the uniformity of curves. For a time-invariant linear system, an identical FRF data should be obtained for every measurement. Repeatability check is done to ensure that the testing condition remains the same and the structure's behaviour is constant. In fact, a linear time-invariant system possesses reciprocity property where the FRF data will be identical although the locations of response and force are exchanged. A reciprocity check helps user to access the reliability and accuracy of the measured FRF data.

After checking the validity of the FRF measurement, a SIMO measurement of FRFs data is made using a block size of 4096S and a sampling rate of 2000S/s. This gives a frequency resolution of 0.4883Hz and a time resolution of 0.0005s. There are several precautions that users need to take into considerations such as the users shall avoid double impact, or else the input spectrum will not produce a flat or smooth spectrum in the frequency of interest. Besides, users need to ensure that both response and force signals have a zero start and zero end because rectangular window is applied. To

achieve this condition, a pre-trigger value of 0.025s and post-trigger value of 2.023s are selected. Trigger level for the force signal of about 5% of the amplitude range would be sufficient, as too low will be accidentally triggered by signal pulse due to poor contact of cabling, while too high may cause non-linearity effect (Rahman, Unpublished). During the FRF measurement, users need to validate the accuracy of the measured FRFs data by using the COH function. As a rule of thumb, only COH measurement that is within 0.9- 1.0 is considered acceptable.

After the FRFs data are acquired by using FRF measurement in DASYLab software, the collected data are post-processed by using ME'Scope software. The modal parameters named damped natural frequencies, modal damping and residue mode shapes are obtained by using the Polynomial curve fitting method. Hence, the mode shape of each vibration modes are animated and recorded. Furthermore, synthesised FRFs can be obtained by using the MTM as shown in Eq. (2.36).

Since acceleration and force signals are used to estimate the FRFs data, this type of FRF is called the accelerance FRF. The measured accelerance residue mode shape is used to synthesise the accelerance FRF previously. To estimate force from various types of responses, the other 2 types of FRFs named the mobility and admittance FRFs must be obtained. It can be done by transforming the measured accelerance residue mode shape into mobility and admittance residue mode shapes as shown in Table 2.2. By using MTM, the synthesis of accelerance, mobility and admittance FRFs can be obtained by using Eqs. (2.40), (2.41) and (2.42).

The synthesised FRFs can be compared with the measured FRFs in order to access the accuracy of the curve fitting result. By using MATLAB software, the cumulative

summation of the correlation between the mean of synthesised and measured FRFs due to force DOF (i.e. impact location 1 has force DOF equal to 1) can be calculated and plotted by using Eq. (2.57). Besides, the condition number of the synthesised FRF matrix can be calculated by using Eq. (2.58) to indicate the condition of the matrix. Note that condition number close to 1 is known as a well-posed problem. For the case of unknown force location, condition number of 15 by 15 synthesised FRF matrix is calculated in this study. On the other hand, condition number of a 15 by 1 synthesised FRF matrix due to the known force DOF (i.e. impact location at point 1) is calculated for the case of known force location.

3.3.2: Methodology of ODS Analysis

ODS analysis is a study used to determine the response of the whole structure during operation or forced vibration. Typically, it is a technique where structural acceleration response's amplitude and phase are determined between a reference location and other response locations. Considering the non-stationary behaviour of the excitation force and the small-scale characteristic of the structure, time-based ODS analysis has been implemented to simultaneously capture all the acceleration signals from 15 accelerometers. From this way, ODS analysis with multiple sensors provides simultaneous amplitude and phase information of the structure motion stored in time domain, whence, the reference location is not needed. The ODS analysis has the similar experimental set-up with the FRF measurement as shown in Figures 3.1 and 3.2.

In this study, an unknown force was excited vertically at one of the points (i.e. point 1) on the test rig and then the impact-induced acceleration responses will be acquired simultaneously by using the DAQ system. A SIMO measurement of acceleration data is made using a sampling rate of 2000S/s and a block size of 4096S. There is no averaging

in the ODS analysis and every measurement is used for the impact force determination. This procedure is repeated by exciting the structure at 15 discrete locations (i.e. points 1 to 15) and hence it generates 15 sets of ODS data separately. It is known that the ODS data will be used to estimate the time history of the unknown force by using impact force determination. Note that modally tuned impact hammer is used as the exciter and force transducer which records the time history of measured force for verification purpose. After obtaining the ODS data, FFT of the acceleration time traces will transform it into frequency domain. Next, the integration of the acceleration response into velocity and displacement responses is done by using Eqs. (2.55) and (2.56).

3.3.3: Methodology of Selecting an Appropriate Analysis Frequency Range Using PSD Tool

It is well-known that noise effect will be amplified during the impact force determination and causes inaccurate force determination result. In this situation, band pass filtering can be used to eliminate or reduce the effect of noises by setting a high pass frequency and low pass frequency. However, it is very difficult to select an appropriate cut-off frequency which is balanced in terms of the signal distortion and contamination of noise. In addition, the actual force excitation frequency is unknown in nature and thus making the selection process very difficult. Typically, residual analysis is used to find the cut-off frequency for the high pass-frequency. However, this method is found to be impractical in the case of time-variant impact force determination where the excitation frequency region may varied from time to time (i.e. the excitation frequency of impact force depends on the impact condition). On the other hand, an appropriate selection of a high pass frequency is important especially for signal obtained from integration process such as velocity and displacement signals. Basically, high pass filter helps to eliminate the intrinsic problem due to integration method. However, it is

not a simple task to find the suitable cut-off frequency. For this reason, PSD tool is recommended to be used in the determination of an appropriate analysis frequency range based on the theory discussed in Section 2.5.

3.3.3.1: Selection of Low Pass Frequency

In fact, PSD tool is able to select an appropriate low pass frequency by considering the power contribution of important signal and unwanted noise. In this case, the PSD tool consists of the residual analysis and acceleration PSD. Experiment procedure to select an appropriate low pass frequency is shown in the following steps:

Step (1) – In a residual analysis, residual of the acceleration response can be calculated by using Eq. (2.60) and hence graph of residual versus frequency can be plotted. Hence, use the curve fitting method as discussed in the Section 2.5.1 to find a balance point where the amount of signal distortion is same with the noise effect. Next, cut-off frequency of the low pass filter is selected at the intersect point between the mean noise line and the residual function.

Step (2) – Next, PSD of the acceleration response in decibel scale can be calculated and plotted using Eqs. (2.61) and (2.62). The statistical functions such as mean and standard deviation are used to represent the statistical value of a PSD sample and it can be calculated in the following Eqs. (2.63) and (2.64). Hence, the cut-off frequency obtained from residual analysis is used to find the power contribution of the mean noise of the raw data, which is known as threshold value in this study. Assuming the system is time-invariant where all the testing conditions are remained constant, the threshold constant can be found by using the Eq. (2.65). In fact, the threshold constant possesses the statistical information of noise data.

Step (3) –Mean and standard deviation are calculated for every new sample of the PSD data. Hence, a new threshold value can be calculated by using the threshold constant and the statistical information of the new PSD data as shown in Eq. (2.66). Hence, the low pass frequency can be found easily by plotting the threshold line on PSD graph. Note that this threshold line has the magnitude as the new threshold value. Signal lower than the threshold line is considered as low power contributed signal with unwanted noise and hence can be eliminated.

3.3.3.2: Selection of High Pass Frequency

PSD tool provides a simple detection method for intrinsic problem and uses an iterative method to find the high pass frequency. In this case, the PSD tool consists of normalised total power of response PSD. Experiment procedure to select an appropriate low pass frequency is shown in the following steps.

Step (1) – Normalised total power of acceleration, velocity and displacement PSD in decibel unit can be calculated and plotted by using Eq. (2.67). Note that intrinsic problem caused by the integration operation will amplify the signal content in low frequency region. Therefore, an intrinsic problem can be detected for signal which has abnormal high normalised total power in the low frequency region.

Step (2) – After detecting the signal that has intrinsic problem, an iterative increasing high pass frequency is applied. At the same time, the changing of the normalised total power is observed. An appropriate high pass frequency can be selected based on the following criteria:

i. Reduction of the abnormal high normalised total power at low frequency region by increasing the high pass frequency indicates the removal of the intrinsic error.

ii. Intrinsic problem is eliminated once the normalised total power is near zero at low frequency region.

iii. Further increment of the high pass frequency above the optimum point will cause signal distortion.

3.3.3.3: Band Pass Filtering

Once low pass frequency and high pass frequency have been determined by using the PSD tool, this information are used to set up a band pass filter for both synthesised FRFs and responses data. In fact, band pass filter truncates the higher modes of a system, however this is possible because the low frequency modes mainly contribute to the structure. Through the band pass filter, the data below the high pass frequency and above the low pass frequency will be removed by setting the data in frequency domain as zero. The data between these 2 cut-off frequencies will be remained and it is used for further impact force determination.

3.3.4: Methodology of Impact Force Determination via MTM

3.3.4.1: By Using Various Types of Responses

The methodology of impact force determination with MTM by using various types of responses has been developed in this research. It enables user to study the effectiveness of the acceleration, velocity and displacement responses on the impact force determination. The schematic block diagram for this method is described in Figure 3.10. Experiment procedure to calculate the unknown force is developed as described in the following steps:

Step (1) – SIMO approach is adopted where multiple acceleration responses are measured simultaneously together with single excitation force. Hence, single column (i.e. 15 by 1) raw accelerance FRF matrix is estimated through FRF measurement as described in Section 3.3.1. A total of 100 averaging is used to reduce the measurement noise. By using Polynomial curve fitting method, modal parameters such as damped natural frequencies, modal damping and accelerance residue mode shapes are extracted from the single column raw accelerance FRF matrix. The accelerance residue mode shape can be converted to mobility and admittance residue mode shapes by using relation as shown in Table 2.2. Hence, synthesis of accelerance, mobility and admittance FRF matrices are computed by using MTM as shown in Eqs. (2.40), (2.41) and (2.42). Note that the inversion of these 3 types of synthesised FRFs become well-posed once the impact location is known in advance.

Step (2) – Vibration pattern of a machine or structure can be recorded and visualised when influenced by its excitation force, which is known as ODS analysis as discussed in Section 3.3.2. In this study, an unknown excitation force is excited by an impact hammer at point 1. Force history data is measured by a force sensor inside the impact hammer's tip for verification purpose. Accelerometers are used to measure acceleration response due to an unknown impact force. Fifteen accelerometers measure acceleration time traces at 15 discrete points of the test rig simultaneously once unknown impact force is released, to form a 15 by 1 response vector. The acceleration time traces are transformed into frequency domain by using forward DFT, computed with FFT algorithm as described in Eq. (2.51). It is integrated into velocity and displacement data in frequency domain by using Eqs. (2.55) and (2.56) respectively.

Step (3) – Impact force determination in frequency domain by using acceleration, velocity and displacement responses is performed by using Eqs. (2.43)-(2.45). Next, it can be transformed into time domain by using backward DFT, computed with IFFT algorithm as shown in Eq. (2.52). Hence, the identified forces by using various types of responses are compared to the measured force obtained from instrumented impact hammer. Force correlograms between the measured force and identified forces are plotted. Besides, the correlation coefficient between the measured and identified forces will be calculated as well.

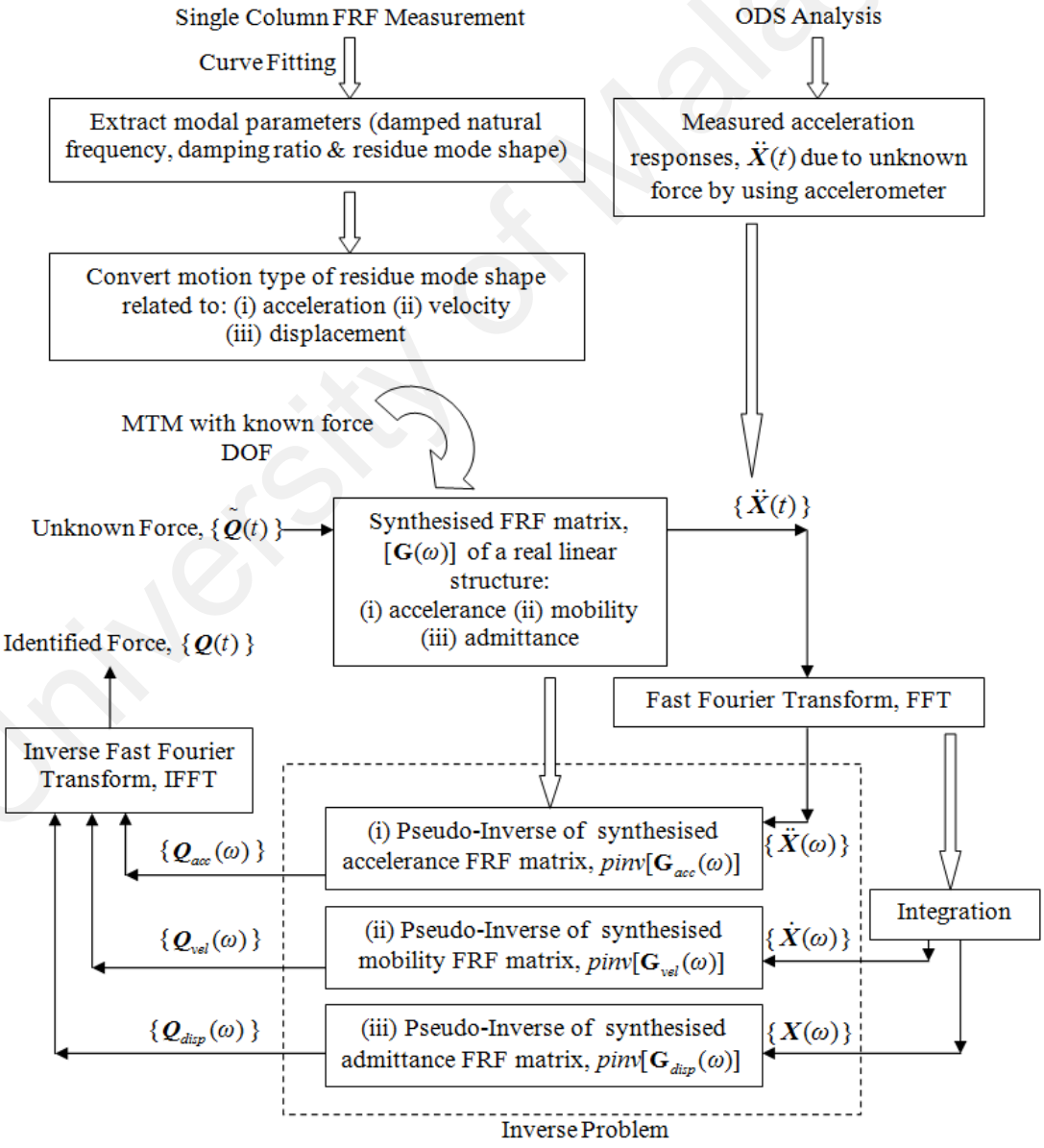

Figure 3.10:
Block Diagram for Force Identification Procedure with MTM via Different Types of Responses

3.3.4.2: By Using Fixed Analysis Frequency Range

In this study impact force determination with MTM by using various types of responses are conducted in different cases of fixed analysis frequency range. It is worthwhile to recall that the selected sampling rate and block size are 2000S/s and 4096S. The frequency resolution is 0.4883Hz (i.e. 2000S/s per 4096S). DC component is suppressed due to accelerometer's measurement limitation and the useful analysis frequency range of positive half spectrum is ranging from 0.5-999.5Hz. With the knowledge of excitation frequency range of measured impact force acting on point 1 (i.e. 0.5-500.0Hz), the fixed analysis frequency ranges are chosen as the following:

i. Under-Estimated case: Analysis frequency range is much smaller than the excitation frequency range. In this case, 206 samples (i.e. (206-1) x 0.4883 = 100.1Hz) of frequency traces for FRF and ODS results have been selected. Thus, the selected analysis frequency range for under-estimated case is 0.5-100.1Hz.

ii. Even-Estimated case: Analysis frequency range is similar with excitation frequency range. In this case, 1025 samples (i.e. (1025-1) x 0.4883 = 500.0Hz) of frequency traces for FRF and ODS results have been selected. Thus, the selected analysis frequency range for even-estimated case is 0.5-500.0Hz.

iii. Over-Estimated case: Analysis frequency range is much larger than the excitation frequency range. In this case, 2048 samples (i.e. (2048-1) x 0.4883 = 999.5Hz) of frequency traces for FRF and ODS results have been selected. Thus, the selected analysis frequency range for over-estimated case is 0.5-999.5Hz.

Experiment procedure to calculate the unknown force acting on point 1 is similar as Section 3.3.4.1 and it is repeated for different cases of fixed analysis frequency range. The effectiveness of the various types of responses is examined in under-estimated case, even-estimated case and over-estimated case respectively. Besides, the identified force for each case of fixed analysis frequency range is compared to the measured force to illustrate the importance of selecting an appropriate analysis frequency range.

3.3.4.3: By Using PSD Tool Selected Analysis Frequency Range

When excitation frequency of an impact force is unknown and time-variant, selection of an appropriate analysis frequency range must be made prior to the impact force determination. In this study, PSD tool is proposed to find a good analysis frequency range in order to enhance the force determination procedure. The schematic block diagram for this method is described in Figure. 3.11. Note that for simplicity, only acceleration response is used for the demonstration purpose. The proposed method is applicable to the other responses in a similar manner. To measure the forces, a set of DSP procedure is designed and developed as described in the following steps.

Step (1) – Single column of FRF measurement is carried out to determine a single reference set of FRFs data as stated in the methodology discussed in Section 3.3.1. This SIMO approach is adopted where multiple responses are measured simultaneously together with single excitation force. Curve fitting the FRFs data to estimate modal parameters such as modal frequencies, modal damping and residue mode shapes. Hence by using mathematical computation software, MTM can be applied to scale the residue mode shape into UMM mode shape. Hence, synthesised FRF can be computed. If the synthesised FRF and measured FRF match each other in the frequency of interest, then the synthesised FRF is accepted. If not, a better curve fitting method will be proposed.

Step (2) – The structural response of the system using ODS analysis is carried out as stated in the methodology discussed in section 3.3.2. After an unknown impact force is acting on the point 1 of the test rig, ODS analysis with multiple sensors acquires simultaneous amplitude and phase information of the structure motion and hence stored it in time domain. The collected acceleration response trace in time domain is transformed to frequency domain using FFT. Note that both FRF measurement and ODS analysis use a sampling rate of 2000S/s and a block size of 4096S.

Step (3) – An appropriate analysis frequency band is chosen by using PSD tool as stated in the methodology presented in Section 3.3.3. First of all, PSD of the mean of the 15 measured acceleration responses is calculated. Then, a threshold constant is obtained from the residual analysis. By using the mean and standard deviation of a new acceleration PSD data, the threshold value differentiates between the high power contributed signal and unwanted noise signal and this can be obtained by using Eq. (2.66). Hence, a low pass frequency can be selected from the acceleration PSD graph. Next, the normalised total power of the acceleration, velocity and displacement PSD data are calculated by using Eq. (2.67). Abnormal high normalised total powers of the PSD data near the DC frequency (i.e. 0Hz) indicate intrinsic problem which amplify the noise contribution in low frequency region. This intrinsic problem can be eliminated by selecting a high pass frequency. Therefore it is suggested to iteratively increase the high pass frequency until the normalised total power of the PSD data drops to a normal value (i.e. close to zero in low frequency region). Note that the high pass frequency shall not be too high because this will cause signal distortion. After obtaining the low pass frequency and high pass frequency, this information is used to set a band pass filter for both ODS data and synthesised FRF data.

Step (4) – Both of the ODS data and synthesised FRF are prepared for the impact force determination which is known as an inversion problem. The pseudo-inverse method is used to carry out matrix inversion in frequency domain, which is well-known in solving the inverse problem by using LS method. Inversion of the synthesised FRF is performed for every discrete frequency component of the FRF, i.e. 4096 times for a 4096 block size of data.

Step (5) – The inversed synthesised FRF is multiplied with the response vector to obtain the force for each frequency. Once the entire force spectrum completed, IFFT transforms the identified force from frequency domain into time domain.

Step (6) – For verification, a comparative study is carried out between the identified force and the measured force by using force correlogram and correlation coefficient function.

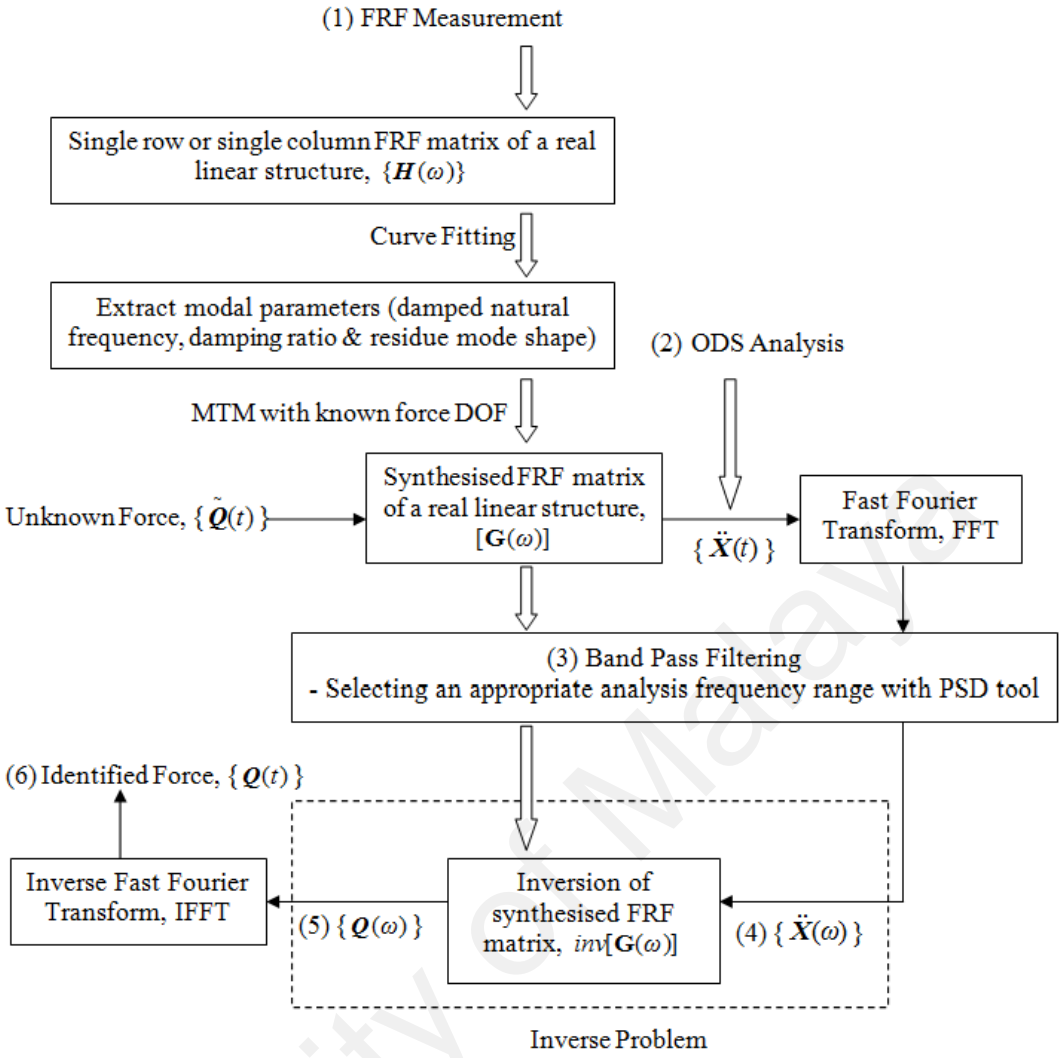

Figure 3.11:
Block Diagram for Force Identification Procedure with MTM via Band Pass Filtering

3.3.4.4: Fixed Analysis Frequency Range versus PSD Tool Selected Analysis Frequency Range

So far, the impact force determination via MTM has been conducted in the 3 cases of fixed analysis frequency range (i.e. under-estimated, even-estimated and over-estimated cases) and in the PSD tool selected analysis frequency range. Moreover, various types of responses such as acceleration, velocity and displacement responses have been used to estimate the unknown force in all the mentioned cases. Therefore, a comparative study is carried out to summarise all those findings by using the correlation coefficient function. Note that correlation coefficient is used because this function effectively

calculates the relation between the entire time traces of measured force and calculate force, which include the loading and unloading parts of impact force. Based on the findings, the most suitable type of response and the most suitable analysis frequency range can be found. Hence, it is proposed to enhance the conventional force determination method.

3.3.4.5: In Collocated and Non-Collocated Cases

Previously, one point analysis was conducted in Sections 3.3.4.1-3.3.4.4 where the impact force determination was examined at single impact location only (i.e. point 1) for simplicity purpose. From the outcomes of force determination, the most suitable analysis frequency range and type of response can be proposed. Hence, this proposed method will be applied to estimate 15 single unknown forces acting on 15 discrete locations for a complete analysis. Note that the impact force determination is conducted to estimate an unknown force at a specific location for every impact force determination, and this procedure is repeated for 15 various locations.

In this research, the effectiveness of the proposed method by using an appropriate analysis frequency range and type of response is examined in the collocated and non-collocated cases. For the collocated case, the impact force determination is carried out by including at least a response sensor, which is close to the impact location. For the non-collocated case, the unknown impact force is estimated by using the sensors, which are far away from the impact location. In this study, 15 accelerometers are used to estimate an unknown force for the collocated case, while only 14 accelerometers (i.e. exclude the sensor that is close to the impact location) are used in non-collocated case.

The experimental configurations for the collocated and non-collocated cases are shown in Table 3.2. By using the proposed method, 15 sets of force determination result can be obtained for each collocated case and non-collocated case. The correlation coefficients between the identified force and measured force are calculated for both collocated and non-collocated cases. Hence the results are compared to the results of impact force determination with a conventional method (i.e. acceleration response for a fixed analysis frequency range of 0.5-999.5Hz).

Table 3.2:
Experimental Configurations for the Collocated and Non-Collocated Cases

Collocated Case		**Non-Collocated Case**	
Measured Responses Location	**Identified Force Location**	**Measured Responses Location**	**Identified Force Location**
All the 15 points	Point 1	14 points without point 1	Point 1
All the 15 points	Point 2	14 points without point 2	Point 2
⋮	⋮	⋮	⋮
All the 15 points	Point 15	14 points without point 15	Point 15

Chapter 4: Results and Discussion

4.1: Introduction

In this chapter, the results of enhancement of impact force determination with MTM by using integration and data filtering approaches are presented and discussed. Firstly, the results prior to impact force determination are presented. For example, the results of accelerance FRF measurement with its COH result are showed. Then, the result of modal parameters estimation by using the curve fitting algorithm such as the damped natural frequencies, modal damping and residue mode shapes are presented. Next, the accuracy of curve fitting result is examined by comparing the synthesised accelerance FRF or modal model build from the modal parameters and MTM. Besides, the correlation between the measured and synthesised accelerance FRFs indicates the accuracy of curve fitting result as well. Furthermore, condition number of 15 by 15 synthesised accelerance FRF matrix and 15 by 1 synthesised accelerance FRF vector are computed to indicate the condition of the matrix for cases that are with or without the priori information of force location.

In this study, force determination will be carried out for different types of responses. Thus, synthesised mobility and admittance FRFs must be obtained before the impact force determination. The result of the synthesis of accelerance, mobility and admittance FRFs are showed. Besides, the measured force is used for the verification purpose. It is assumed to be unknown and to be estimated through the impact force determination. The impact-induced acceleration responses, which are measured simultaneously at 15 locations, are presented as well. The velocity and displacement responses obtained from the single integration and double integration of the acceleration responses respectively are shown.

After obtaining results from FRF measurement and ODS analysis, impact force determination via MTM by using various types of responses was conducted to determine the unknown force. First of all, the impact force determination was carried out in the case of fixed analysis frequency range. The force determination result for under-estimated, even-estimated and over-estimated cases are presented and discussed. Combining the findings from these 3 cases, the ideal case of selecting an appropriate analysis frequency range is discussed. Then, selection of a good analysis frequency range based on the PSD tool is demonstrated. By the way, the elimination of high frequencies noise and intrinsic problem through the PSD tool is highlighted. Hence, the force determination result by using the PSD tool selected analysis frequency range is presented.

Furthermore, comparison between the force determination result by using fixed frequency range and PSD tool selected frequency range in various types of responses is conducted. This comparison enables the author to select and propose the most suitable type of response and analysis frequency range for impact force determination via MTM. Furthermore, the proposed method is used to identify 15 unknown impact forces that are acting on 15 various locations on the test rig for both collocated and non-collocated cases. The effectiveness of the proposed method is shown when comparing the correlation coefficient result to the conventional method one.

4.2: Results Prior to Impact Force Determination

4.2.1: FRF Measurement

In this study, the FRF measurement was done by using a reference force at a specific point (i.e. point 1 of the test rig) and 15 accelerometers. The accelerance FRF can be obtained by dividing the output acceleration response with the input force. By using 100

averages, measurement noise can be reduced. The imaginary part of 15 measured accelerance FRFs is shown in Figure 4.1 (a). The quality of the FRF measurement is indicated by the COH analysis as shown in Figure 4.1 (b). In fact, the FRF measurement is considered good for COH that is greater than 0.9. The quality of FRF measurement must be high especially at the natural frequencies regions because poor COH at these natural frequencies will affect the accuracy of force determination. In this study, it is found that the frequency range of 0.5-500.0Hz has COH value above 0.9. Note that the DC frequency (i.e. 0Hz) is not valid in this analysis, which is limited by the specification of accelerometer.

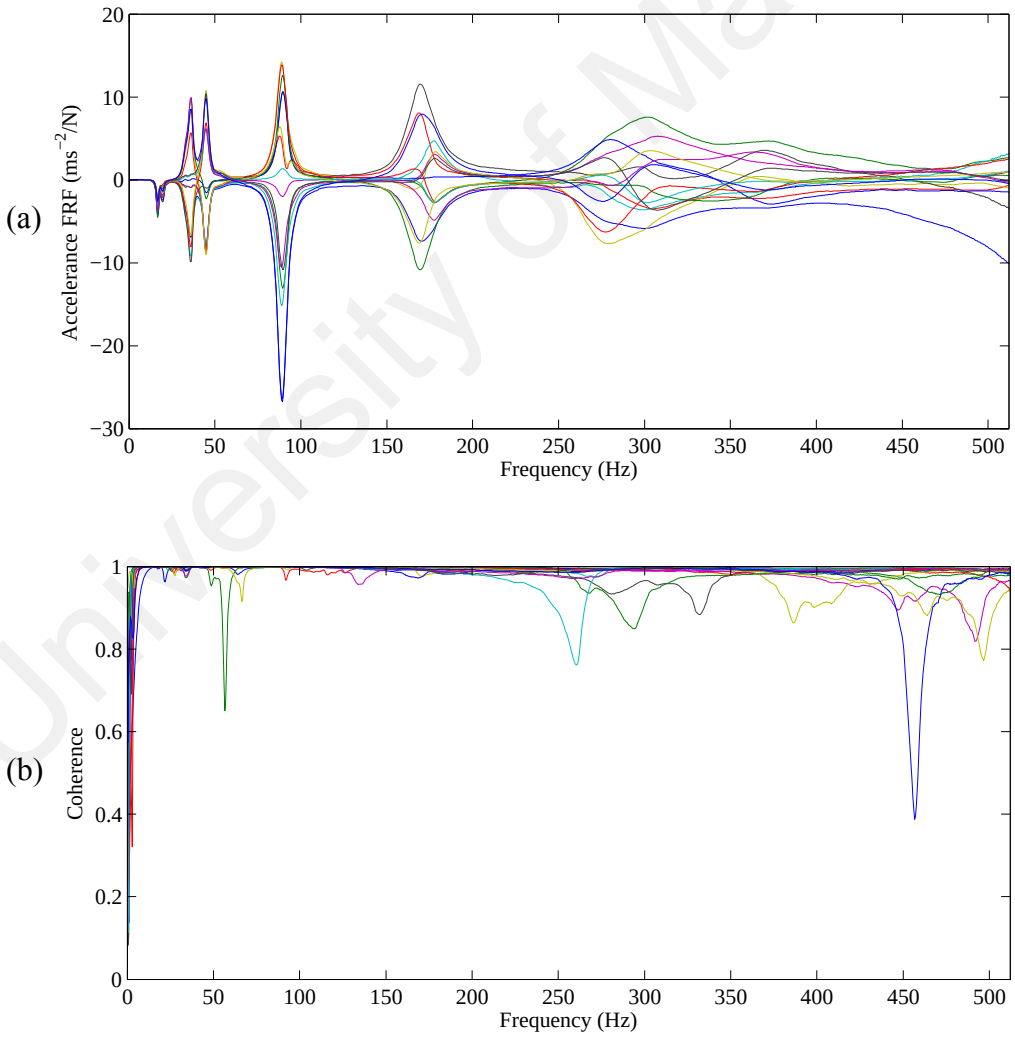

Figure 4.1:
FRF and COH Measurement Result: (a) Imaginary Part of 15 Measured Accelerance FRFs, (b) 15 Measured COHs due to Reference Force at Point 1

4.2.2: Modal Parameters Estimation

By using curve fitting algorithm such as Polynomial method, modal parameters for one or more modes can be estimated from the raw accelerance FRFs at a time. A total number of 9 modes have been extracted by using this method. The result of curve fitting consists of the damped natural frequency, modal damping and residue mode shapes. In fact, these modal parameters represent the dynamic characteristic of the test rig. The obtained damped natural frequencies and modal damping is shown in Table 4.1. The means of COHs for the accelerance FRFs measurement at all the modes are provided in Table. 4.1 as well to indicate the accuracy of the FRFs measurement. Since all the COHs at all the modes are greater than 0.9, thus it is considered that the accelerance FRF measurement is accurate for the mode extraction.

Table 4.1:
Damped Natural Frequencies and Modal Damping Extracted from Single Column FRF Matrix by Using Curve Fitting Algorithm with Their Respective COH Value

Mode	Damped Natural Frequency (Hz)	Modal Damping (%)	COH
1	16.7800	4.4488	0.9985
2	20.0060	6.0736	0.9992
3	36.6260	5.2989	0.9963
4	45.1690	4.5908	0.9975
5	89.5810	3.8190	0.9989
6	172.1700	4.3701	0.9910
7	276.0400	6.2063	0.9837
8	299.8900	7.4933	0.9863
9	363.7800	6.7644	0.9897

The obtained accelerance residue mode shapes are shown in Table A.1 in Appendix A. By using MTM, the accelerance residue mode shapes are converted to the accelerance UMM mode shapes. The accelerance UMM mode shapes are shown in Table A.2. Instead of accelerance UMM mode shape, the mobility and admittance UMM mode shapes are required for the force determination by using velocity and displacement responses. The mobility and admittance residue mode shapes can be obtained by using the conversion of the unit of residue as shown in Table 2.2. Hence, the mobility and admittance UMM mode shapes are obtained through MTM. The results are shown in Tables A.3 and A.4 respectively.

The graphical form of the mode shape is provided in Figure 4.2 for a better vision purpose. Figure 4.2 shows that the Perspex plate test rig consists of heaving mode (i.e. mode 1 and mode 2), rolling mode (i.e. mode 3) and pitching mode (i.e. mode 4). It contains all the significant vibration modes for the motions of a vehicle body in low frequency region. This shows that the test rig produces similar dynamic behaviour as in an actual vehicle body and it is suitable for impact force determination purpose.

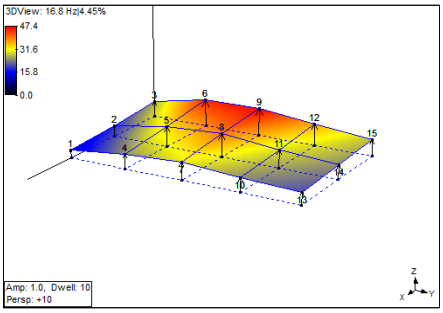

(a) Mode 1

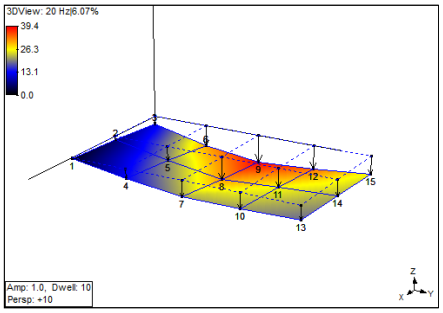

(b) Mode 2

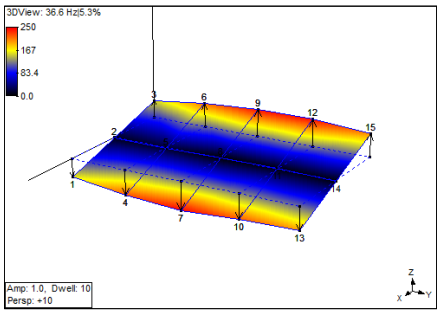

(c) Mode 3

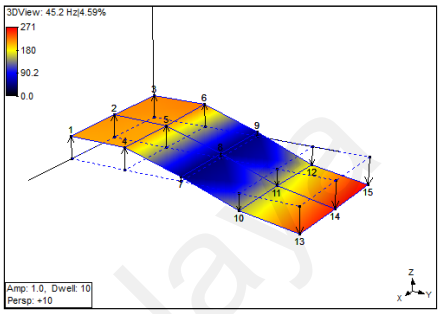

(d) Mode 4

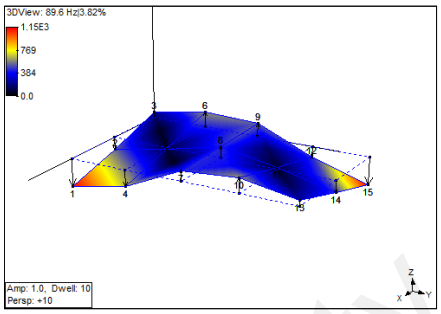

(e) Mode 5

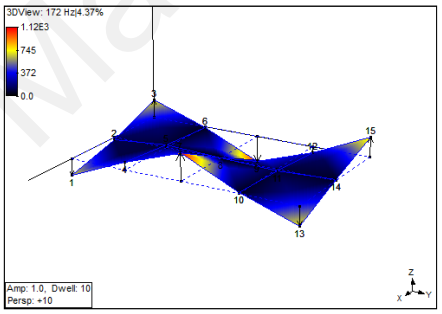

(f) Mode 6

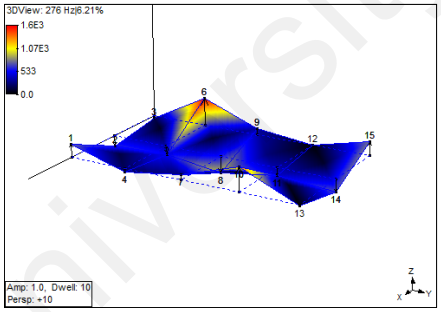

(g) Mode 7

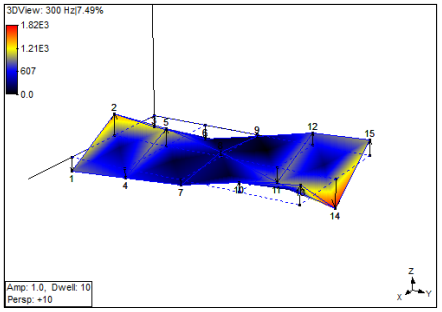

(h) Mode 8

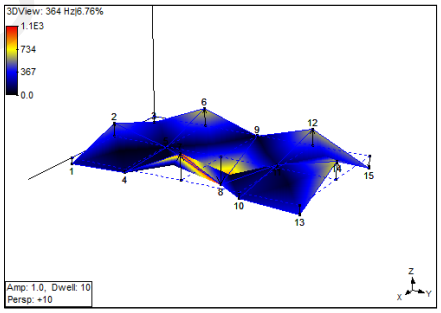

(i) Mode 9

Figure 4.2:
Mode Shape of the Test Rig: (a)-(i) Mode 1-9

4.2.3: Accuracy of Curve Fitting Result

4.2.3.1: Comparison between Synthesised and Measured FRFs

In fact, the accuracy of force determination via MTM primary depends on the accuracy of the FRF measurement and the curve fitting result. Extraction of modal parameters would be straightforward and easy, however fitting a modal model with the extracted modal parameters has some limitations. This modal model is known as the synthesised FRF in this study. The comparison between the mean of 15 synthesised and measured accelerance FRFs due to force DOF 1 in the Cartesian domain is shown in Figure 4.3.

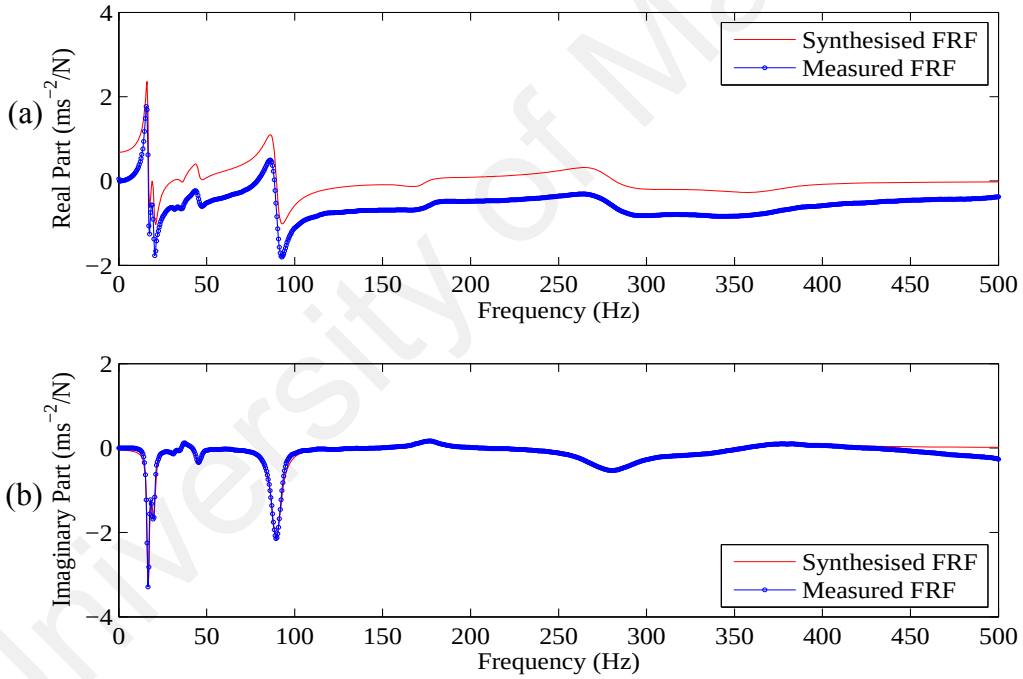

Figure 4.3:
Comparison between Synthesised and Measured Accelerance FRFs in Cartesian Domain: (a) Real Part, (b) Imaginary Part

It is found that there is an offset between the real part of the measured and synthesised data. This bias is due to out-of-band mode contribution, accounted by using extra polynomial terms. However, the shape and magnitude of the imaginary part of the synthesised data closely match the measured data in the frequency range of 0.5-

500.0Hz. Vibrant Technology stated that the modal parameters are still considered accurate in the frequency range 0.5-500.0Hz since the imaginary parts of the synthesised FRF match the "shape" of measured FRF (Vibrant Technology, 2001).

4.2.3.2: Correlation between Synthesised and Measured FRFs

The cumulative summation of correlation between the mean of synthesised and measured data is plotted in Figure 4.4 for the real part, imaginary part and for overall (i.e. real plus imaginary parts). It is found that the correlation for a 0.5-500.0Hz analysis frequency range has an overall value of 0.4297 only. The low correlation is due to the bias in real part. This fitting error may reduce the accuracy of force determination and it is required to take action to compensate with this fitting error. The correlation for 0.5-100.1Hz and 0.5-999.5Hz fixed analysis frequency ranges are also shown in Table 4.2 for reference purpose. In overall, 0.5-100.1Hz analysis frequency range has the best correlation followed by the 0.5-500.0Hz and 0.5-999.5Hz.

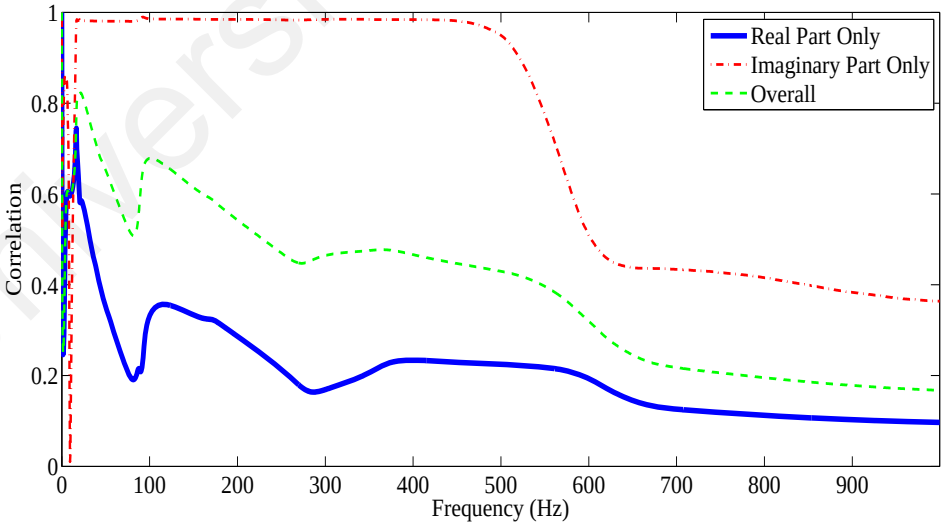

Figure 4.4:
Graph of Cumulative Summation of Correlation between Mean of Synthesised and Measured Accelerance FRFs in Cartesian Domain

Table 4.2:
Correlation between Synthesised and Measured FRFs for Different Fixed Analysis Frequency Ranges in Cartesian Domain

Frequency Range	0.5-100.1Hz	0.5-500.0Hz	0.5-999.5Hz
Real Part	0.3316	0.2245	0.0969
Imaginary Part	0.9858	0.9494	0.3639
Overall	0.6785	0.4297	0.1676

4.2.4: Condition Number of Synthesised FRF

The cumulative summation of condition number graphs of the 15 by 15 synthesised accelerance FRFs matrix and 15 by 1 synthesised accelerance FRFs matrix due to force DOF 1 are shown in Figures 4.5 and 4.6 respectively. The condition number graphs of other force DOFs for various types of FRFs such as the mobility and admittance FRFs are similar and hence they are not shown in this study. Without the knowledge of impact force location in advance, the force is estimated at 15 locations. In fact, actual force excited at one of the 15 locations, leaving forces at other locations to be zero. In this case, the calculated condition number of this 15 by 15 synthesised accelerance FRFs matrix is very high (i.e. power of 18). This is known as ill-posed problem where small error can be amplified and causes meaningless force identification result.

With priori information of impact location, the force DOF can be selected for the synthesised accelerance FRFs. The calculated condition number of this 15 by 1 synthesised accelerance FRFs vector is equal to 1 for whole frequency range. Thus the impact force determination is well-posed. In this study, the impact location is assumed known in advance, only the time history of the force is unknown and will be reconstructed by using MTM pseudo-inverse technique.

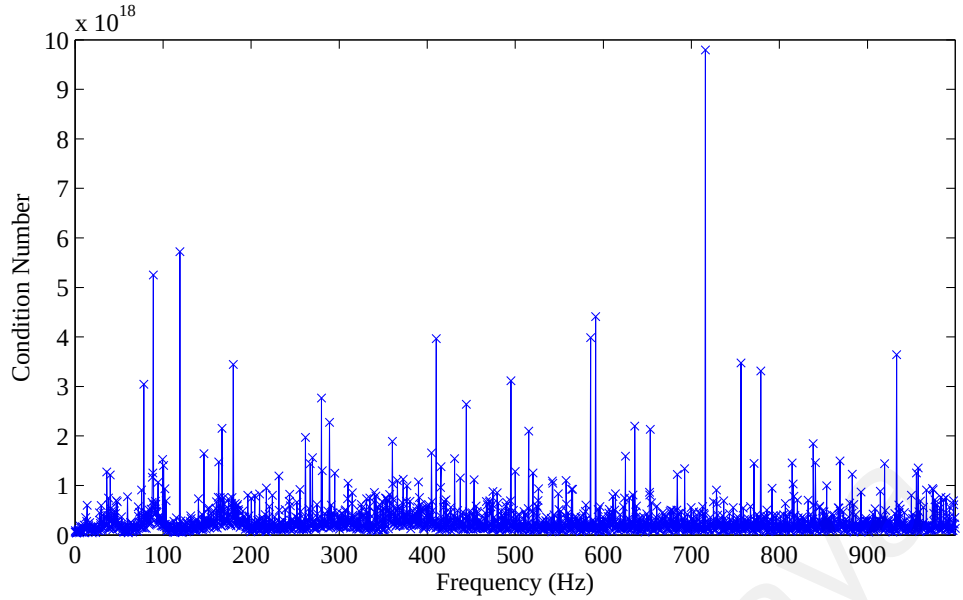

Figure 4.5:
Graph of Condition Number of 15 by 15 Synthesised Accelerance FRFs Vector due to Force DOFs 1-15 versus Frequency

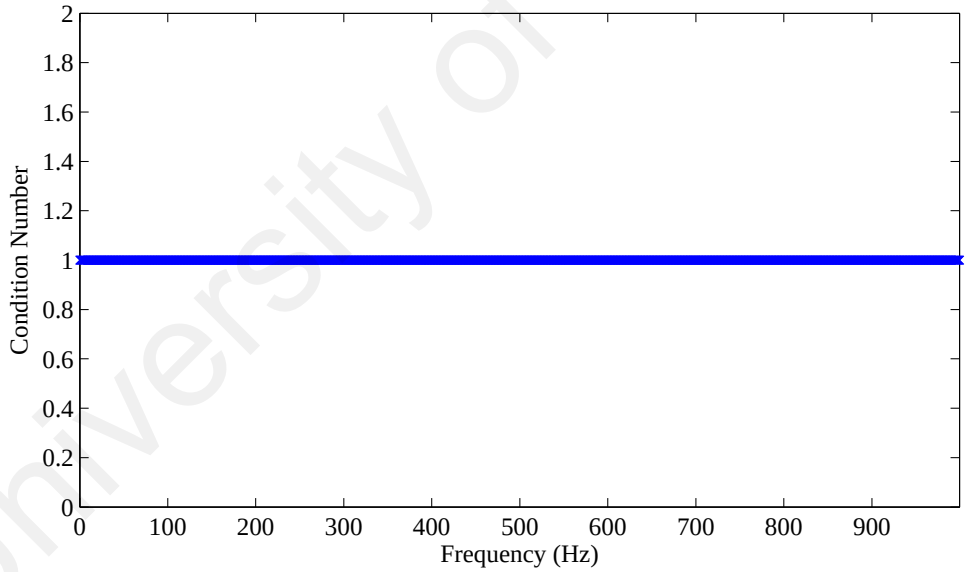

Figure 4.6:
Graph of Condition Number of 15 by 1 Synthesised Accelerance FRFs Vector due to Force DOF 1 versus Frequency

4.2.5: Synthesised Accelerance, Mobility and Admittance FRFs

From Section 4.2.2, modal parameters such as damped natural frequencies, modal damping plus accelerance, mobility and admittance UMM mode shapes were obtained through Polynomial curve fitting method. These parameters are essential to synthesise the accelerance, mobility and admittance FRFs due to specific force DOF through MTM. Note that this force DOF is related to the identified impact location, i.e. to estimate an unknown force at point 1 requires the synthesised FRF due to force DOF 1. Positive half spectrums of the synthesised accelerance, mobility and admittance FRFs due to force DOF 1 are shown in Figure 4.7. In fact, complex spectrum of a real signal consists of a 2-sided spectrum (i.e. positive and negative half spectrums). Both half spectrums are symmetrical around DC. Thus, the negative half spectrum is redundant and it not shown here. The result for the other force DOF is not shown here because the pattern is similar.

Figure 4.7 (a) shows that the synthesised accelerance FRF is sensitive at high range of frequency. The mobility FRF and admittance FRF are sensitive in a moderate and low frequency ranges respectively as shown in Figures 4.7 (b) and (c). In fact, accelerance, mobility and admittance FRFs have the units proportional to the units of acceleration, velocity and displacement respectively. The transformation from accelerance FRF to mobility and admittance FRFs involves integration method which possesses low pass characteristic. Therefore, the gain at high frequency region for the admittance FRF is the lowest, followed by mobility and accelerance FRFs.

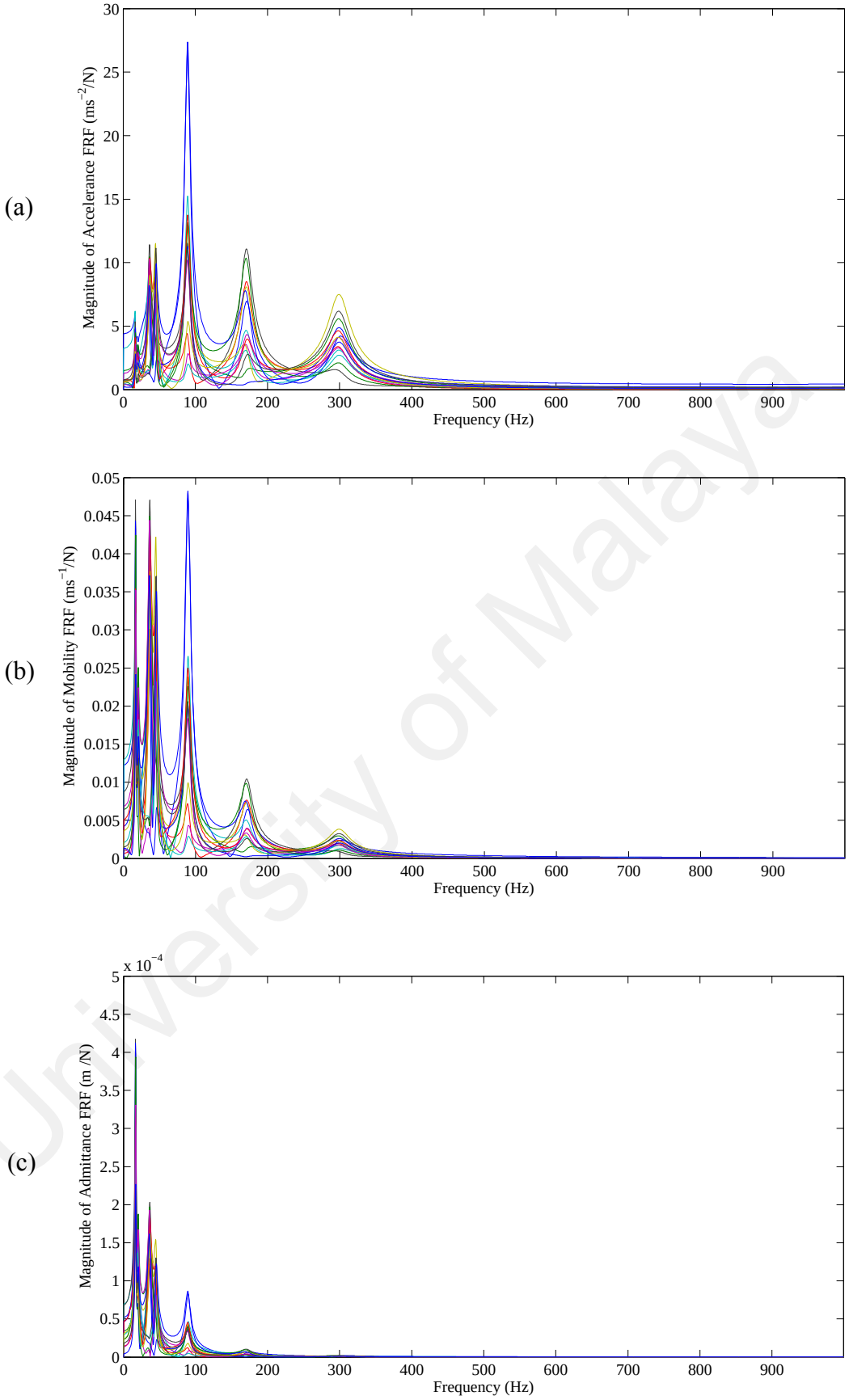

Figure 4.7:
Graph of Various Synthesised FRFs in Frequency Domain: (a) Accelerance, (b) Mobility, (c) Admittance

4.2.6: Measured Force and the Impact-Induced Responses

Firstly, a modally tuned impact hammer with force transducer at its tip was used to excite the test rig at point 1. By using ODS analysis, the impact force acting on the rectangular plate is measured simultaneously with the acceleration responses of the structure at 15 discrete locations. The results of measured force and the impact-induced responses are shown in Figure 4.8. The amplitude of impact force is 31.927N and its impact duration is around 0.009s as shown in Figure 4.8 (a). The measured impact force with magnitude of 31.927N is assumed unknown and will be recovered from known responses by using impact force determination. The measured force is used to verify the force identified by impact force determination. All the measured acceleration responses diminished to zero within 0.4s due to damping effect as shown in Figure 4.8 (b).

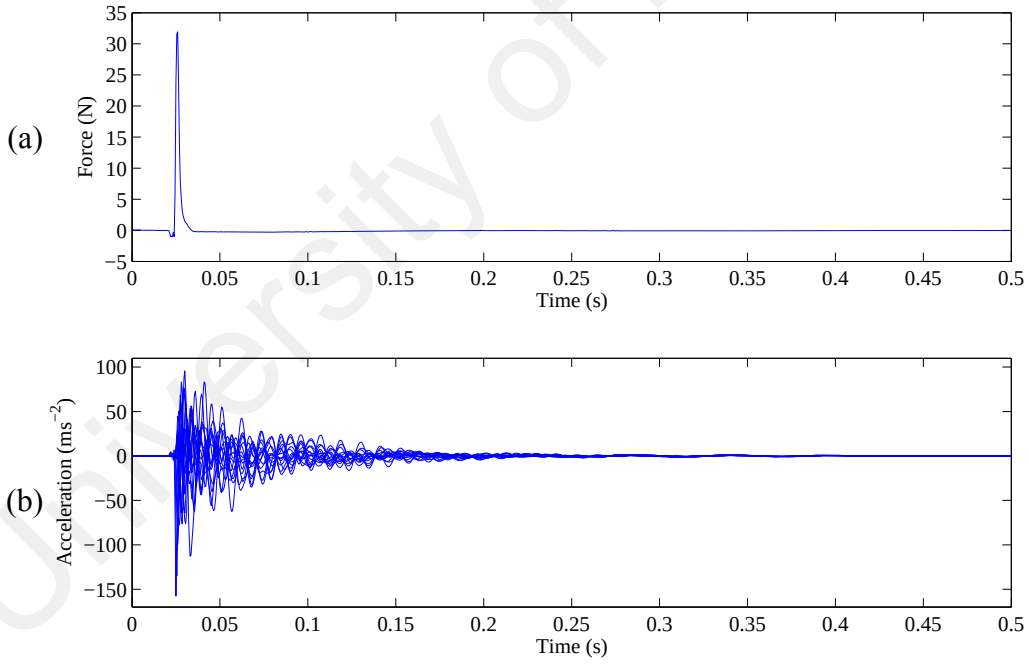

Figure 4.8:
Graph of Measured Input Force and Output Responses in Time Domain: (a) Original Impact Force Exciting at Point 1, (b) Measured Responses at 15 Discrete Locations on Test Rig

4.2.7: Integration of Acceleration Responses in Frequency Domain

Measured acceleration responses in time domain were transformed into frequency domain by using DFT, computed with FFT algorithm as followed Eq. (2.51). By using integration and double integration in frequency domain as followed Eqs. (2.55) and (2.56) respectively, measured acceleration signals were converted to velocity and displacement signals separately as shown in Figure 4.9.

Positive half spectrums of acceleration, velocity and displacement responses in frequency domain are plotted in Figures 4.9 (a), (b) and (c) respectively. It is found that gain of a signal is significant in relatively large frequency range in terms of acceleration, moderate frequency range in terms of velocity, and relatively small frequency range in terms of displacement. This is because the sensitivity of various responses is different in different frequency range. For example, the acceleration responses are more sensitive at high frequencies than at low frequencies (Karrenberg, 2002). Velocity responses are evenly sensitive and displacement responses are more sensitive at low frequencies than at high frequencies (Karrenberg, 2002).

The sensitivity characteristics of various types of responses are different, therefore it is valuable to examine their performances in the impact force determination with MTM. Furthermore, integrated signals such as velocity and displacement signals possess a low pass characteristic in nature (Karrenberg, 2002). Thus, they are used to reduce the noise effect in high frequency region so that the conventional impact force determination with MTM by using measured acceleration signal can be enhanced.

(a)

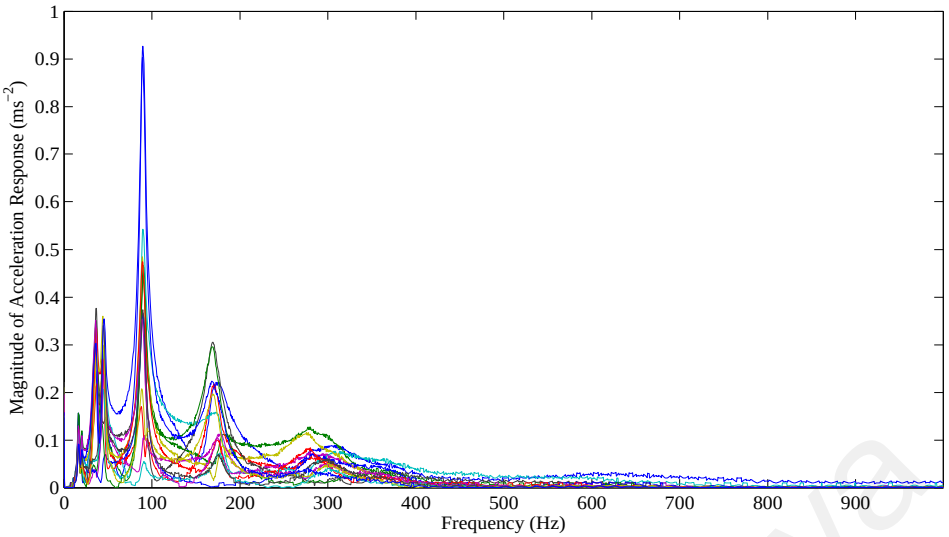

(b)

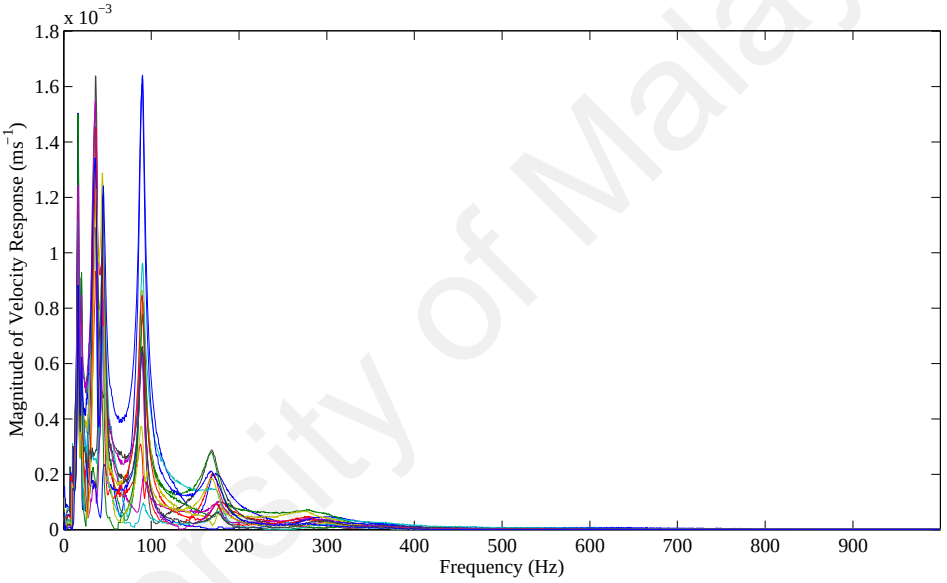

(c)

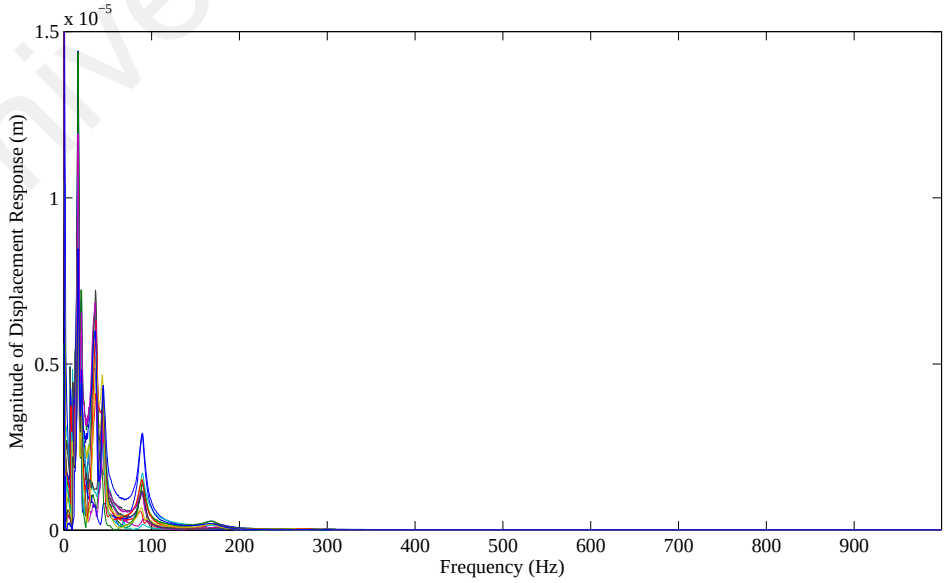

Figure 4.9:
Graph of Various Types of Responses in Frequency Domain: (a) Acceleration, (b) Velocity, (c) Displacement

4.3: Impact Force Determination via MTM by Using Various Types of Responses

4.3.1: Fixed Analysis Frequency Range

By using various types of responses, the impact force determination via MTM is conducted in the fixed analysis frequency range. The effectiveness of different types of responses is examined in 3 cases: under-estimated case, even-estimated case and over-estimated case. Since the excitation frequency range of impact force acting on point 1 is around 0.5-500.0Hz, the fixed analysis frequency ranges are chosen as 0.5-100.1Hz, 0.5-500.0Hz and 0.5-999.5Hz for under-estimated case, even-estimated case and over-estimated case respectively. The identified forces are compared with the measured forces in both time and frequency domains. Besides, force correlogram and correlation coefficient are used for quantitative results.

4.3.1.1: Force Determination for Under-Estimated Case

For the under-estimated case, a fixed analysis frequency range of 0.5-100.1Hz is used. The results are shown in Figures 4.10-4.12. It shows that all the identified forces do not match well with the measured forces in time domain as shown in Figure 4.10 (a), 4.11 (a) and 4.12 (a). However in frequency domain, it is found that the identified force from displacement response matches well with the measured force compared to the forces estimated by using other types of responses as shown in Figure 4.10 (b), 4.11 (b) and 4.12 (b). The force correlograms between the identified forces and the measured forces in under-estimated case are shown in Figure 4.13. Identified data fall within ±10% from the actual value are considered good and acceptable (Liu & Shepardjr, 2005). Considering the measurement noise effect and the curve fitting error, this offset value is adopted in this study, which is set at around ±3.2N since the maximum measured force is 31.927N.

In the under-estimated case, all the correlation coefficients between the measured forces and the identified forces by various types of responses are low, which are around 0.67-0.72. This shows that the agreement between identified forces and the measured forces is bad and hence not satisfied. Impact force determination shall be avoided to be carried out in the under-estimated case because this type of impact force determination is not accurate. In fact, the identified force by MTM is the summation of mode contribution distributing along the frequency region. Since there is a truncation of important mode contributing to the estimation of the identified force, the identified force will be under-estimated. This explains why all the identified forces by all types of responses are less than the measured forces.

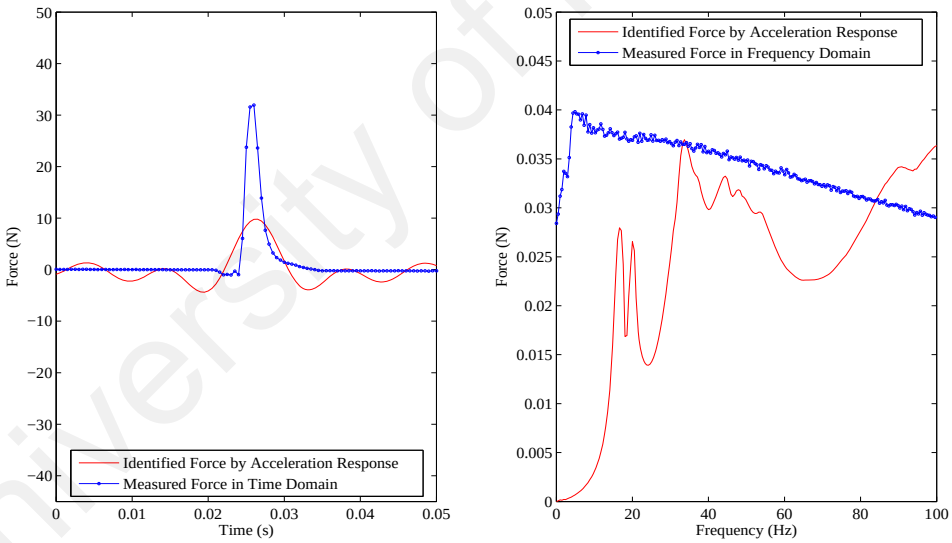

(a) (b)

Figure 4.10:
Graph of Comparison between Identified Force by Acceleration Response and Measured Force at Point 1 in the 0.5-100.1Hz Analysis Frequency Range: (a) Time Domain, (b) Frequency Domain

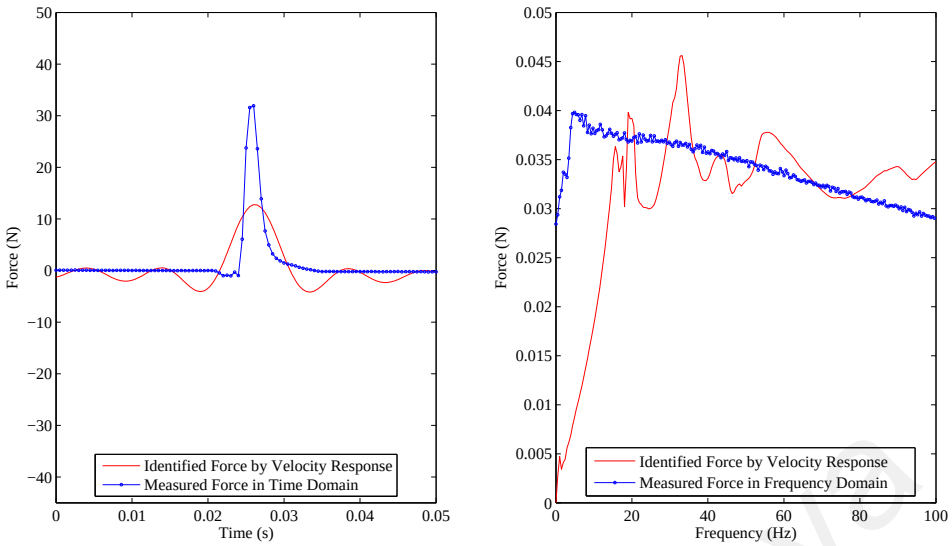

Figure 4.11:
Graph of Comparison between Identified Force by Velocity Response and Measured Force at Point 1 in the 0.5-100.1Hz Analysis Frequency Range: (a) Time Domain, (b) Frequency Domain

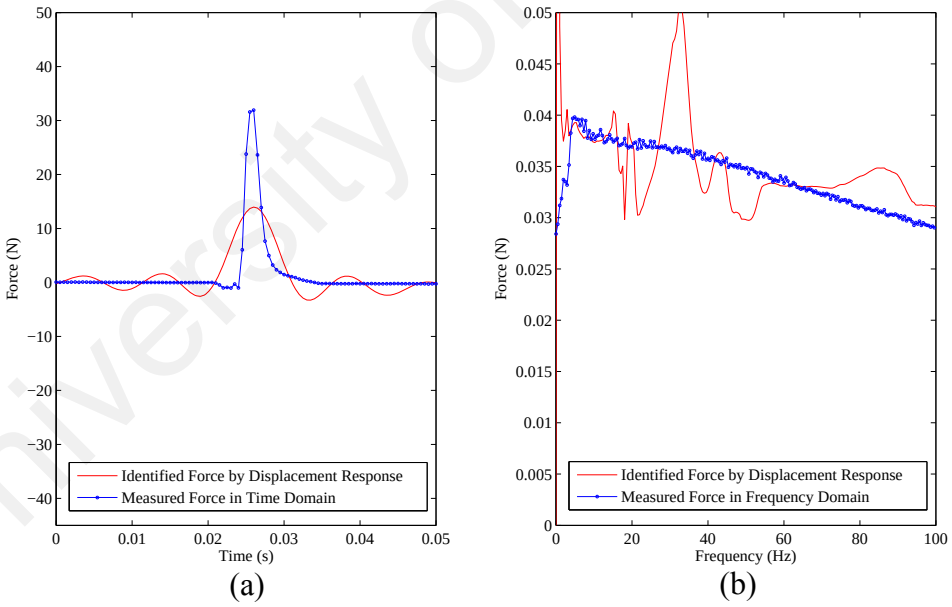

Figure 4.12:
Graph of Comparison between Identified Force by Displacement Response and Measured Force at Point 1 in the 0.5-100.1Hz Analysis Frequency Range: (a) Time Domain, (b) Frequency Domain

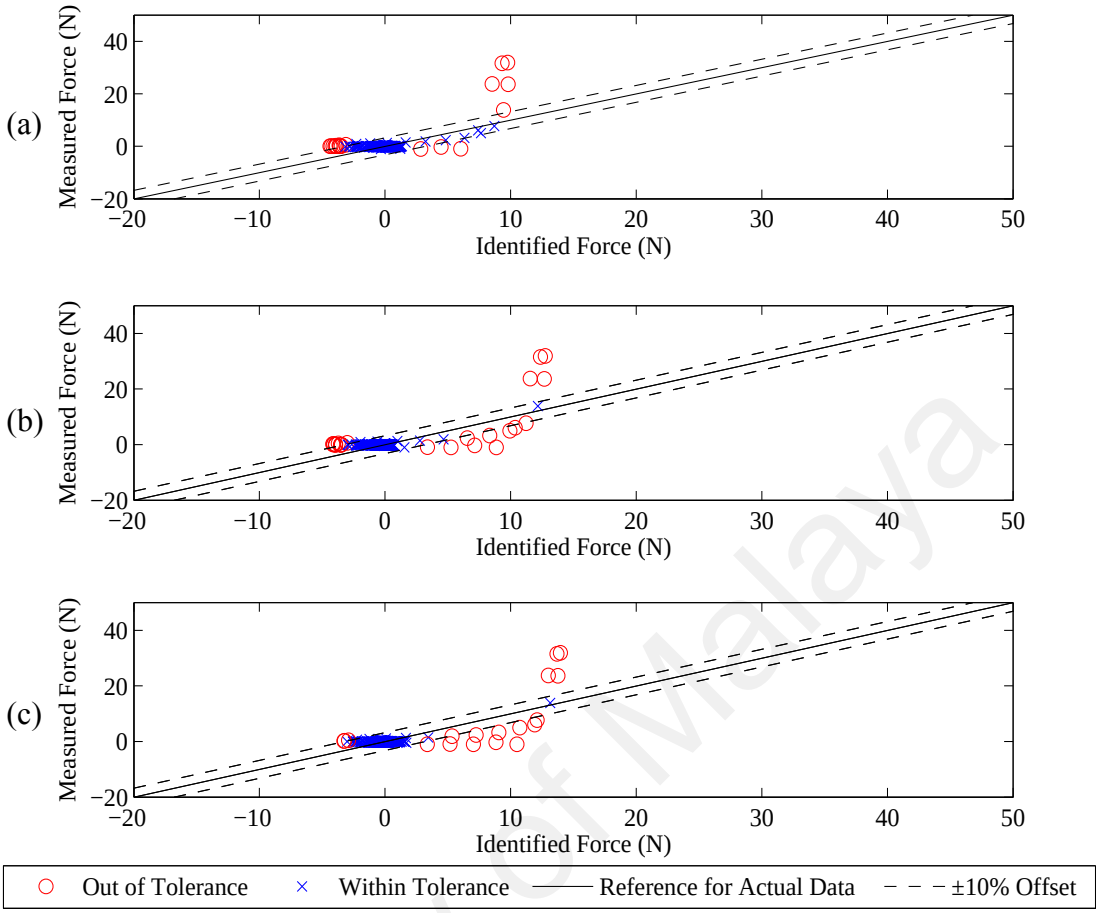

Figure 4.13:
Force Correlogram by Using Different Types of Responses in a Fixed 0.5-100.1Hz Analysis Frequency Range: (a) Acceleration, (b) Velocity, (c) Displacement

4.3.1.2: Force Determination for Even-Estimated Case

For the even-estimated case, the force determination was carried out by using a fixed analysis frequency range which is similar to the actual excitation frequency range (i.e. 0.5-500.0Hz). The comparison between the measured forces with the identified forces by acceleration, velocity and displacement responses in both time and frequency domains are shown in Figures 4.14-4.16. It is found that all the identified forces in time domain agree well to the measured forces in time domain. For acceleration feedback, it is found that the identified force result is affected by noise in high frequency region as shown in Figure 4.14 (b). The velocity unit obtained from single integration and displacement unit obtained from double integration are able to reduce the noise effect as

shown in Figures 4.15 (b) and 4.16 (b). In the frequency domain, it is found that the displacement feedback results in better force determination result.

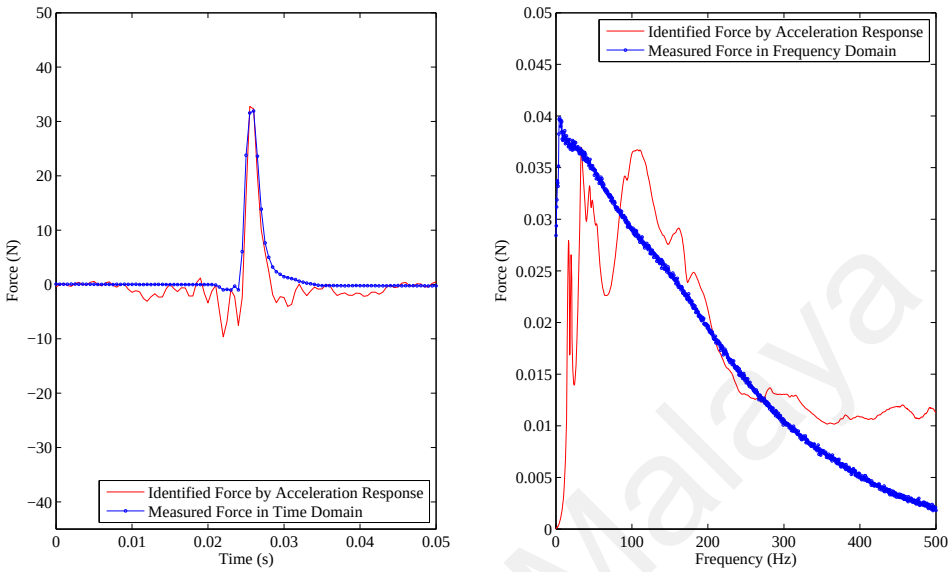

(a) (b)

Figure 4.14:
Graph of Comparison between Identified Force by Acceleration Response and Measured Force at Point 1 in the 0.5-500.0Hz Analysis Frequency Range: (a) Time Domain, (b) Frequency Domain

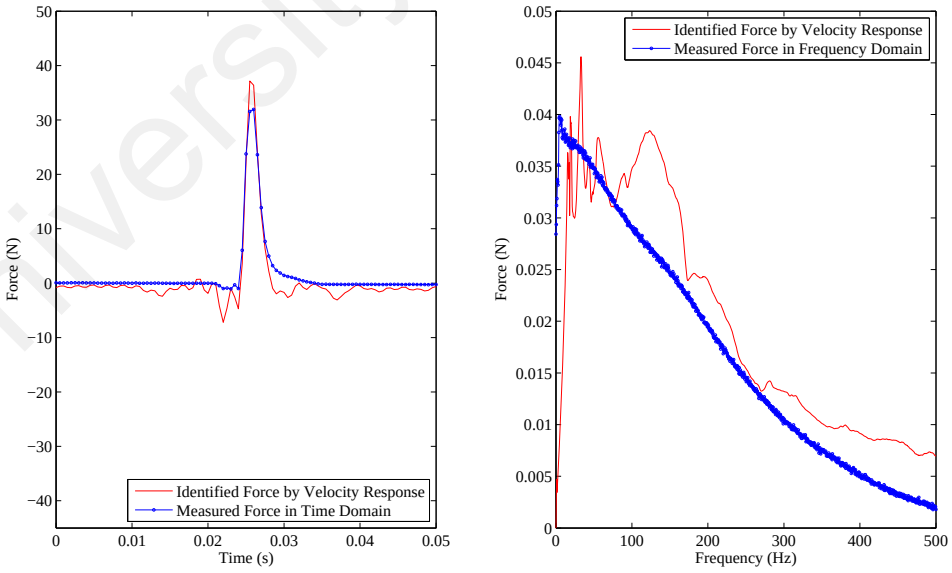

(a) (b)

Figure 4.15:
Graph of Comparison between Identified Force by Velocity Response and Measured Force at Point 1 in the 0.5-500.0Hz Analysis Frequency Range: (a) Time Domain, (b) Frequency Domain

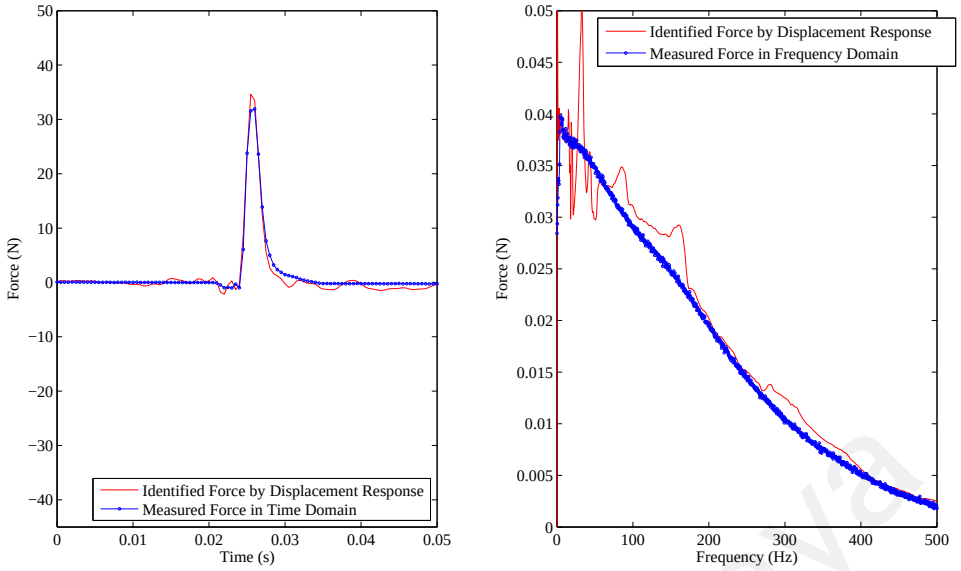

Figure 4.16:
Graph of Comparison between Identified Force by Displacement Response and Measured Force at Point 1 in the 0.5-500.0Hz Analysis Frequency Range: (a) Time Domain, (b) Frequency Domain

The force correlograms for the identified forces and measured forces in time domain are plotted in Figure 4.17. It is found that acceleration feedback has the largest number of points that is out of tolerance, followed by velocity and displacement feedbacks. All the correlation coefficients between measured forces and the identified forces by all types of responses in time domain are above 0.9. This shows that the identified forces agree well with the measured data. In overall, results show that the displacement is the most suitable type of response for the impact force determination via MTM in even-estimated case.

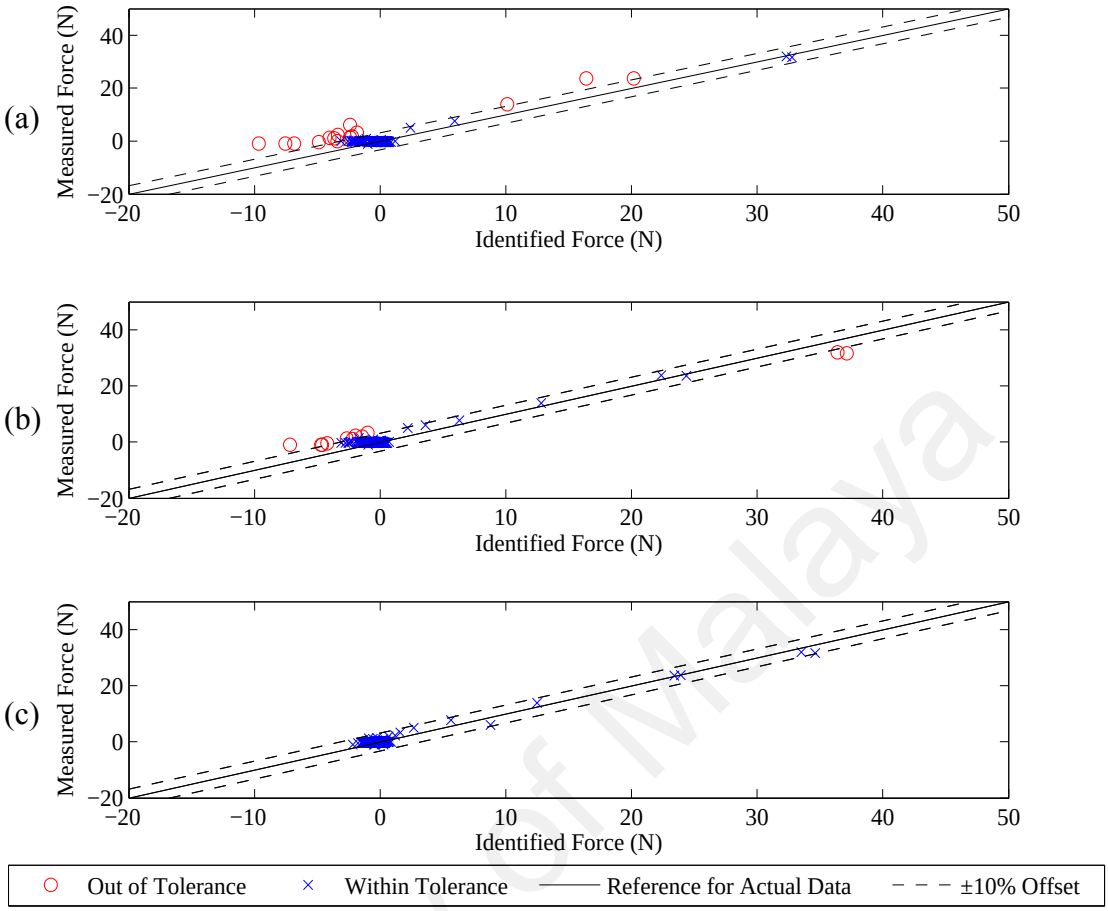

Figure 4.17:
Force Correlogram by Using Different Types of Responses in a Fixed 0.5-500.0Hz Analysis Frequency Range: (a) Acceleration, (b) Velocity, (c) Displacement

4.3.1.3: Force Determination for Over-Estimated Case

For the under-estimated case, a fixed analysis frequency range of 0.5-100.1Hz is used. In this case, the force determination results by various types of responses are shown in Figures 4.18-4.20.

For the acceleration feedback, the force determination result is inaccurate in time domain since it has a lot of large oscillating components as shown in Figure 4.18 (a). From the Figure 4.18 (b), it is found that the identified force does not match with the measured force especially in high frequency region above actual excitation frequency.

This inaccuracy of force determination is primarily due to measurement noise of response data and the low quality of synthesised FRF (i.e. 0.5-999.5Hz analysis frequency range has the worst correlation as shown in Section 4.2.3.2). As mentioned earlier, acceleration unit is sensitive in high frequency region. Thus, the contamination of noise occurs in high frequency region will be amplified during the impact force determination when acceleration unit is used.

For the velocity feedback as shown in Figure 4.19, the force determination result matches better with the measured force in time domain and frequency domain. There is some small oscillating components appear in the identified force result as shown in Figure 4.19 (a). The contribution of these noise elements can be observed by analysing the identified force in the frequency domain as shown in Figure 4.19 (b). It is found that the identified force is inaccurate especially in frequency region above the actual excitation frequency where the noise contamination is the highest.

For the displacement feedback, it is found that the identified force matches very well with the measured force with no oscillating component as shown in Figure 4.20 (a). The noise effect of identified force in frequency domain especially the high frequency region is minimized. Besides, it is found that the identified force agrees very well with the measured force in frequency domain as shown in Figure 4.20 (b).

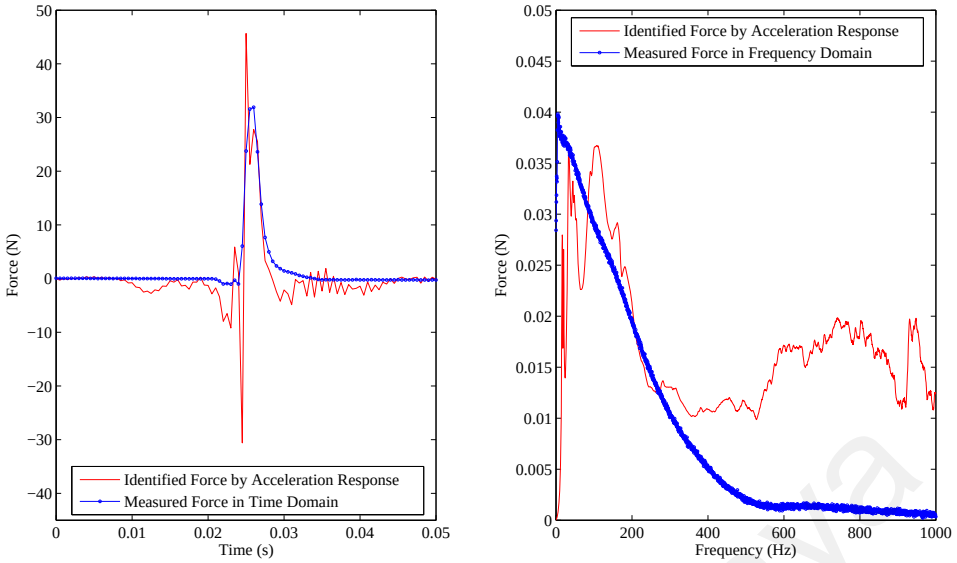

(a) (b)

Figure 4.18:
Graph of Comparison between Identified Force by Acceleration Response and Measured Force at Point 1 in the 0.5-999.5Hz Analysis Frequency Range: (a) Time Domain, (b) Frequency Domain

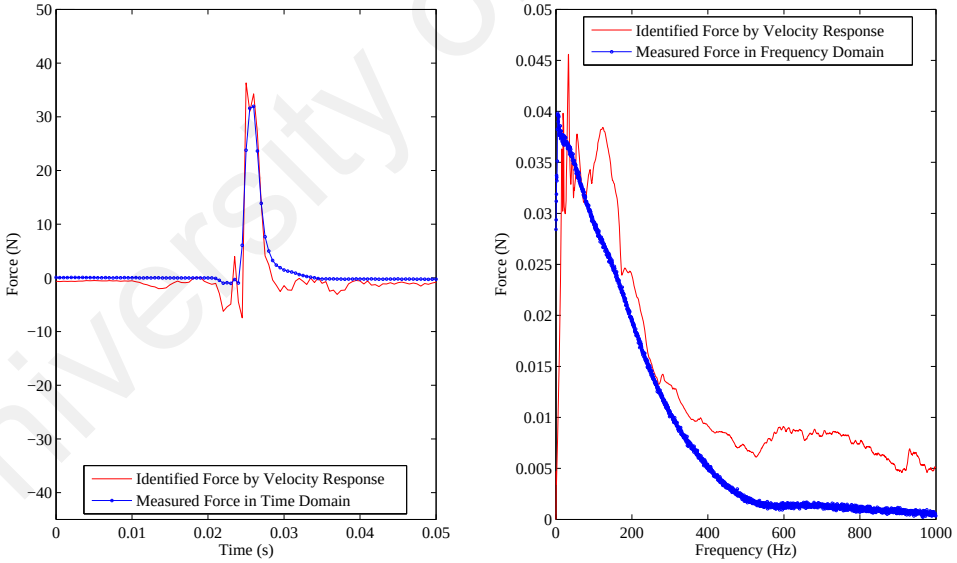

(a) (b)

Figure 4.19:
Graph of Comparison between Identified Force by Acceleration Response and Measured Force at Point 1 in the 0.5-999.5Hz Analysis Frequency Range: (a) Time Domain, (b) Frequency Domain

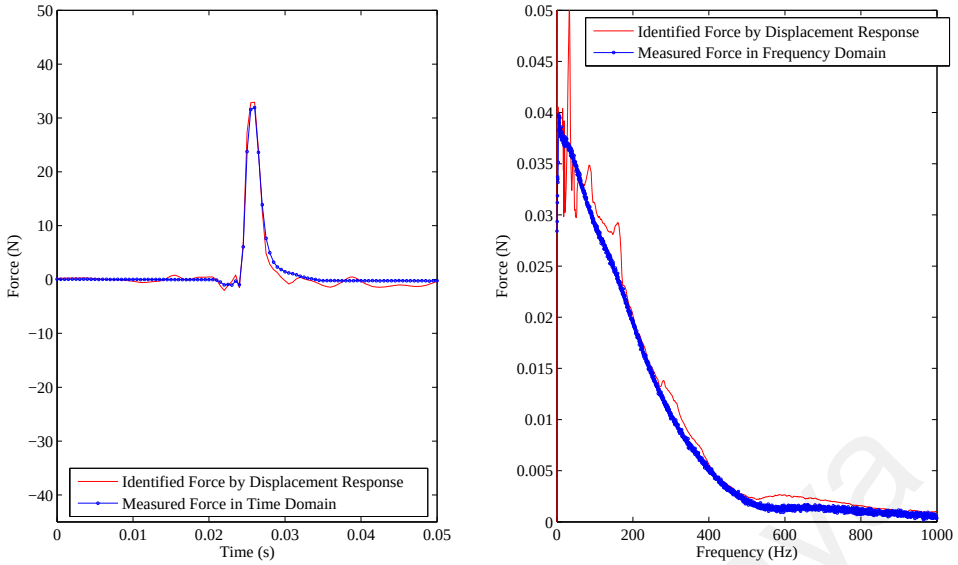

Figure 4.20:
Graph of Comparison Between Identified Force by Displacement Response and Measured Force at point 1 in the 0.5-999.5Hz Analysis Frequency Range: (a) Time Domain, (b) Frequency Domain

Next, the force correlograms between identified forces and measured forces in over-estimated case are shown in Figure 4.21. It is found that acceleration feedback has the largest number of points that is out of tolerance, followed by velocity and displacement feedbacks. Surprisingly, the identified force by using displacement response has the best accuracy with only one point slightly out of the tolerance. Moreover, the acceleration feedback has the worst correlation coefficient (i.e. 0.74). The correlation coefficients between measured force and the identified force by velocity and displacement feedback in time domain are above 0.90 and are within acceptable range.

In overall, results show that the displacement is the most suitable type of response in fixed 0.5-999.5Hz analysis frequency range where the analysis frequency range is much higher than the excitation frequency range. In fact, contamination of noise occurs in high frequency region and the noise effect is significant to impact force determination result, especially for the acceleration feedback as shown in Figure 4.18. It is found that

displacement unit obtained from double integration is superior to the other units (i.e. velocity and displacement units) for the impact force determination via MTM in over-estimated case. The insensitive behaviour of a displacement unit in high frequency region helps to reduce the effect of noise in high frequency. Displacement unit is more sensitive in low frequency region as the unknown impact force has the highest mode contribution in low frequency region, this explains why a displacement feedback has the best force determination result. Therefore, it is suggested to use displacement response to estimate unknown impact force via MTM in over-estimated case.

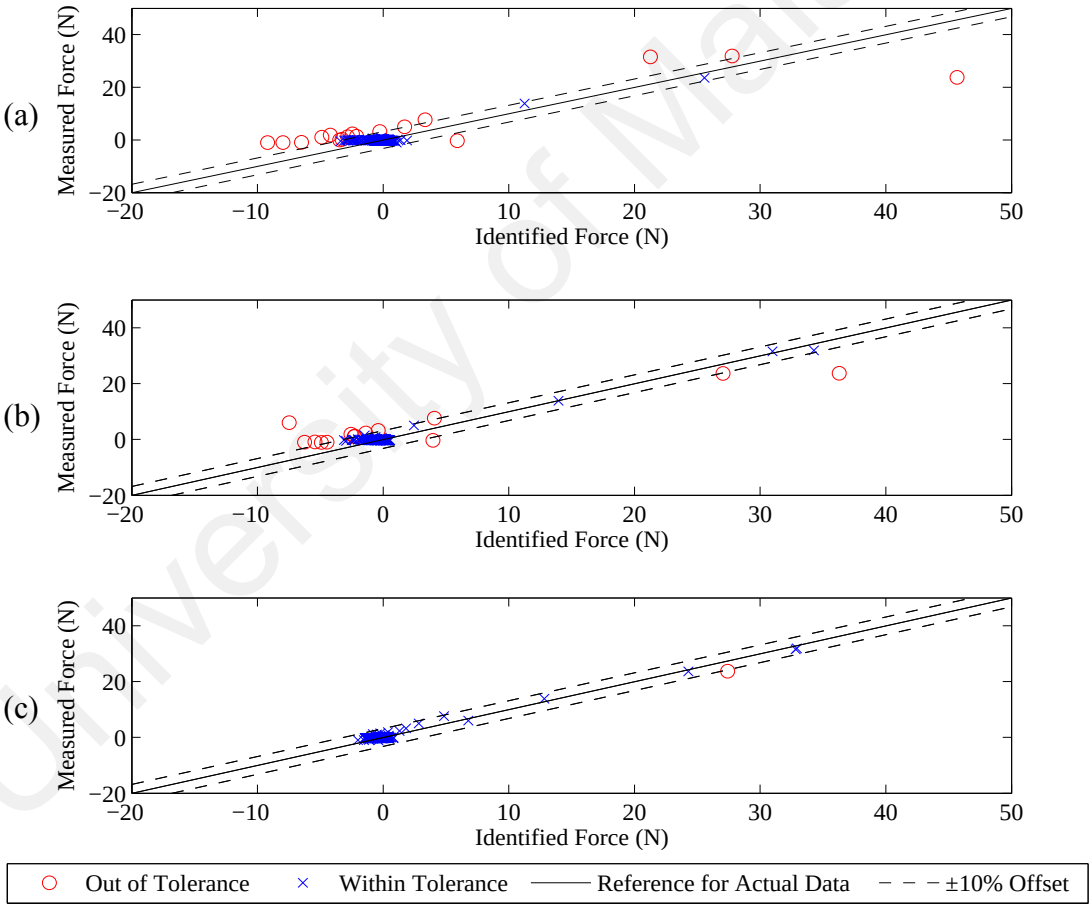

Figure 4.21:
Force Correlogram by Using Different Types of Responses in a Fixed 0.5-999.5Hz Analysis Frequency Range: (a) Acceleration, (b) Velocity, (c) Displacement

4.3.1.4: Force Determination for Ideal Case

Combining force determination results for under-estimated, even-estimated and over-estimated cases, several important findings are summarised and listed as follows:

i. The analysis frequency range must contain the entire significant excitation regions, or else the force determination by using various types of responses will be inaccurate eventually.
ii. If the analysis frequency range is close to the actual excitation region, the force determination result by using various types of responses will have a satisfied accuracy.
iii. If the analysis frequency range is too broad and it contains a lot of noise especially in the high frequency region, displacement is the best vibration unit for the impact force determination via MTM.

The force determinations in 3 cases of fixed analysis frequency range were conducted by knowing the actual excitation frequency in advance. However the actual excitation frequency is unknown in nature. Besides, the excitation frequency of an unknown impact force may be time-variant, which may change from time to time depends on the impact condition (Halvorsen & Brown, 1977). In this case, it is very hard to determine and justify which analysis frequency range is suitable for the impact force determination. Therefore, an effective tool to select an ideal analysis frequency range must be obtained to further enhance the force determination procedure.

In fact, an ideal analysis frequency range can be defined as the frequency range that contains all excitation force regions and without any contribution of noise inside the analysis frequency range. However this would be practically hard to achieve in real

applications. In real situation, at least a good analysis frequency range including a significant and highly contributed excitation frequency region with allowable amount of noise contamination must be obtained to ensure an accurate force determination result. Details on the technique to obtain a good analysis frequency range will be discussed in Section 4.3.2.

4.3.2: PSD Tool Selected Analysis Frequency Range

In this study, selection of a good analysis frequency range for impact force determination via MTM is done by using a PSD tool. The PSD tool consists of the residual analysis, acceleration PSD and normalised total power of response PSD. In general, a good analysis frequency range for impact force determination must have an optimum cut-off frequency of low pass filter to eliminate the noise at high frequency region. There are 2 main criteria that these cut-off frequencies must follow:

i. The cut-off frequency must not be too high, or else high amount of unwanted noise will be included.
ii. The cut-off frequency must not be too low, or else signal distortion will occur.

4.3.2.1: Residual Analysis

From the residual analysis of raw acceleration response in frequency domain, the low pass frequency can be selected. In this study, 15 raw acceleration responses were used to estimate the unknown force. The mean of these data is used for the residual analysis. By using the Eq. (2.60), the residual can be calculated in the function of frequency. The residual data versus the frequency are plotted in Figure 4.22. Theoretically, the cut-off frequency is a reasonable selection of frequency which balances the amount of noise and signal distortion. With proper following the procedure of the residual analysis, the

cut-off frequency is found at the interception between the horizontal intercept line and the sampled data. It is 451.2Hz. Next, this cut-off frequency is plotted in the PSD graph in order to get the threshold line for the differentiation between the high power contributed and low power contributed frequency region.

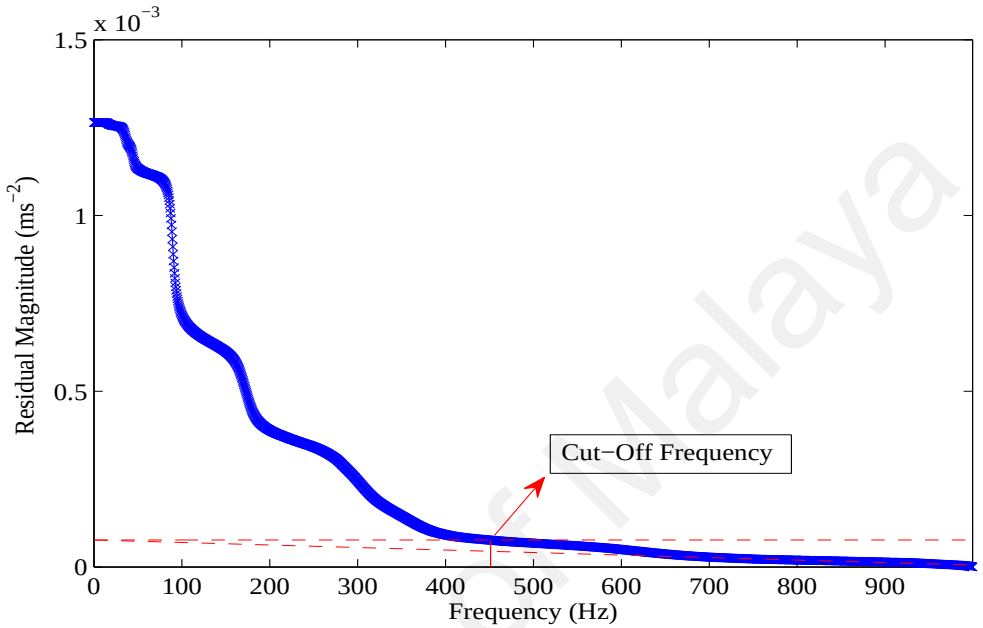

Figure 4.22:
Residual Analysis for the Determination of an Appropriate Cut-Off Frequency by Using Mean of 15 Raw Acceleration Responses

4.3.2.2: PSD of Acceleration Response

In this study, the impact excitation frequency was unknown. However, it is well-known that the excitation characteristic of impact force in the frequency domain is broadband and diminishing with increasing frequency. In other words, the impact force will eventually excite several modes of a structure simultaneously in the frequency domain. The excited modes will appear as peaks represented in the PSD graph.

By using Eq. (2.61), the acceleration PSD can be calculated by using the mean of 15 measured acceleration responses in frequency domain. The result is shown in Figure 4.23. It was chosen to analyse the PSD data in decibel scale because decibel scale

provides a clearer vision of the data compared to linear scale. In fact, the PSD graph shows the power distribution of the data in frequency domain. With the cut-off frequency determined from the residual analysis, a threshold line differentiating the high power contributed signal and low power contributed signal with unwanted noise can be obtained. The magnitude of this threshold line is known as threshold value and it is found as -35.98dB from Figure 4.23(b). This threshold value contains the statistical information of noise in high frequency region.

In fact, a good cut-off frequency should include all the highly contributed excited modes, or else poor mode truncation will happen and the unknown force will be under-estimated. Mean and standard deviation are used to characterise the PSD data and they can be calculated in the following Eqs. (2.63) and (2.64). They are shown in Figure 4.23(b) as top line, middle line and bottom line which represent the mean plus standard deviation of PSD data, mean of PSD data, and mean minus standard deviation of PSD data respectively. PSD data that is above the upper line is considered as significant data for the force recovery. Thus, the significant data must be included in the analysis frequency range and shall not be eliminated. PSD data that is above the mean line is also important and should be taken into account. The PSD data below the middle line and bottom line are less significant and can be filtered out if its value is negligible compared to the overall PSD data.

From the PSD graph as shown in Figure 4.23(b), it is observed that there are several significant modes excited by the unknown force that falls within 0-350Hz. There are several important modes drop within 350-400Hz for acceleration PSD in the region between mean line and upper line. The cut-off frequency, 451.17Hz for the force determination at point 1 is determined by using residual analysis in Section 4.3.2.1. It is

found that the cut-off frequency is able to include all of these high power contributed signal. Besides, it is observed that the power distribution of signals above the cut-off frequency is very low and hence contributes less to the recovery of force. The low power contributed signal in this region will be eliminated to avoid the amplification of noise during the impact force determination and causes undesired force determination result.

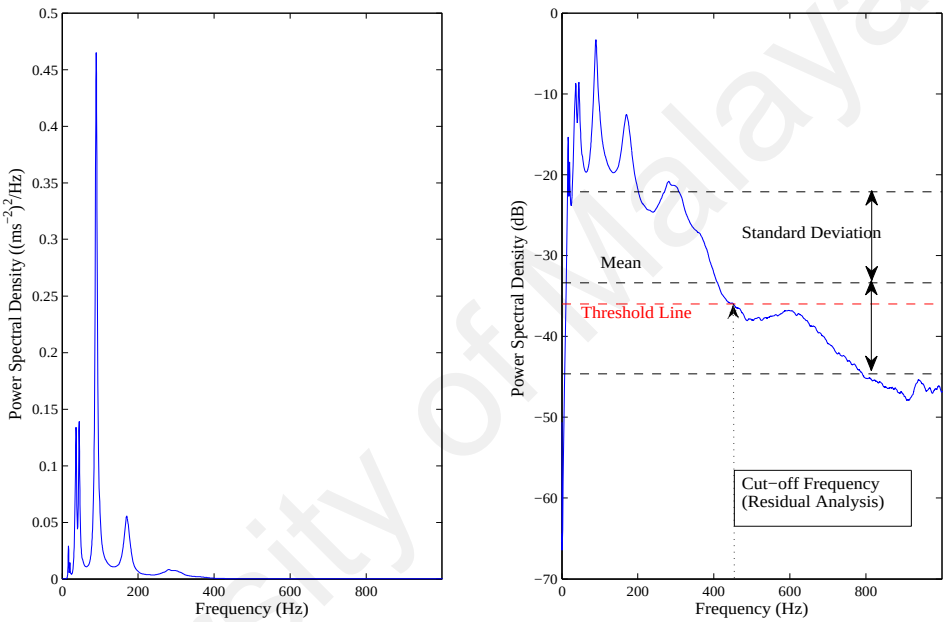

Figure 4.23:
Graph of Mean of Acceleration PSD due to Unknown Impact Force at Point 1 with the Cut-Off Frequency Determined from Residual Analysis: (a) Linear, (b) Decibel Scale

Assuming the power contribution of the noise region is constant relative to the mean and standard deviation of a sample (i.e. acceleration PSD), hence, the threshold line, mean and standard deviation can be related to find the threshold constant as follows Eq. (2.65). The acceleration PSD analysis result for force determination at point 1 is shown in Table. 4.3. The threshold constant is equal to -0.23.

Table 4.3:
Determination of Threshold Constant from Acceleration PSD Analysis Result and Residual Analysis for Force Determination at Point 1

Point	Mean of PSD (dB)	Standard Deviation of PSD (dB)	Cut-Off Frequency from Residual Analysis (Hz)	Threshold value (dB)	Threshold constant
1	-33.38	11.27	451.17	-35.98	-0.23

The threshold constant is utilized further to obtain the low pass frequency for every new sample of PSD data. An example of the determination of the cut-off frequency for force determination acting on Point 2 is shown in Table 4.4 and Figure 4.24. Note that once the mean and standard deviation of the new PSD sample are calculated, threshold value of a new PSD sample can be calculated by using Eq. (2.66). This threshold value is used to set a threshold line in the PSD graph. Hence the cut-off frequency, 435.55Hz for the force determination at point 2 can be obtained from the PSD graph as shown in Figure 4.24. By using this approach, the cut-off frequency for unknown force determination acting on Points 1-15 can be determined and they are shown in Tables B.1 and B.2.

The approach of finding cut-off frequency with the assistance of the PSD tool enhances the extraction process. In fact, finding cut-off frequency by using the residual analysis is time consuming as it requires extra care on curve fitting the data. Imagine we need to curve fit the residual response data one by one for every new response data. This would be impractical for the impact force determination. In this study, PSD tool is presented as an effective tool to find the cut-off frequency. Only a set of residual analysis is required to find the threshold constant, and then the cut-off frequency for every new sample of response can be obtained by using the statistic characteristics of the PSD data and the PSD graph. Indeed this approach is time efficient and produces more consistent result.

By assuming the total power must be conserved for various types of responses in a specific frequency range, the velocity and displacement data share the same cut-off frequency as the acceleration data in this study.

Table 4.4:
Determination of Cut-Off Frequency by Using the Threshold Constant and Acceleration PSD Analysis Result for Force Determination at Point 2

Point	Mean of new acceleration PSD (dB)	Standard Deviation of new acceleration PSD (dB)	Threshold constant	New Threshold value (dB)	Cut-Off Frequency from PSD graph (Hz)
2	-48.76	12.90	-0.23	-51.73	435.55

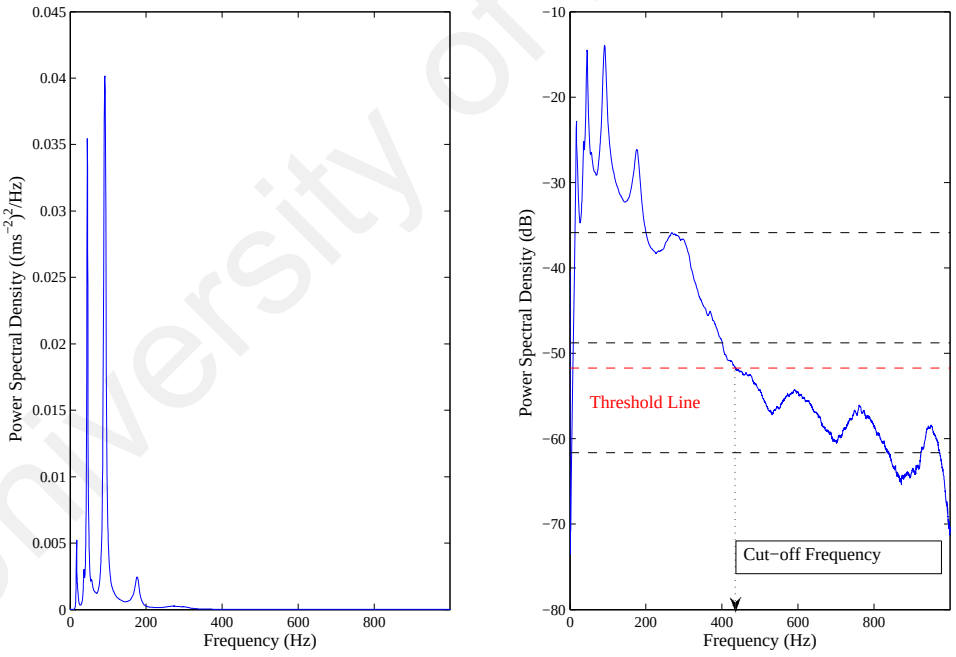

Figure 4.24:
Graph of Mean of Acceleration PSD due to Unknown Impact Force at Point 2 with the Cut-Off Frequency Determined from PSD Graph: (a) Linear, (b) Decibel Scale

4.3.2.3: Intrinsic Problem of Integration Method

Intrinsic problem can occur during integration process, which magnifies the noise in the low frequency region. It is noted that high pass filter can be adopted to remove these spurious trends without corrupting the data. However, it is not a simple task to discriminate between real low frequency data and low frequency noise with intrinsic problem (Audenino & Belingardi, 1996).

In this study, the PSD tool is used as a simple method to detect this intrinsic problem. Firstly, total powers of acceleration, velocity and displacement PSDs are calculated by summing up the total areas below their PSD curves. It can be done by using trapezoidal numerical integration as follows Eq. (2.67). The magnitude of the calculated total power is proportional to the exact total power value, which have the unit of (unit response)^2. Normalised magnitude is implemented to make the analysis and comparison easier between the various response data. The cumulative summation of the normalised total powers of the acceleration, velocity and displacement PSDs are shown in Figure 4.25.

From the Figures 4.25 (a) and (b), it is found that the total power near to the DC frequency is close to zero for both acceleration and velocity graphs. This shows that the integration resulted from the acceleration to the velocity data is satisfied where the noise in low frequency region do not affect and contribute to the total power of the signal significantly and thus can be ignored. Therefore the intrinsic problem is not significant for the single integration process in this study. However for the displacement graph as shown in Figure 4.25 (c)., it shows that the total power near to the DC frequency is very large, i.e. 0.35 of the total power. This observation shows that the double integration gives rise to the intrinsic problem. The noise at the low frequency region has been magnified and contributes to the total power of the displacement data badly.

To avoid the intrinsic problem occurs in the displacement data, a high pass frequency must be set. In this study, the cut-off frequency was found by utilising the cumulative summation of the normalised total power graph. By increasing the high pass frequency iteratively, the output result (i.e. cumulative summation of normalised total power) is overlaid in Figure 4.26. It is found that the output result becomes stable after selecting the high pass frequency at 2.0Hz onwards. Below this frequency, the output normalised value is unacceptably high. Thus, by setting the high pass frequency at 2.0Hz, the unreasonably high amplified noises during the double integration process have been removed. This is verified by the observation that the output normalised value drops to zero when approaching DC frequency. Note that the high pass frequency must not be too high because it may cause signal distortion. By using this simple method, an adequate high pass frequency is selected at 2.0Hz.

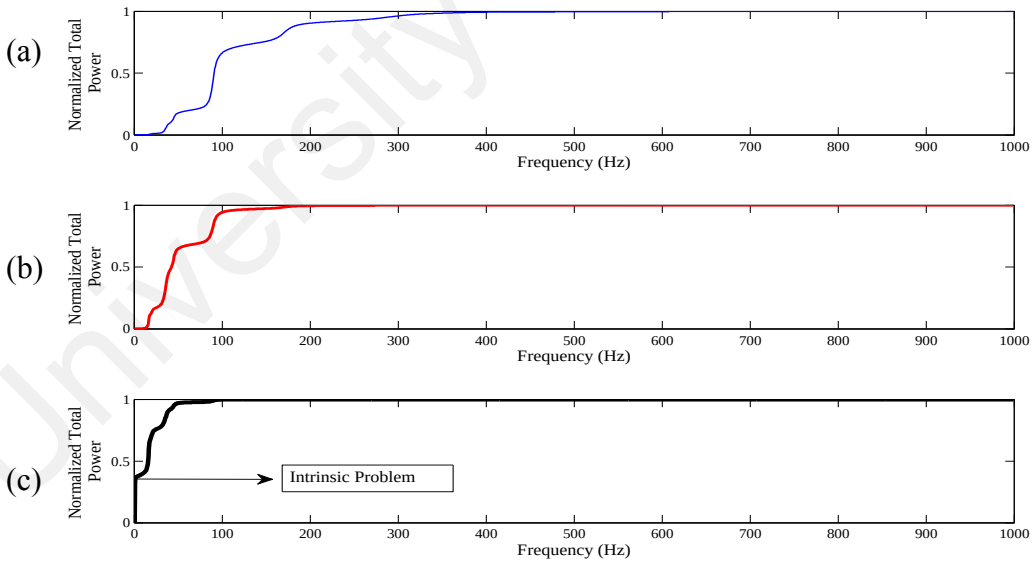

Figure 4.25:
Cumulative Summation of Normalised Total Power of the Different Types of Response PSDs in Frequency Domain: (a) Acceleration, (b) Velocity, (c) Displacement PSDs

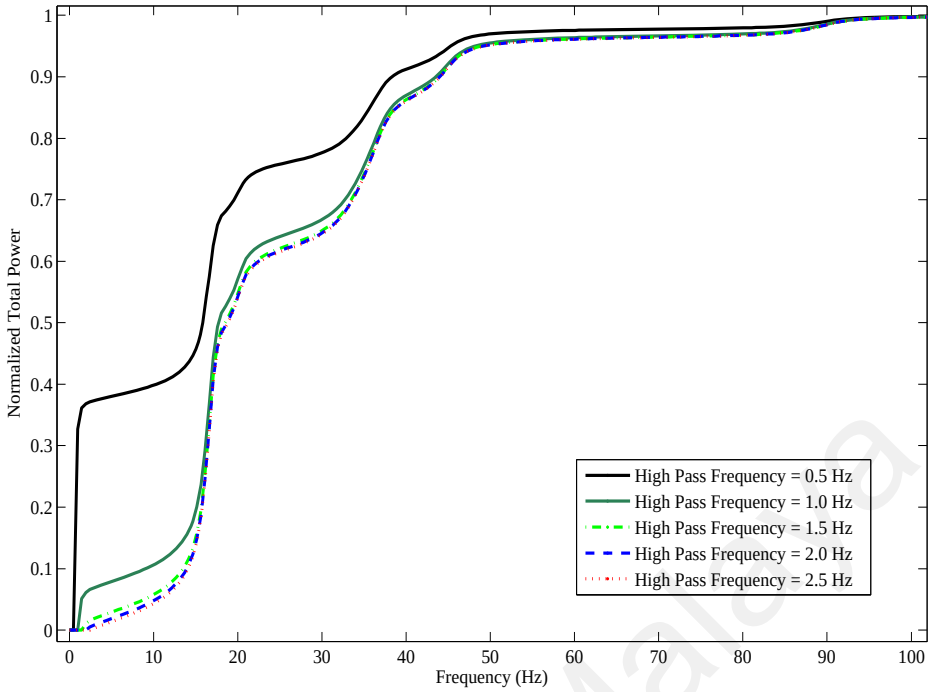

Figure 4.26:
Cumulative Summation of Normalised Total Power of the Displacement PSD for an Iteratively Increasing High Pass Frequency

4.3.2.4: Band Pass Filtering

After performing the residual analysis and utilizing the PSD tool, band pass filtering is set by using the calculated high pass frequency and low pass frequency. For example, the selected high pass frequency is 0.5Hz for acceleration and velocity data and 2.0Hz for displacement data. The low pass frequency is selected at 451.2Hz for the force determination at point 1 labelled on the test rig. The selected low pass frequency is same for all types of responses. The data outside the selected frequency range will be filtered out by setting the value to zero in the frequency domain. This selected analysis frequency range is good in terms of low noise and high contribution of power, therefore it is predicted that the force determination accuracy will be enhanced by using the PSD tool selected analysis frequency range, instead of using the fixed analysis frequency range.

4.3.2.5: Force Determination By Using PSD Tool Selected Analysis Frequency Range

Once the cut-off frequencies for band pass filter were determined by using the PSD tool, force determination via MTM was conducted by using various types of responses with their respective selected analysis frequency ranges. The force determination results were plotted in Figures 4.27, 4.28 and 4.29 for acceleration, velocity and displacement feedbacks respectively. By comparing the force determination results in the time domain, it is found that all the identified force results are satisfied. This shows that the PSD tool selected analysis frequency range effectively removes the unwanted noise from the calculation of unknown impact force. At the same time, it chooses the high power contributed signal into the impact force determination and therefore improves the accuracy of the force determination result.

The impact force reconstructed by displacement response is excellent in terms of accuracy where it has no oscillating components in the time trace compared to the acceleration and velocity feedback result. Besides, it is found that the identified force by displacement response matches most closely to the measured force in the frequency domain, followed by velocity and acceleration feedback result.

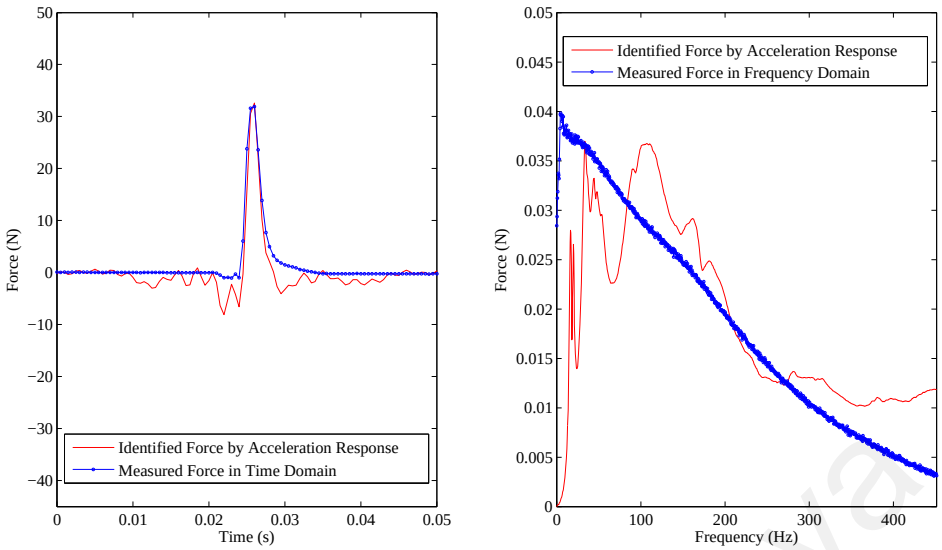

(a) (b)

Figure 4.27:
Graph of Comparison between Identified Force by Acceleration Response and Measured Force at Point 1 in the Selected 0.5-451.2Hz Analysis Frequency Range by Using PSD Tool: (a) Time Domain, (b) Frequency Domain

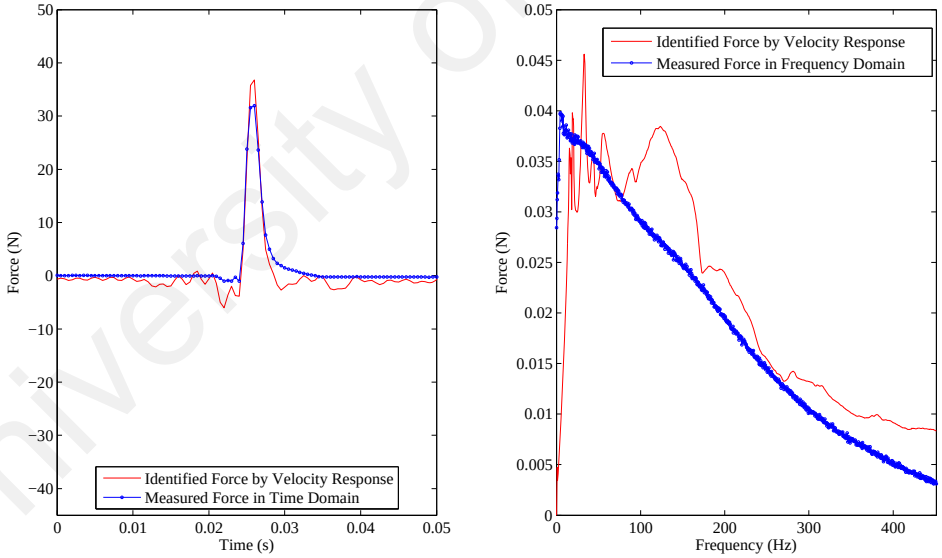

(a) (b)

Figure 4.28:
Graph of Comparison between Identified Force by Velocity Response and Measured Force at Point 1 in the Selected 0.5-451.2Hz Analysis Frequency Range by Using PSD Tool: (a) Time Domain, (b) Frequency Domain

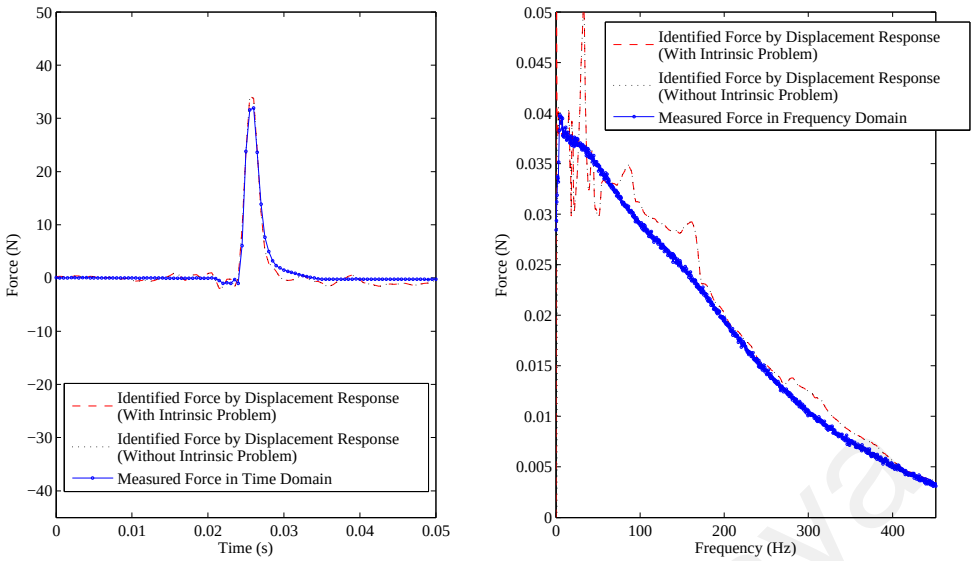

(a) (b)

Figure 4.29:
Graph of Comparison between Identified Force by Displacement Response and Measured Force at Point 1 in the Selected 0.5-451.2Hz and 2.0-451.2Hz Analysis Frequency Range by Using PSD Tool: (a) Time Domain, (b) Frequency Domain

The identified forces with and without the intrinsic problem are compared in a zoom-in time range and a zoom-in frequency range as shown in Figure 4.30. It is found that the identified force with intrinsic problem has a supreme high value near the DC frequency as shown in Figure 4.30 (b). This indicate that the displacement feedback with a high pass frequency of 0.5Hz suffers the intrinsic problem as discussed in Section 4.3.2.3. It is recommended to increase the high pass frequency to 2.0Hz to reduce the effect of intrinsic problem. By using the appropriate high pass frequency selected by using PSD tool (i.e. 2.0Hz), this undesired frequency region was eliminated as shown in Figure 4.30 (b). Hence, it improves the force accuracy in the time domain.

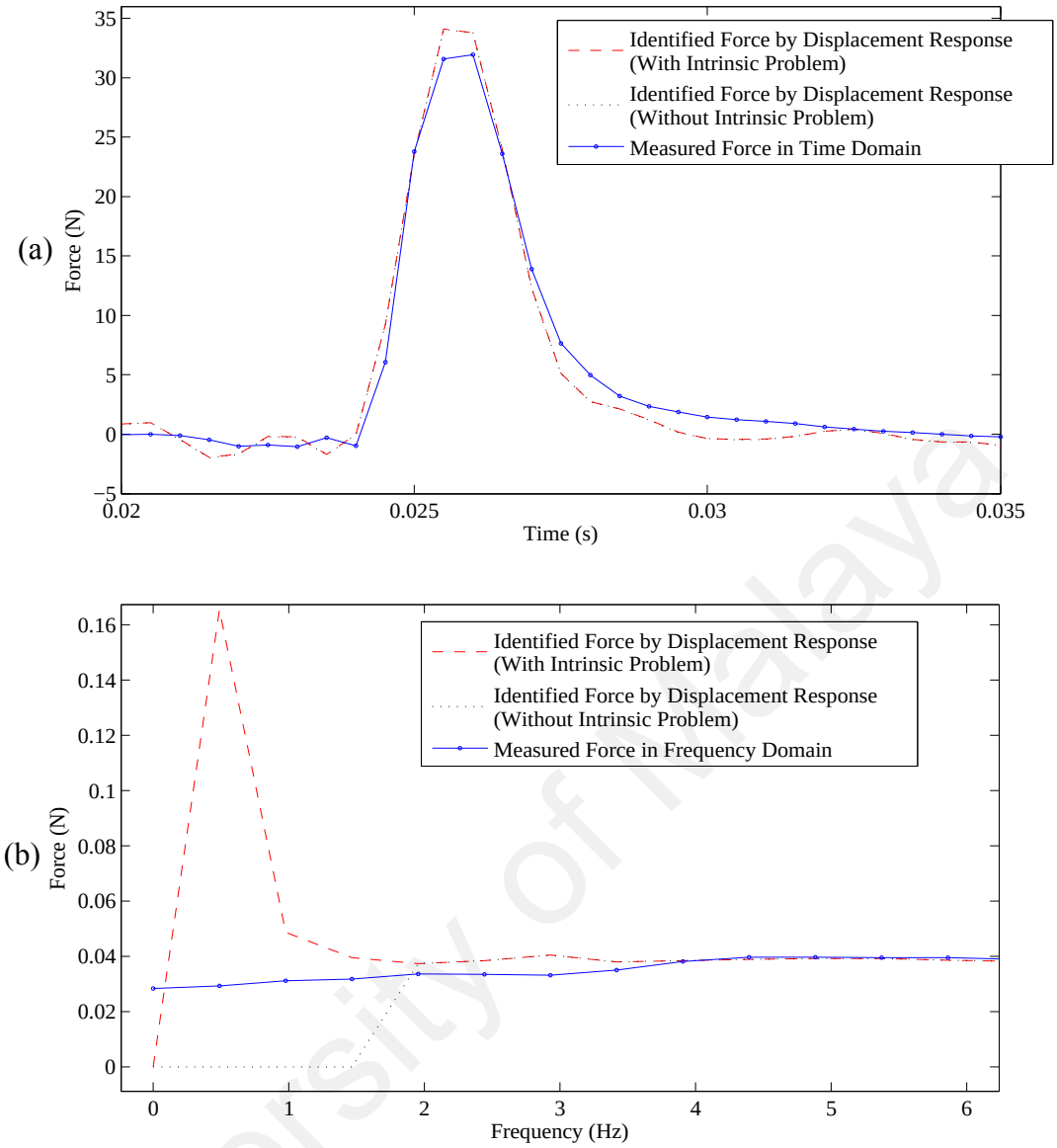

Figure 4.30:
Graph of Comparison between Identified Force with and without Intrinsic Problem and Measured Force: (a) Zoom-In Time Range, (b) Zoom-In Frequency Range

The force correlograms for the identified forces by using PSD tool selected analysis frequency range in various types of responses are shown in the Figure 4.31. The result shows that the number of points out of the tolerance is the highest for acceleration feedback, followed by the velocity and displacement feedback. It is found that displacement feedback has the best accuracy where all the points fall within the acceptable range. Besides, it is found that the correlation coefficient of the identified force by using the displacement response is improved significantly when the intrinsic

problem has been removed by using the band pass filter. The correlation coefficient increases from 0.9458 (i.e. with intrinsic problem) to 0.9816 (i.e. without intrinsic problem). Therefore it is suggested to use 2.0Hz as the high pass frequency for the displacement unit in this study instead of 0.5Hz. The force determination results for acceleration and velocity feedback are satisfied, which have the correlation coefficients of 0.9136 and 0.9588 respectively. The good force determination result by all types of responses shows the importance of selecting a good analysis frequency range, which is done by utilizing PSD tool in this study.

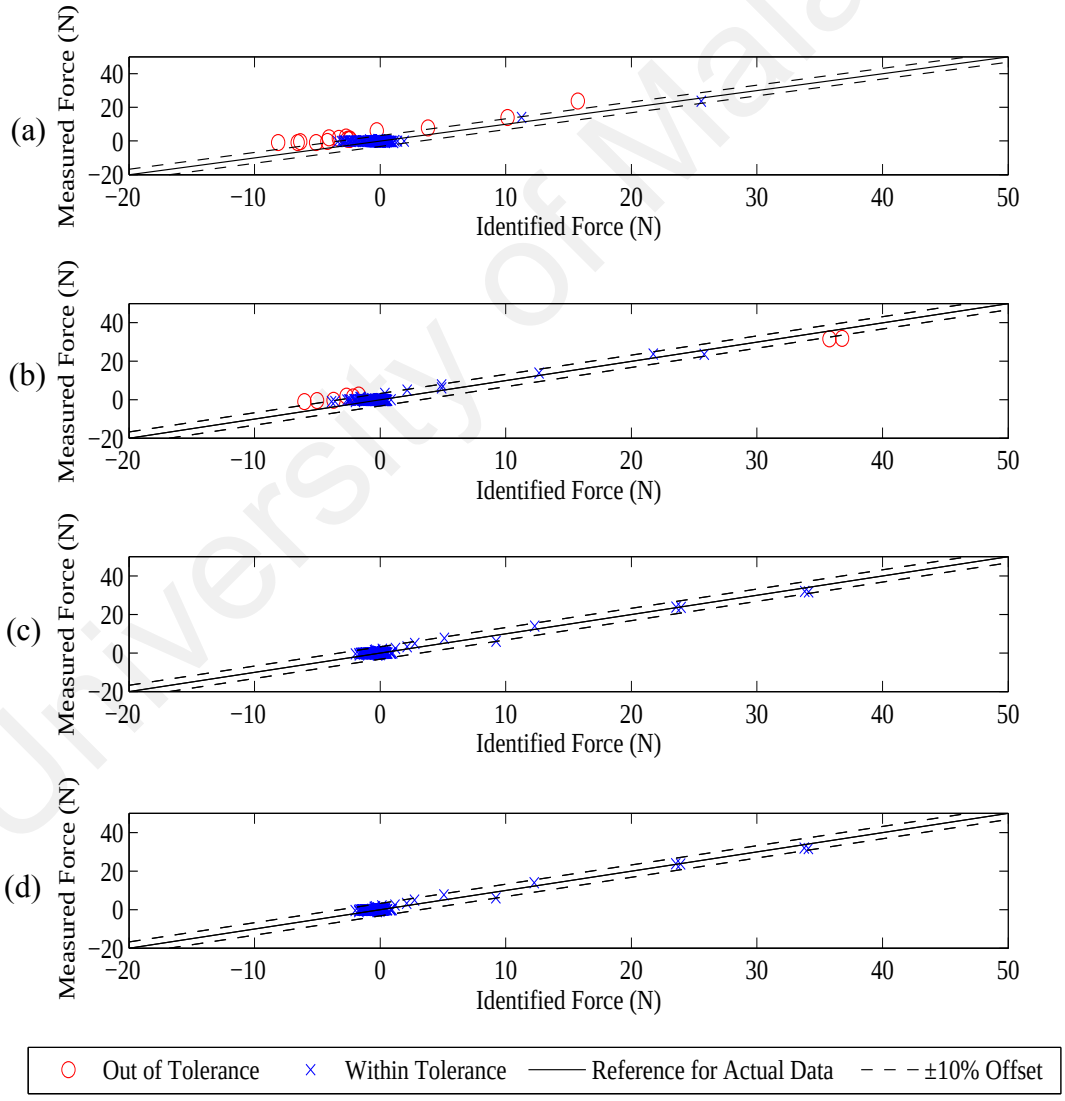

Figure 4.31:
Force Correlogram by Using PSD Tool Selected Analysis Frequency Range in Various Types of Responses: (a) Acceleration, (b) Velocity, (c) Displacement (Intrinsic Problem), (d) Displacement (Without Intrinsic Problem)

In summary, PSD tool is an effective tool which extends the capability of residual analysis in selecting an appropriate cut-off frequency. Selection of an appropriate analysis frequency range through PSD tool is fast because it does not need extensive care and attention on curve fitting the data to obtain the cut-off frequency. The capability of the PSD tool to determine a good analysis frequency range enables it applicable in impact force determination especially for the case where the actual excitation frequency is unknown and time-variant.

4.3.3: Comparison between Force Determination Result by Using Fixed Analysis Frequency Range and PSD Tool Selected Analysis Frequency Range

Previously in Sections 4.3.1-4.3.2, the impact force determination via MTM by using fixed analysis frequency range and PSD tool selected analysis frequency range was conducted. The findings of all the force determination results for fixed and PSD tool selected analysis frequency ranges were compared by using the correlation coefficients between the identified forces and measured forces in the time domain. The results are plotted in Figure 4.32. In fact, the force accuracy is satisfied if the correlation coefficient is within 0.9-1.0. It is found that the acceleration feedback has the worst force determination result for all cases, followed by velocity and displacement feedbacks.

Besides, it is found that the under-determined case has the worst force determination result as shown in Figure 4.32. This showed that an analysis frequency range of impact force determination must include the entire highly contributed excitation frequency region, or else the force accuracy will be very bad no matter which types of responses are used. The second lowest correlation coefficient is the impact force determination in the over-determined case. In the over-determined case, it is found that the force

determination result by using acceleration feedback is inaccurate; however the force accuracy is improved by using the velocity and displacement responses. In this case, the displacement feedback shows a superior behaviour in filtering the noise effect in high frequency region and therefore has the highest force accuracy.

The correlation coefficient for the even-estimated case shows a satisfied force determination result for all the response feedbacks since all the correlation coefficients are greater than 0.9. In the even-estimated case, the analysis frequency range is similar to the excitation frequency region. The analysis frequency range in the even-estimated case includes all the highly contributed excitation regions with insignificant amount of noise. Therefore it ensures a good force determination result.

Furthermore, PSD tool solves the difficulty of determining a good analysis frequency range when the actual excitation frequency is unknown and time-variant. From the Figure 4.32, it is found that the correlation coefficient of force determination by using PSD tool selected analysis frequency range has a good force determination result for all the responses feedbacks. In overall, the displacement response with PSD tool selected analysis frequency range has the best correlation coefficient compared to the force results obtained from fixed analysis frequency range.

It is shown that by selecting a suitable response unit and an appropriate selection of analysis frequency range, the accuracy of the impact force determination by using MTM can be enhanced significantly. From the results, the proposed analysis frequency range and the proposed type of response are PSD tool selected frequency range and displacement response respectively.

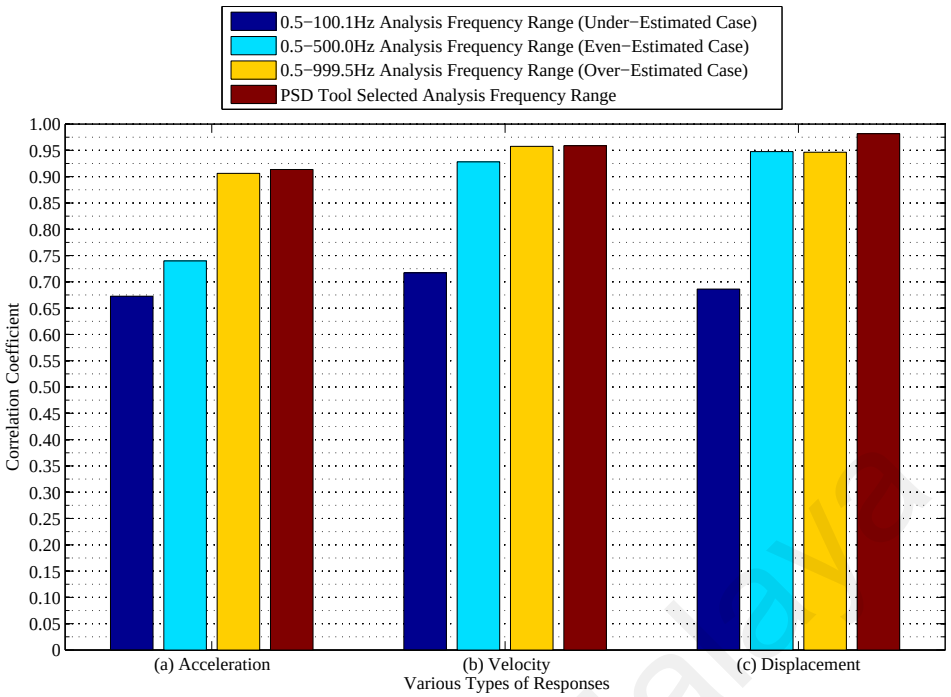

Figure 4.32:
Graph of Comparison between Correlation Coefficient of the Impact Force Determination Result for Fixed Analysis Frequency Range and PSD Tool Selected Analysis Frequency Range by Using Various Types of Responses: (a) Acceleration, (b) Velocity, (c) Displacement

4.3.4: Effectiveness of the Proposed Force Determination Method in Collocated and Non-Collocated Cases

Previously, the accuracy enhancement of the impact force determination via MTM by using integration method and data filtering approach was presented. It showed that the combination of the displacement feedback and an appropriate selection of analysis frequency range obtained from PSD tool have the best force determination accuracy. The effectiveness of the proposed methods are examined in the collocated and non-collocated cases in this section. Hence it is compared to the conventional force determination method (i.e. acceleration raw data for a fixed analysis frequency range of 0.5-999.5Hz). The correlation coefficient for the force determination result by using the conventional method is compared to the result of the proposed method for both

collocated and non-collocated cases. The results are shown in Figures 4.33 and 4.34 respectively.

For the collocated case as shown in Figure 4.33, it is found that the force accuracy by using the conventional method with acceleration raw data is not satisfied, i.e. the correlation coefficients are less than 0.9 for the force determination results at 15 impact locations. In fact, the force accuracy is mainly affected by the following factor: measurement noise during FRF measurement and ODS analysis, curve fitting error especially the bias error in real part, contamination of the noise frequency region in the analysis frequency range and amplification of the noise through impact force determination. From the Figure 4.33, it is found that the proposed method has a better results of correlation coefficients for the force determination results at 15 impact locations. The average of correlation coefficients for the proposed method's result achieves a satisfied force determination result of 0.9245, a significant accuracy improvement of 34.28% compared to the force determination result by using the conventional method, i.e. 0.6885.

For the non-collocated case as shown in Figure 4.34, it is found that the force determination result by using the conventional method is not satisfied as most of the correlation coefficients are less than 0.9. The average of the correlation coefficients for the conventional method's result is 0.7851. By using the proposed method, it is found that the force accuracy is enhanced. It is observed that the correlation coefficients of the force determination result by using the proposed method are higher than the conventional method's result at all the examined 15 locations. The average of the correlation coefficients for the proposed method is 0.9234 (i.e. an increment of 17.62%), which indicates a good force determination result.

By comparing the force determination result in collocated and non-collocated cases as shown in Figures 4.33 and 4.34, it is found that the proposed method is able to enhance the poor force determination result by the conventional method. Both cases have the average values of correlation coefficients greater than 0.92 by using the proposed method and less than 0.79 by using the conventional method. This shows the effectiveness of the proposed method in enhancing the conventional force determination method. In summary, the enhancement of impact force determination via MTM by using the proposed method is successful to be applied in the collocated and non-collocated cases.

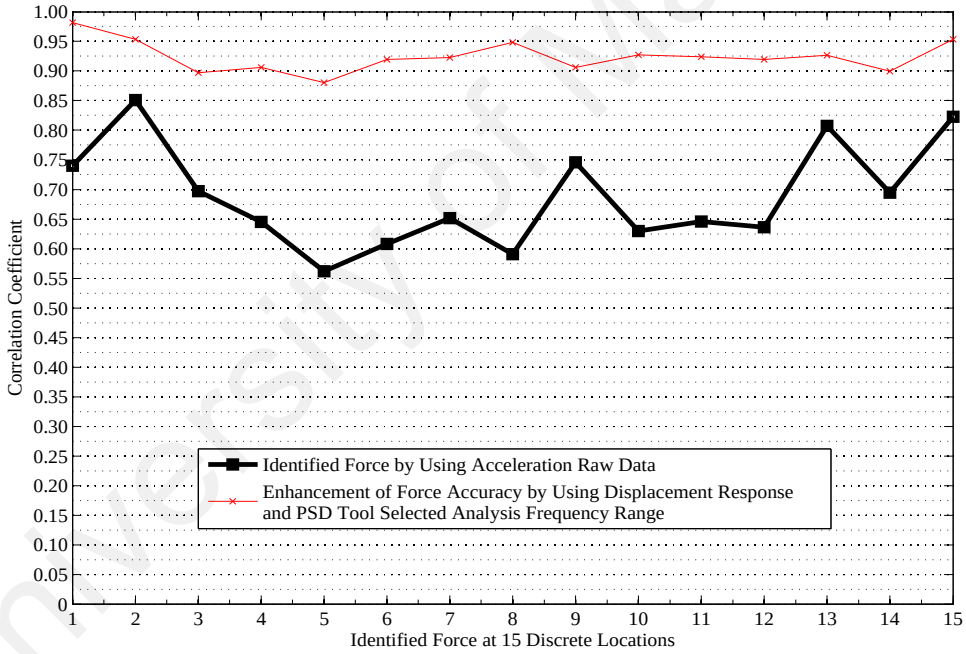

Figure 4.33:
Graph of Comparison between the Correlation Coefficient of the Impact Force Determination Result at 15 Impact Locations by Using the Conventional Acceleration Responses and the Proposed Method in a Collocated Case

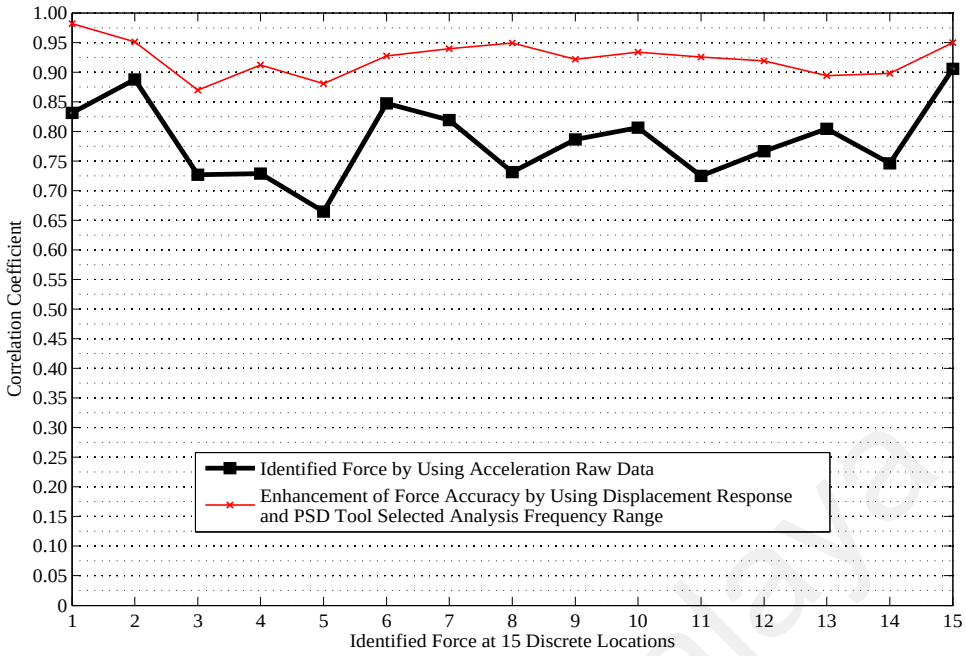

Figure 4.34:
Graph of Comparison between the Correlation Coefficient of the Impact Force Determination Result at 15 Impact Locations by Using the Conventional Acceleration Response and the Proposed Method in a Non-Collocated Case

Chapter 5: Conclusions and Recommendations

5.1: Conclusions

In conclusion, an accuracy enhancement of the impact force determination via MTM by using integration method and data filtering approach is successfully established. Several objectives have been achieved as follows:

i. The accuracy of impact force determination via MTM by using fixed analysis frequency range in various types of responses has been studied. Hence, the first objective is achieved. In this study, it was found that the unknown force is impossible to be reconstructed if the analysis frequency range excludes the highly contributed excitation frequency region (i.e. under-estimated case). The impact force determination result in under-determined case has the lowest correlation coefficient, which is less than 0.75 by using various types of responses. An accurate force determination result can only be obtained if the analysis frequency range contains all the highly contributed excitation frequency regions with less contamination of noise (i.e. the correlation coefficients for even-estimated case are greater than 0.9 for the force determination result by using various types of responses). The noise effect in the over-estimated case is the largest compared to under-estimated and even-estimated cases and it causes an inaccurate force determination result especially when acceleration response is used (i.e. the acceleration feedback has a poor correlation coefficient of 0.7398). This study shows the superior low pass characteristic of integration method in reducing noise effect especially in high frequency region, which indirectly enhances the force determination result (i.e. force determination result by using the velocity and displacement feedbacks have the correlation coefficients of

0.9281 and 0.9477 respectively for the over-estimated case). The findings in the case of the fixed analysis frequency range highlight the importance of having an appropriate analysis frequency range in the impact force determination.

ii. The accuracy of impact force determination via MTM by using PSD tool selected analysis frequency range in various types of responses has been studied. Hence, the second objective is achieved. In this study, a frequency range determinator named PSD tool has been developed for the case of unknown exciting frequency range of impact force. This study successfully utilizes the PSD tool to acquire a suitable low pass frequency to eliminate the insignificant low power contributed signal and unwanted noise in the high frequency region. Furthermore, the PSD tool is able to detect and solve the intrinsic problem by selecting a suitable high pass frequency in a simple and easy way (i.e. high pass frequency of 2.0Hz has been set for the displacement feedback). Band pass filtering is set based on the high pass and low pass frequencies and hence an appropriate analysis frequency range is selected for the force determination purpose. Force determination results by using various types of responses are satisfied by adopting the PSD tool selected analysis frequency range. The correlation coefficients are all above 0.9. Therefore it is concluded that the PSD tool is able to assist the user to obtain an appropriate analysis frequency range for the impact force determination purpose, which indirectly helps to enhance the accuracy of the identified force.

iii. The most suitable analysis frequency range and type of response in impact force determination via MTM have been proposed. Hence, the third objective is achieved. The comparison and analysis of outcomes from the cases of fixed

analysis frequency range and PSD tool selected analysis frequency range encourages the user to conduct the impact force determination by using the displacement feedback obtained from the integration method and by using the PSD tool selected analysis frequency range.

iv. The effectiveness of the proposed force determination method in both collocated and non-collocated cases, in comparison to the conventional method has been studied. Hence, the fourth objective is achieved. In this study, a comparison has been made between force determination result of the proposed method and the conventional method. Note that the force determination by using a conventional method utilizes an acceleration feedback and an over-estimated fixed analysis frequency range (i.e. 0.5-999.5Hz analysis frequency range). The result shows a significant improvement of force determination result for both collocated and non-collocated cases when the proposed method is adopted, compared to the result of the conventional method. The proposed method enhances the force determination result by an increment of 34.28% and 17.62% of the correlation coefficients for the collocated and the non-collocated cases respectively, compared to the result of the conventional method. The averages of the correlation coefficients of the force determination result by using the conventional method are low, i.e. 0.6885 and 0.7851 for the collocated and non-collocated cases respectively. The force determination result by using the conventional method is inaccurate mainly due to the effect of noise in high frequency region and the curve fitting error during the modal parameters extraction. However, this inaccurate force determination method can be improved by using the proposed method. The averages of the correlation coefficients of the force determination results by using the proposed method are

above 0.9 for both collocated and non-collocated cases. This implies that the force determination result by using the proposed method is satisfied and hence applicable in both mentioned cases.

5.2: Recommendations

In future, the modal parameters extraction process can be enhanced further by using a multiple reference testing instead of using a single reference testing of FRF. In this study, only a single column or single reference of FRF matrix is measured through the FRF measurement and curve fitting is performed to estimate the modal parameters of the test rig. In fact, this is known as a single reference testing where there is only a single fixed exciter location. For the multiple reference testing, it requires a multiple fixed exciters or multiple fixed response transducers. The multiple reference testing is able to identify closely coupled modes or repeated roots of a structure while the single reference testing is insufficient to identify that. Thus, by applying a multiple reference curve fitting, more accurate modal parameters can be obtained and this will eventually improve the accuracy of the force determination result.

There is a curve fitting error observed during the modal extraction process which is unavoidable by the current polynomial curve fitting algorithm. The quality of fitting reduces especially when the modal model is used to synthesise the FRF (i.e. it shows bias in the real part of the synthesised FRF). This bias is primary due to the effect of out-of-band mode contribution. This curve fitting error must be solved in order to have a better force determination result. So, there is a need to develop a curve fitting algorithm so that the extracted modal parameters are able to fit the modal model nicely. In other words, the synthesised FRF must be closely matched to the measured FRF.

In this study, due to the limitation of MTM, the force determination becomes well-posed only when a single impact location is known in advance. The force determination results are ill-posed when multiple forces are to be estimated from various discrete locations. To overcome this limitation, the modal filtering method is recommended for the force determination in future where this method is suitable for the multiple input identification case. Therefore, the effectiveness of the proposed method can be further examined in the case of multiple input identifications with unknown impact locations.

Impact-type force is accounted for the force determination in this research. The effectiveness of the proposed method on recovering the other type of forces (i.e. motor force and sinusoidal force) are to be worthy of notice as well. Besides, single-axis impact force determination is accounted in this research. The effectiveness of the proposed method on recovering the tri-axis or oblique impact force determination is recommended for future work. Furthermore, it is valuable to assess the proposed method for anisotropic material such as composites in future.

References

Allemang, R. J., & Brown, D. L. (1998). A unified matrix polynomial approach to modal identification. *Journal of Sound and Vibration, 211*(3), 301-322. doi: DOI: 10.1006/jsvi.1997.1321

Allen, M. S., & Carne, T. G. (2006). Comparison of inverse structural filter (ISF) and sum of weighted accelerations technique (SWAT) time domain force identification methods. In American Institute of Aeronautics and Astronautics (Ed.), *A collection of technical papers: Proceedings of the 47th AIAA/ASME/ASCE/AHS/ASC Structures, Structural Dynamics, and Materials Conference, Newport, Rhode Island* (pp. 1-24). Reston, VA: American Institute of Aeronautics and Astronautics. Retrieved from http://silver.neep.wisc.edu/~msallen/Allen_Carne_ISFvsSWAT_SDMConf_AIAAv6final.pdf

Allen, M. S., & Carne, T. G. (2008). Delayed, multi-step inverse structural filter for robust force identification. *Mechanical Systems and Signal Processing, 22*(5), 1036-1054. doi: 10.1016/j.ymssp.2007.11.022

Allen, M. S., & Ginsberg, J. H. (2006). A global, single-input–multi-output (SIMO) implementation of the algorithm of mode isolation and application to analytical and experimental data. *Mechanical Systems and Signal Processing, 20*(5), 1090-1111. doi: 10.1016/j.ymssp.2005.09.007

Atobe, S., Fukunaga, H., & Hu, N. (2011). Impact force identification of CFRP structures using experimental transfer matrices. *Computers Materials and Continua, 26*(1), 67.

Audenino, A. L., & Belingardi, G. (1996). Processing of simultaneous mechanical random response signals: integration, differentiation and phase shifts correction. *Mechanical Systems and Signal Processing, 10*(3), 277-291. doi: 10.1006/mssp.1996.0021

Avitabile, P. (2001). Experimental modal analysis. *Sound and Vibration, 35*(1), 20-31.

Baharin, N. H., & Rahman, R. A. (2009). Effect of accelerometer mass on thin plate vibration. *Jurnal Mekanikal, 29*, 100-111.

Biewener, A. A., & Full, R. J. (1992). Force platform and kinematic analysis. *Biomechanics–Structures and Systems: A Practical Approach* (pp. 45-73). USA: Oxford University Press.

Blau, M. (1999). Indirect measurement of multiple excitation force spectra by FRF matrix inversion: influence of errors in statistical estimates of FRFs and response spectra. *Acta Acustica united with Acustica*, 85(4), 464-479.

Brandt, A. (2011), *Noise and vibration analysis: Signal analysis and experimental procedures*. United Kingdom: John Wiley and Sons.

Boukria, Z., Perrotin, P., & Bennani, A. (2011). Experimental impact force location and identification using inverse problems: application for a circular plate. *International Journal of Mechanics, 5*(1), 48-55.

Briggs, J. C., & Tse, M. -K. (1992). Impact force identification using extracted modal parameters and pattern matching. *International Journal of Impact Engineering, 12*(3), 361-372. doi: 10.1016/0734-743x(92)90123-b

Cardi, A. A., Adams, D. E., & Walsh, S. (2006a). Ceramic body armor single impact force identification on a compliant torso using acceleration response mapping. *Structural Health Monitoring, 5*(4), 355-372. doi: 10.1177/1475921706067763

Cardi, A. A., Adams, D. E., & Walsh, S. (2006b). Locating and quantifying ceramic body armor impact forces on a compliant torso using acceleration mapping. In *Nondestructive Evaulation for Health Monitoring and Diagnostics* (pp. 617714-617714). International Society for Optics and Photonics. doi: 10.1117/12.658245

Carne, T. G., Bateman, V. I., & Mayes, R. L. (1992). Force reconstruction using a sum of weighted accelerations technique. In D. J. DeMichele (Ed.), *Proceedings of the 10th International Modal Analysis Conference, Town and Country Hotel, San Diego, California* (pp. 291-298). Bethel, CT.: Society for Experimental Mechanics, Inc.

Chang, C., & Sun, C. (1989). Determining transverse impact force on a composite laminate by signal deconvolution. *Experimental Mechanics, 29*(4), 414-419. doi: 10.1007/bf02323860

Chella, M. A., Tørum, A., & Myrhaug, D. (2012). An overview of wave impact forces on offshore wind turbine substructures. *Energy Procedia, 20*(0), 217-226. doi: 10.1016/j.egypro.2012.03.022

Chen, C., & Yuan, F. G. (2010). Impact source identification in finite isotropic plates using a time-reversal method: theoretical study. *Smart Materials and Structures, 19*(10), 105028.

Choi, H. G., Thite, A. N., & Thompson, D. J. (2006). A threshold for the use of Tikhonov regularisation in inverse force determination. [doi: DOI: 10.1016/j.apacoust.2005.11.003]. *Applied Acoustics, 67*(7), 700-719.

Choi, H. G., Thite, A. N., & Thompson, D. J. (2007). Comparison of methods for parameter selection in Tikhonov regularisation with application to inverse force determination. *Journal of Sound and Vibration, 304*(3-5), 894-917. doi: 10.1016/j.jsv.2007.03.040

Cooley, J. W., & Tukey, J. W. (1965). An algorithm for the machine calculation of complex Fourier series. *Mathematics of computation*, 297-301.

Derrick, T.R. (2004). Signal processing. In D. G. E. Robertson, G. E. Hamill, G. Kamen, & Whittlesey (Eds.), *Research methods in biomechanics* (pp. 227-238). Champaign, Illinois: Human Kinetics.

Desanghere, G., & Snoeys, R. (1985). Indirect identification of excitation forces by modal coordinate transformation. In D. J. DeMichele (Ed.), *Proceedings of the 3rd International Modal Analysis Conference, Orlando Marriott Inn, International Drive, Orlando, Florida* (pp. 685-690). Schenectady, N.Y.: Union College.

DeVis, D., Gielen, L., Verhoeven, J., Nordmann, R., & Neumer, T. (1992). Indirect identification of fluid structure interaction forces in boilerfeed pumps. In D. J. DeMichele (Ed.), *Proceedings of the 10th International Modal Analysis Conference, Town and Country Hotel, San Diego, California* (pp. 47-53). Bethel, CT.: Society for Experimental Mechanics, Inc.

Dishan, H. (1995). Phase error in fast Fourier transform analysis. *Mechanical Systems and Signal Processing, 9*(2), 113-118. doi: 10.1006/mssp.1995.0009

Dobson, B. J., & Rider, E. (1990). A review of the indirect calculation of excitation forces from measured structural response data. *Proceedings of the Institution of Mechanical Engineers, Part C: Journal of Mechanical Engineering Science, 204*(2), 69-75. doi: 10.1243/pime_proc_1990_204_080_02

Doyle, J. (1997). A wavelet deconvolution method for impact force identification. *Experimental Mechanics, 37*(4), 403-408. doi: 10.1007/bf02317305

Feng, W., & Chen, L. (2010). The impact of the orientation angles uncertainty of instrument polarizers on polarization measurement accuracy. *Optik - International Journal for Light and Electron Optics, 121*(24), 2276-2279. doi: http://dx.doi.org/10.1016/j.ijleo.2009.08.004

Fu, Z. F., & He, J. (2001). *Modal analysis.* Oxford : Butterworth-Heinemann.

Goldsmith, W. (1960). *Impact: The theory and physical behaviour of colliding solids*. London: Edwards Arnold Ltd.

Golub, G. H., & Loan, C. F. V. (1996). *Matrix computations* (3rd ed.). Baltimore: Johns Hopkins University Press.

Goodier, J., Jahsman, W., & Ripperger, E. (1959). An experimental surface-wave method for recording force-time curves in elastic impacts. *ASME J. Appl. Mech, 26*, 3-7.

Gu, G., Kapoor, A., & Lilley, D. M. (2008). Calculation of dynamic impact loads for railway bridges using a direct integration method. *Proceedings of the Institution of Mechanical Engineers, Part F: Journal of Rail and Rapid Transit, 222*(4), 385-398.

Guillaume, P., Parloo, E., Verboven, P., & De Sitter, G. (2002). An inverse method for the identification of localized excitation sources. In A. L. Wicks (Ed.), *A Conference & Exposition on Structural Dynamics: Smart Structures and Transducer: Proceedings of the 20th International Modal Analysis Conference, the Westin Los Angeles Airport, Los Angeles, California* (pp. 1382-1388). Bethel, CT.: Society for Experimental Mechanics, Inc.

Gunawan, F. E. (2012). Levenberg–Marquardt iterative regularisation for the pulse-type impact-force reconstruction. *Journal of Sound and Vibration, 331*(25), 5424-5434. doi: http://dx.doi.org/10.1016/j.jsv.2012.07.025

Gunawan, F. E., Homma, H., & Kanto, Y. (2006). Two-step B-splines regularisation method for solving an ill-posed problem of impact-force reconstruction. *Journal of Sound and Vibration, 297*(1–2), 200-214. doi: 10.1016/j.jsv.2006.03.036

Gunawan, F. E., Homma, H., & Morisawa, Y. (2008). Impact-Force Estimation by Quadratic Spline Approximation. *Journal of Solid Mechanics and Materials Engineering, 2*(8), 1092-1103.

Hadamard, J. (1923). *Lectures on Cauchy problem in linear partial differential equations*. New Haven, CT: Yale University Press.

Halvorsen, W. G., & Brown, D. L. (1977). Impulse technique for structural frequency response testing. *Sound and Vibration, 11*(11), 8-21.

Hansen, P. C. (2001). The L-curve and its use in the numerical treatment of inverse problems. In P. Johnston (Ed.), *Computational inverse problems in electrocardiology* (pp. 119-142). Southampton: WIT Press.

Hansen, P. C., Kilmer, M. E., & Kjeldsen, R. H. (2006). Exploiting residual information in the parameter choice for discrete ill-posed problems. *BIT Numerical Mathematics, 46*(1), 41-59. doi: 10.1007/s10543-006-0042-7

Hollandsworth, P. E., & Busby, H. R. (1989). Impact force identification using the general inverse technique. *International Journal of Impact Engineering, 8*(4), 315-322. doi: 10.1016/0734-743X(89)90020-1

Hu, N., & Fukunaga, H. (2005). A new approach for health monitoring of composite structures through identification of impact force. *Journal of Advanced Science, 17*(1&2), 82-89.

Hu, N., Matsumoto, S., Nishi, R., & Fukunaga, H. (2007). Identification of impact forces on composite structures using an inverse approach. *Structural Engineering and Mechanics, 27*(4), 409-424.

Huang, C.-H., Shih, C.-C., & Kim, S. (2009). An inverse vibration problem in estimating the spatial and temporal-dependent external forces for cutting tools. *Applied Mathematical Modelling, 33*(6), 2683-2698. doi: 10.1016/j.apm.2008.08.001

Huang, H., Pan, J., & McCormick, P. G. (1997). Prediction of impact forces in a vibratory ball mill using an inverse technique.. *International Journal of Impact Engineering, 19*(2), 117-126. doi: 10.1016/S0734-743X(96)00018-8

Hundhausen, R. J., Adams, D. E., & Derriso, M. (2007). Impact loads identification in standoff metallic thermal protection system panels. *Journal of Intelligent Material Systems and Structures, 18*(6), 531-541. doi: 10.1177/1045389x06067141

Hundhausen, R. J., Adams, D. E., Derriso, M., Kukuchek, P., & Alloway, R. (2005). Transient loads identification for a standoff metallic thermal protection system panel. In SEM (Ed.), *A conference & exposition on structural dynamics: Structural health monitoring: Proceedings of the 23th International Modal Analysis Conference, Orlando, Florida* (pp. 1-15). Bethel, CT.: Society for Experimental Mechanics, Inc. Retrieved from http://sem-proceedings.com/23i/sem.org-IMAC-XXIII-Conf-s03p01-Transient-Loads-Identification-Standoff-Metallic-Thermal-Protection.pdf

Hwang, J. -S., Kareem, A., & Kim, H. (2011). Wind load identification using wind tunnel test data by inverse analysis. *Journal of Wind Engineering and Industrial Aerodynamics, 99*(1), 18-26. doi: 10.1016/j.jweia.2010.10.004

Inoue, H., Harrigan, J. J., & Reid, S. R. (2001). Review of inverse analysis for indirect measurement of impact force. *Applied Mechanics Reviews, 54*(6), 503-524.

Jacquelin, E., Bennani, A., & Hamelin, P. (2003). Force reconstruction: analysis and regularisation of a deconvolution problem. *Journal of Sound and Vibration, 265*(1), 81-107. doi: 10.1016/s0022-460x(02)01441-4

Jang, T. S., Baek, H., Han, S. L., & Kinoshita, T. (2010). Indirect measurement of the impulsive load to a nonlinear system from dynamic responses: Inverse problem formulation. *Mechanical Systems and Signal Processing, 24*(6), 1665-1681. doi: 10.1016/j.ymssp.2010.01.003

Jiang, X., & Hu, H. (2008). Reconstruction of distributed dynamic loads on an Euler beam via mode-selection and consistent spatial expression. *Journal of Sound and Vibration, 316*(1-5), 122-136. doi: 10.1016/j.jsv.2008.02.038

Jiang, X. Q., & Hu, H. Y. (2009). Reconstruction of distributed dynamic loads on a thin plate via mode-selection and consistent spatial expression. *Journal of Sound and Vibration, 323*(3-5), 626-644. doi: 10.1016/j.jsv.2009.01.008

Kang, D., Ming, X., & Xiaofei, Z. (2000). Phase difference correction method for phase and frequency in spectral analysis. *Mechanical Systems and Signal Processing, 14*(5), 835-843. doi: 10.1006/mssp.1999.1284

Karrenberg, U. (2002). *An interactive multimedia introduction to signal processing.* Berlin: Springer Verlag.

Kim, S. -J., & Lee, S. -K. (2009). Experimental identification for inverse problem of a mechanical system with a non-minimum phase based on singular value decomposition. *Journal of Mechanical Science and Technology, 22*(8), 1504-1509. doi: 10.1007/s12206-008-0312-1

Kim, Y. -R., & Kim, K. -J. (1999). Indirect input identification by modal filter technique. *Mechanical Systems and Signal Processing, 13*(6), 893-910. doi: 10.1006/mssp.1999.1240

Kim, Y., & Lee, C. (1986). Finite element analysis of rotor bearing systems using a modal transformation matrix. *Journal of Sound and Vibration, 111*(3), 441-456.

Kriel, T. E. S. (2000). *Assessment of frequency domain force identification procedures* (Master's Thesis, University of Pretoria, Pretoria, South Africa). Retrieved from http://upetd.up.ac.za/thesis/available/etd-01122007-131828/

Lee, M. -H., & Chen, T. -C. (2011). Intelligent fuzzy weighted input estimation method for the forces generated by an operating rotating machine. *Measurement, 44*(5), 917-926. doi: 10.1016/j.measurement.2011.02.013

Lee, S. (2008). Identification of impact force in thick plates based on the elastodynamics and time-frequency method (I). *Journal of Mechanical Science and Technology, 22*(7), 1349-1358. doi: 10.1007/s12206-008-0319-7

Lee, T. K., & Kim, B. S. (2008). Vibration analysis of automobile tire due to bump impact. *Applied Acoustics, 69*(6), 473-478. doi: 10.1016/j.apacoust.2007.12.003

Liu, G. R., & Han, X. (2003). *Computational inverse techniques in nondestructive evaluation.* Florida: CRC Press.

Liu, J., & Han, X. (2009). Computational inverse procedure for identification of structural dynamic loads. In Z. H. Yao & M. W. Yuan (Eds.), *Computational mechanics* (pp. 323). Beijing: Springer Berlin Heidelberg.

Liu, Y., & Shepardjr, W. (2005). Dynamic force identification based on enhanced least squares and total least-squares schemes in the frequency domain. *Journal of Sound and Vibration, 282*(1-2), 37-60. doi: 10.1016/j.jsv.2004.02.041

LMS International (2000). *The LMS theory and background*. Leuven, Belgium: LMS International. Retrieved from http://read.pudn.com/downloads71/ebook/257215/Complete%20theory.pdf

Lourens, E., Reynders, E., De Roeck, G., Degrande, G., & Lombaert, G. (2012). An augmented Kalman filter for force identification in structural dynamics. *Mechanical Systems and Signal Processing, 27*(0), 446-460. doi: 10.1016/j.ymssp.2011.09.025

Ma, C. -K., & Ho, C. -C. (2004). An inverse method for the estimation of input forces acting on non-linear structural systems. *Journal of Sound and Vibration, 275*(3–5), 953-971. doi: 10.1016/s0022-460x(03)00797-1

Ma, C. -K., Lin, D. -C., & Chang, J. -M. (1999). Estimation of forces generated by a machine mounted upon isolators under operating conditions. *Journal of the Franklin Institute, 336*(5), 875-892. doi: 10.1016/s0016-0032(99)00012-5

Mao, Y. M., Guo, X. L., & Zhao, Y. (2010). A state space force identification method based on Markov parameters precise computation and regularisation technique. *Journal of Sound and Vibration, 329*(15), 3008-3019. doi: 10.1016/j.jsv.2010.02.012

Martin, M. T., & Doyle, J. F. (1996a). Impact force identification from wave propagation responses. *International Journal of Impact Engineering, 18*(1), 65-77. doi: 10.1016/0734-743x(95)00022-4

Martin, M. T., & Doyle, J. F. (1996b). Impact force location in frame structures. *International Journal of Impact Engineering, 18*(1), 79-97. doi: 10.1016/0734-743x(95)00016-9

McCarthy, D. J. (1997). Short-time coherence functions: instantaneous and tuned. *Mechanical Systems and Signal Processing, 11*(2), 169-185. doi: 10.1006/mssp.1996.0073

McCarthy, D. J., & Lyon, R. H. (1995). Recovery of impact signatures in machine structures. *Mechanical Systems and Signal Processing, 9*(5), 465-483. doi: 10.1006/mssp.1995.0036

McDonough, R. N., & Whalen, A. D. (1995). *Detection of signals in noise.* San Diego, CA: Academic Press.

Mendrok, K., & Uhl, T. (2010). Load identification using a modified modal filter technique. *Journal of Vibration and Control, 16*(1), 89-105. doi: 10.1177/1077546309103274

Norton, M. P., & Karczub, D. G. (2003). *Fundamentals of noise and vibration analysis for engineers.* Cambridge: Cambridge University Press.

O'Callahan, J., & Piergentili, F. (1996). Force estimation using operational data. In A. L. Wicks (Ed.), *A conference & exposition on structural dynamics: noise and vibration harshness (NVH): Proceedings of the 14th International Modal Analysis Conference, Hyatt Regency Dearborn Hotel, Dearborn, Michigan* (pp. 1586 - 1592). Bethel, CT.: Society for Experimental Mechanics, Inc.

Ödeen, S., & Lundberg, B. (1991). Prediction of impact force by impulse response method. *International Journal of Impact Engineering, 11*(2), 149-158. doi: 10.1016/0734-743x(91)90002-w

Okubo, N., Tanabe, S., & Tatsuno, T. (1985). Identification of forces generated by a machine under operating condition. In D. J. DeMichele (Ed.), *Proceedings of the 3rd International Modal Analysis Conference, Orlando Marriott Inn, International Drive, Orlando, Florida* (pp. 920-927). Schenectady, N.Y.: Union College.

Ong, Z. C., Khoo, S. Y., Rahman, A. G. A., Ismail, Z., & Noroozi, S. (2011). *Effect of cyclic force in performing Impact-Synchronous Modal Analysis (ISMA)*. Manuscript submitted for publication.

Otsuka, T., Okada, T., Ikeno, T., Shiomi, K., & Okuma, M. (2007). Force identification of an outboard engine by experimental means of linear structural modeling and equivalent force transformation. *Journal of Sound and Vibration, 308*(3–5), 541-547. doi: 10.1016/j.jsv.2007.04.004

Ouyang, H. (2011). Moving-load dynamic problems: A tutorial (with a brief overview). *Mechanical Systems and Signal Processing, 25*(6), 2039-2060. doi: 10.1016/j.ymssp.2010.12.010

Pesterev, A., Bergman, L., Tan, C., & Yang, B. (2005). Assessing tire forces due to roadway unevenness by the pothole dynamic amplification factor method. *Journal of Sound and Vibration, 279*(3-5), 817-841. doi: 10.1016/j.jsv.2003.11.060

Rahman, A. G. A. (Unpublished). *Dynamic of machine structures- Theory and industrial case studies* (1st ed.). University of Malaya, Kuala Lumpur.

Rahman, A. G. A., & Iwankiewicz, R. (2005). Determination of excitations from known responses using measured frequency response function inverse technique. *International Journal of Comadem, 8*, 6-12.

Rahman, A. G. A.,Ong, Z.C., & Ismail, Z. (2011a). Effectiveness of Impact-Synchronous Time Averaging in determination of dynamic characteristics of a rotor dynamic system. *Measurement, 44*(1), 34-45. doi: 10.1016/j.measurement.2010.09.005

Rahman, A. G. A., Ong, Z. C., & Ismail, Z. (2011b). Enhancement of coherence functions using time signals in Modal Analysis. *Measurement, 44*(10), 2112-2123. doi: 10.1016/j.measurement.2011.08.003

Rainer, J. H. (1986). Applications of the Fourier transform to the processing of vibration signals. *Building Research Note*, 233, 24.

Ribeiro, J., de Castro, J., & Freire, J. (2001). New improvements in the digital double integration filtering method to measure displacements using accelerometers. In A. L. Wicks (Ed.), *Future directions in structural dynamics: Proceedings of 19th International Modal Analysis Conference, Hyatt Orlando, Kissimmee, Florida* (pp. 538 - 542). Bethel, CT.: Society for Experimental Mechanics, Inc.

Richardson, M., & Jamestown, C. (2000). Modal mass, stiffness and damping. *Vibrant Technology, Inc., Jamestown, CA*, 1-5.

Richardson, M., & Schwarz, B. (2003). Modal parameter estimation from operating data. *Sound and Vibration, 37*(1), 28-39.

Ryu, B. -J., Han, H. -H., Lee, G. -S., Ahn, K. -Y., & Lee, C. -R. (2010). Dynamic response analysis of a cantilevered beam due to an elastic impact. *International Journal of Precision Engineering and Manufacturing, 11*(4), 539-547. doi: 10.1007/s12541-010-0062-8

Sekula, K., & Holnicki, -S. (2007). Comparison of real time impact load identification procedures. In E.Ostachowicz, J. Holnicki-Szulc, C. Mota Soares et al. (Eds.), *Smart structures and materials: Proceedings of the III Eccomas Thematic Conference, Gdańsk, Poland*. Retrieved from http://smart.ippt.gov.pl /dok/referaty/2007%20Comparison%20of%20real%20time%20impact%20load %20identification%20procedures.pdf

Schwarz, B. J., & Richardson, M. H. (1999). Experimental modal analysis. In *Proceedings of the CSI Reliability week*, Orlando, Fla, USA (pp. 30-32). Retrieved from http://vibetech.com/assets/papers/paper28.pdf

Schwarz, B. J., & Richardson, M. H. (2006). *Using FEA modes to scale experimental mode shapes.* IMAC In SEM (Ed.), *A conference & exposition on structural dynamics: Looking forward: Technologies for IMAC: Proceedings of the 24th International Modal Analysis Conference* (pp. 1-8)*, St. Louis, Missouri*. Bethel, CT.: Society for Experimental Mechanics. Retrieved from http://www.systemplus.co.jp/support/data/techpaper/mescope/tech/46.pdf

Schwarz, B. J., Richardson, M. H., & Avitabile, P. (2002). *Locating optimal references for modal testing using CMIF*. In SEM (Ed.), *A conference & exposition on structural dynamics: Smart structures and transducer: Proceedings of the 20th International Modal Analysis Conference, Los Angeles, California* (pp. 984-990). Bethel, CT.: Society for Experimental Mechanics, Inc.

Sewell, P., Noroozi, S., Vinney, J., Amali, R., & Andrews, S. (2010). Improvements in the accuracy of an Inverse Problem Engine's output for the prediction of below-knee prosthetic socket interfacial loads. *Engineering Applications of Artificial Intelligence, 23*(6), 1000-1011.

Shih, C., Zhang, Q., & Allemang, R. (1989). Force identification by using principle and modal coordinate transformation method. *Vibration analysis- Techniques and applications*, 303-309.

Shin, E. S. (2000). Real-time recovery of impact force based on finite element analysis. *Computers & Structures, 76*(5), 621-635.

SKF Condition Monitoring, Inc. (1999). Vibration sensors. Retrieved from http://www.exvalos.cz/soubory/File/SKF/SNIMACE_VIBRACI.pdf

Soon, B. Y., Eloe, P. W., & Kammler, D. (2001). The fast Fourier transform method and ill-conditioned matrices. *Applied Mathematics and Computation, 117*(2–3), 117-129. doi: 10.1016/s0096-3003(99)00171-x

Starkey, J., & Merrill, G. (1989). On the ill-conditioned nature of indirect force-measurement techniques. *Journal of Modal Analysis, 4*(3), 103-108.

Steltzner, A. D., & Kammer, D. C. (1999). *Input force estimation using an inverse structural filter.* In A. L. Wicks, D. J. DeMichele, & SEM (Eds.), *Modal analysis: Reducing the time to market: Proceedings of the 17th International Modal Analysis Conference, Kissimmee, Florida* (pp.954-960). Bethel, CT.: Society for Experimental Mechanics, Inc.

Stevens, K. K. (1987). Force identification problems- An overview. In SEM (Ed.), In *Proceedings of the Society of Experimental Mechanics (SEM) Spring Conference on Expeimental Mechanics, Houston, Texas, June 14-19, 1987* (pp. 838-844). Bethel, CT.: Society for Experimental Mechanics.

Thite, A., & Thompson, D. (2006). Selection of response measurement locations to improve inverse force determination. *Applied Acoustics, 67*(8), 797-818. doi: 10.1016/j.apacoust.2006.01.001

Uhl, T. (2006). The inverse identification problem and its technical application. *Archive of Applied Mechanics, 77*(5), 325-337. doi: 10.1007/s00419-006-0086-9

Vibrant Technology, Inc. (2001). Multiple reference curve fitting to find closely coupled modes. *VES App. Note # 15*. Retrieved from http://www.vibetech.com/assets/papers/VESAppNote15.pdf

Vibrant Technology, Inc. (2012). *Fourier spectra, auto spectra, and PSDs; Curve fiting; Mode indicator methods; Curve fitting methods; Curve fitting guidelines; Counting the modes in a band. Estimating frequency & damping; Estimating residues; Saving shapes.* Product Help, ME'Scope V4.0.0.99.

Vold, H., Schwarz, B., & Richardson, M. (2000). Measuring operating deflection shapes under non-stationary conditions. In A. L. Wicks, D. J. DeMichele, SEM, & SPIE (Eds.), *Computational challenges in structural dynamics: Proceedings of the 18th International Modal Analysis Conference, the Westin La Cantera Resort, San Antonio, Texas (pp. 1655-1660)*. Bethel, CT.: Society for Experimental Mechanics, Inc.

Wang, B. -T. (2002). Prediction of impact and harmonic forces acting on arbitrary structures: theoretical formulation. *Mechanical Systems and Signal Processing, 16*(6), 935-953. doi: 10.1006/mssp.2002.1505

Wang, B. -T. (2003). Determination of unknown impact force acting on a simply supported beam. *Mechanical Systems and Signal Processing, 17*(3), 683-704. doi: 10.1006/mssp.2001.1463

William, T. T., & Marie, D. D. (1998). *Theory of vibration with applications* (5th ed.). New Jersey: Prentice Hall.

Yan, G., & Zhou, L. (2009). Impact load identification of composite structure using genetic algorithms. *Journal of Sound and Vibration, 319*(3-5), 869-884. doi: 10.1016/j.jsv.2008.06.051

Yoon, J. -Y., & Singh, R. (2010). Indirect measurement of dynamic force transmitted by a nonlinear hydraulic mount under sinusoidal excitation with focus on super-harmonics. *Journal of Sound and Vibration, 329*(25), 5249-5272. doi: 10.1016/j.jsv.2010.06.026

Yoon, J. -Y., & Singh, R. (2011). Estimation of interfacial forces in a multi-degree of freedom isolation system using a dynamic load sensing mount and quasi-linear models. *Journal of Sound and Vibration, 330*(18-19), 4429-4446. doi: 10.1016/j.jsv.2011.04.033

Yu, L. (2003). Moving force identification based on the frequency–time domain method. *Journal of Sound and Vibration, 261*(2), 329-349. doi: 10.1016/s0022-460x(02)00991-4

Zhang, E., Antoni, J., & Feissel, P. (2012). Bayesian force reconstruction with an uncertain model. *Journal of Sound and Vibration, 331*(4), 798-814. doi: http://dx.doi.org/10.1016/j.jsv.2011.10.021

Zheng, S., Zhou, L., Lian, X., & Li, K. (2011). Technical note: Coherence analysis of the transfer function for dynamic force identification. *Mechanical Systems and Signal Processing, 25*(6), 2229-2240. doi: 10.1016/j.ymssp.2011.01.015

Appendix A

Table A.1:
Accelerance Residue Mode Shape Extracted from Single Column Accelerance FRFs Matrix by using Curve Fitting Method

Response DOF	Force DOF	Residue Mode Shape 1		Residue Mode Shape 2		Residue Mode Shape 3		Residue Mode Shape 4		Residue Mode Shape 5	
		Magnitude ((m/s^2)/Ns)	Phase (Degree)	Magnitude ((m/s^2)/Ns)	Phase (Degree)	Magnitude ((m/s^2)/Ns)	Phase (Degree)	Magnitude ((m/s^2)/Ns)	Phase (Degree)	Magnitude ((m/s^2)/Ns)	Phase (Degree)
1	1	12.58	4.70	13.18	-77.47	160.59	-24.69	212.91	-4.74	1153.20	-1.78
2	1	18.50	-0.79	9.35	-46.07	16.08	-80.48	219.38	-5.10	543.63	0.20
3	1	26.61	-1.23	12.14	17.03	155.13	163.92	222.44	-3.96	210.77	167.70
4	1	25.03	6.56	19.25	-40.47	223.08	-21.77	211.38	-1.45	671.27	-3.98
5	1	33.17	2.88	21.21	-8.36	16.05	-47.16	212.08	-1.48	95.50	-8.93
6	1	44.79	1.24	31.50	19.28	212.29	160.67	227.11	-0.39	603.33	177.80
7	1	30.63	5.15	28.49	-31.61	250.20	-20.93	42.16	8.12	441.13	-177.95
8	1	39.79	2.06	32.79	-9.72	7.69	-119.27	41.88	4.94	447.38	-177.47
9	1	47.38	0.07	39.44	6.57	245.72	162.41	45.63	3.30	532.93	-177.74
10	1	24.77	4.06	24.89	-24.39	220.33	-19.09	155.87	174.40	610.84	176.92
11	1	29.53	0.23	27.67	-11.49	6.56	-153.62	159.83	176.70	65.47	177.07
12	1	36.78	-3.06	34.36	-3.68	247.76	163.45	179.62	179.31	445.22	-3.85
13	1	20.88	6.56	18.85	-1.34	200.61	-15.03	250.04	173.66	249.42	166.05
14	1	24.73	2.14	22.53	3.59	7.64	38.81	263.10	175.49	462.82	3.27
15	1	27.88	-1.71	25.91	6.40	204.65	161.50	270.54	177.42	1149.20	-0.63

Table A.1:
Continued

Response DOF	Force DOF	Residue Mode Shape 6		Residue Mode Shape 7		Residue Mode Shape 8		Residue Mode Shape 9	
		Magnitude ((m/s^2)/Ns)	Phase (Degree)	Magnitude ((m/s^2)/Ns)	Phase (Degree)	Magnitude ((m/s^2)/Ns)	Phase (Degree)	Magnitude ((m/s^2)/Ns)	Phase (Degree)
1	1	686.26	2.34	772.71	25.08	897.62	38.75	436.68	-12.79
2	1	248.72	53.98	615.13	-155.94	1518.10	-158.80	538.37	-148.17
3	1	740.89	155.36	171.54	173.55	850.62	14.64	326.66	10.52
4	1	454.49	-142.80	207.72	169.24	889.71	-7.29	245.74	-12.43
5	1	273.57	-116.66	543.61	-160.11	1198.80	-125.36	174.41	121.74
6	1	373.42	-92.23	1597.50	13.76	1009.80	24.23	752.91	-158.28
7	1	1117.20	171.41	383.05	-26.61	605.03	95.49	1044.20	-144.67
8	1	4.34	-43.04	938.18	-159.70	276.32	-158.74	1101.30	44.61
9	1	1069.10	-10.08	408.42	42.04	952.08	120.35	758.38	-41.75
10	1	313.28	89.62	1405.80	24.35	601.47	-147.16	347.20	-7.29
11	1	251.88	62.51	436.32	-155.93	1022.80	14.97	135.04	-163.54
12	1	422.82	45.91	192.93	108.34	881.97	-118.85	858.76	-177.21
13	1	751.76	-24.67	181.79	108.84	1220.00	-149.23	387.94	72.26
14	1	257.92	-111.71	767.35	-142.26	1821.10	37.35	691.95	-127.95
15	1	824.06	-176.83	783.93	18.36	996.70	-149.73	465.74	38.11

Table A.2:
Accelerance UMM Mode Shape

Response DOF	Force DOF	UMM Mode Shape 1		UMM Mode Shape 2		UMM Mode Shape 3		UMM Mode Shape 4		UMM Mode Shape 5	
		Magnitude ((m/s^2)/Ns)	Phase (Degree)	Magnitude ((m/s^2)/Ns)	Phase (Degree)	Magnitude ((m/s^2)/Ns)	Phase (Degree)	Magnitude ((m/s^2)/Ns)	Phase (Degree)	Magnitude ((m/s^2)/Ns)	Phase (Degree)
1	1	36.42	2.35	40.71	-38.73	192.24	-12.34	245.81	-2.37	805.66	-0.89
2	1	53.54	-3.14	28.87	-7.34	19.25	-68.13	253.28	-2.73	379.79	1.10
3	1	77.02	-3.58	37.50	55.77	185.70	176.26	256.82	-1.59	147.25	168.59
4	1	72.44	4.21	59.45	-1.73	267.05	-9.43	244.05	0.92	468.97	-3.08
5	1	96.01	0.53	65.49	30.37	19.22	-34.82	244.86	0.89	66.72	-8.04
6	1	129.64	-1.12	97.26	58.01	254.13	173.01	262.21	1.98	421.50	178.69
7	1	88.66	2.80	87.98	7.13	299.51	-8.58	48.67	10.49	308.19	-177.06
8	1	115.18	-0.29	101.25	29.01	9.21	-106.93	48.35	7.31	312.55	-176.58
9	1	137.13	-2.28	121.78	45.31	294.15	174.75	52.69	5.67	372.32	-176.85
10	1	71.70	1.71	76.86	14.34	263.75	-6.74	179.96	176.77	426.75	177.81
11	1	85.47	-2.12	85.45	27.24	7.85	-141.28	184.53	179.07	45.74	177.96
12	1	106.45	-5.42	106.11	35.05	296.59	175.79	207.38	-178.32	311.04	-2.95
13	1	60.42	4.21	58.20	37.39	240.15	-2.69	288.68	176.03	174.25	166.94
14	1	71.58	-0.21	69.56	42.32	9.14	51.15	303.76	177.86	323.34	4.16
15	1	80.69	-4.06	80.00	45.14	244.98	173.84	312.35	179.79	802.86	0.26

Table A.2:
Continued

Response DOF	Force DOF	UMM Mode Shape 6		UMM Mode Shape 7		UMM Mode Shape 8		UMM Mode Shape 9	
		Magnitude ((m/s^2)/Ns)	Phase (Degree)	Magnitude ((m/s^2)/Ns)	Phase (Degree)	Magnitude ((m/s^2)/Ns)	Phase (Degree)	Magnitude ((m/s^2)/Ns)	Phase (Degree)
1	1	861.61	1.17	1157.67	12.54	1300.52	19.37	999.06	-6.39
2	1	312.27	52.81	921.58	-168.48	2199.51	-178.17	1231.71	-141.78
3	1	930.20	154.19	257.00	161.01	1232.42	-4.73	747.35	16.92
4	1	570.62	-143.97	311.20	156.70	1289.06	-26.66	562.22	-6.04
5	1	343.47	-117.83	814.43	-172.65	1736.89	-144.73	399.02	128.13
6	1	468.84	-93.40	2393.36	1.22	1463.05	4.86	1722.55	-151.89
7	1	1402.67	170.24	573.88	-39.15	876.60	76.12	2388.97	-138.28
8	1	5.45	-44.21	1405.57	-172.24	400.35	-178.11	2519.61	51.01
9	1	1342.28	-11.24	611.89	29.50	1379.43	100.98	1735.06	-35.36
10	1	393.33	88.45	2106.16	11.81	871.44	-166.53	794.34	-0.90
11	1	316.24	61.34	653.69	-168.47	1481.89	-4.40	308.95	-157.15
12	1	530.86	44.74	289.05	95.80	1277.85	-138.22	1964.71	-170.82
13	1	943.85	-25.84	272.36	96.30	1767.60	-168.60	887.55	78.65
14	1	323.82	-112.88	1149.64	-154.80	2638.51	17.97	1583.08	-121.56
15	1	1034.63	-178.00	1174.48	5.81	1444.07	-169.10	1065.54	44.50

Table A.3:
Mobility UMM Mode Shape

Response DOF	Force DOF	UMM Mode Shape 1		UMM Mode Shape 2		UMM Mode Shape 3		UMM Mode Shape 4		UMM Mode Shape 5	
		Magnitude ((m/s)/Ns)	Phase (Degree)	Magnitude ((m/s)/Ns)	Phase (Degree)	Magnitude ((m/s)/Ns)	Phase (Degree)	Magnitude ((m/s)/Ns)	Phase (Degree)	Magnitude ((m/s)/Ns)	Phase (Degree)
1	1	3.55	-43.92	3.63	-85.47	12.66	-58.86	14.58	-48.69	33.95	-46.99
2	1	5.21	-49.41	2.57	-54.08	1.27	-114.65	15.03	-49.04	16.00	-45.00
3	1	7.50	-49.86	3.34	9.02	12.23	129.74	15.24	-47.91	6.20	122.50
4	1	7.05	-42.07	5.30	-48.47	17.59	-55.95	14.48	-45.40	19.76	-49.18
5	1	9.35	-45.74	5.84	-16.37	1.27	-81.34	14.53	-45.42	2.81	-54.13
6	1	12.62	-47.39	8.67	11.27	16.74	126.49	15.56	-44.33	17.76	132.60
7	1	8.63	-43.48	7.84	-39.61	19.73	-55.10	2.89	-35.83	12.99	136.85
8	1	11.21	-46.56	9.02	-17.73	0.61	-153.45	2.87	-39.00	13.17	137.33
9	1	13.35	-48.56	10.85	-1.43	19.38	128.23	3.13	-40.65	15.69	137.06
10	1	6.98	-44.56	6.85	-32.40	17.37	-53.26	10.68	130.45	17.98	131.72
11	1	8.32	-48.40	7.61	-19.50	0.52	172.20	10.95	132.75	1.93	131.87
12	1	10.36	-51.69	9.46	-11.69	19.54	129.27	12.30	135.36	13.11	-49.05
13	1	5.88	-42.07	5.19	-9.35	15.82	-49.21	17.13	129.71	7.34	120.85
14	1	6.97	-46.48	6.20	-4.42	0.60	4.63	18.02	131.54	13.62	-41.93
15	1	7.85	-50.34	7.13	-1.60	16.14	127.32	18.53	133.47	33.83	-45.83

Table A.3:
Continued

Response DOF	Force DOF	UMM Mode Shape 6		UMM Mode Shape 7		UMM Mode Shape 8		UMM Mode Shape 9	
		Magnitude ((m/s)/Ns)	Phase (Degree)	Magnitude ((m/s)/Ns)	Phase (Degree)	Magnitude ((m/s)/Ns)	Phase (Degree)	Magnitude ((m/s)/Ns)	Phase (Degree)
1	1	26.18	-45.08	27.77	-34.24	29.92	-27.77	20.87	-53.33
2	1	9.49	6.56	22.11	144.74	50.60	134.68	25.73	171.28
3	1	28.27	107.94	6.17	114.23	28.35	-51.88	15.61	-30.02
4	1	17.34	169.78	7.47	109.92	29.65	-73.81	11.75	-52.98
5	1	10.44	-164.08	19.54	140.57	39.96	168.12	8.34	81.19
6	1	14.25	-139.65	57.41	-45.56	33.66	-42.29	35.99	161.17
7	1	42.63	123.99	13.77	-85.93	20.17	28.97	49.91	174.78
8	1	0.17	-90.46	33.72	140.98	9.21	134.74	52.64	4.07
9	1	40.79	-57.50	14.68	-17.28	31.73	53.83	36.25	-82.30
10	1	11.95	42.20	50.52	-34.97	20.05	146.32	16.60	-47.84
11	1	9.61	15.09	15.68	144.75	34.09	-51.55	6.45	155.91
12	1	16.13	-1.51	6.93	49.02	29.40	174.63	41.05	142.24
13	1	28.68	-72.09	6.53	49.52	40.66	144.25	18.54	31.71
14	1	9.84	-159.13	27.58	158.42	60.70	-29.18	33.07	-168.50
15	1	31.44	135.75	28.17	-40.97	33.22	143.75	22.26	-2.44

Table A.4:
Admittance UMM Mode Shape

Response DOF	Force DOF	UMM Mode Shape 1		UMM Mode Shape 2		UMM Mode Shape 3		UMM Mode Shape 4		UMM Mode Shape 5	
		Magnitude ((m)/Ns)	Phase (Degree)	Magnitude ((m)/Ns)	Phase (Degree)	Magnitude ((m)/Ns)	Phase (Degree)	Magnitude ((m)/Ns)	Phase (Degree)	Magnitude ((m)/Ns)	Phase (Degree)
1	1	0.35	89.80	0.32	47.78	0.83	74.62	0.87	85.00	1.43	86.92
2	1	0.51	84.31	0.23	79.18	0.08	18.83	0.89	84.64	0.67	88.91
3	1	0.73	83.87	0.30	142.28	0.81	-96.77	0.90	85.78	0.26	-103.60
4	1	0.69	91.66	0.47	84.78	1.16	77.54	0.86	88.28	0.83	84.73
5	1	0.91	87.98	0.52	116.89	0.08	52.14	0.86	88.26	0.12	79.77
6	1	1.23	86.33	0.77	144.53	1.10	-100.02	0.92	89.35	0.75	-93.50
7	1	0.84	90.25	0.70	93.65	1.30	78.38	0.17	97.86	0.55	-89.25
8	1	1.09	87.16	0.80	115.53	0.04	-19.96	0.17	94.68	0.55	-88.77
9	1	1.30	85.17	0.97	131.83	1.28	-98.28	0.19	93.04	0.66	-89.04
10	1	0.68	89.16	0.61	100.86	1.14	80.22	0.63	-95.86	0.76	-94.38
11	1	0.81	85.33	0.68	113.76	0.03	-54.31	0.65	-93.56	0.08	-94.23
12	1	1.01	82.04	0.84	121.57	1.29	-97.24	0.73	-90.95	0.55	84.86
13	1	0.57	91.66	0.46	123.91	1.04	84.27	1.02	-96.60	0.31	-105.25
14	1	0.68	87.24	0.55	128.84	0.04	138.11	1.07	-94.77	0.57	91.97
15	1	0.76	83.39	0.64	131.66	1.06	-99.19	1.10	-92.84	1.43	88.07

Table A.4:
Continued

Response DOF	Force DOF	UMM Mode Shape 6		UMM Mode Shape 7		UMM Mode Shape 8		UMM Mode Shape 9	
		Magnitude ((m)/Ns)	Phase (Degree)	Magnitude ((m)/Ns)	Phase (Degree)	Magnitude ((m)/Ns)	Phase (Degree)	Magnitude ((m)/Ns)	Phase (Degree)
1	1	0.80	88.66	0.67	-81.02	0.69	-74.92	0.44	79.73
2	1	0.29	140.31	0.53	97.96	1.16	87.53	0.54	-55.66
3	1	0.86	-118.31	0.15	67.45	0.65	-99.03	0.33	103.04
4	1	0.53	-56.47	0.18	63.14	0.68	-120.96	0.25	80.08
5	1	0.32	-30.33	0.47	93.79	0.92	120.97	0.17	-145.75
6	1	0.43	-5.91	1.38	-92.34	0.77	-89.44	0.75	-65.77
7	1	1.30	-102.26	0.33	-132.71	0.46	-18.18	1.04	-52.16
8	1	0.01	43.29	0.81	94.20	0.21	87.59	1.10	137.13
9	1	1.24	76.25	0.35	-64.06	0.73	6.68	0.76	50.76
10	1	0.36	175.95	1.21	-81.75	0.46	99.17	0.35	85.22
11	1	0.29	148.84	0.38	97.97	0.78	-98.70	0.13	-71.03
12	1	0.49	132.24	0.17	2.24	0.68	127.48	0.86	-84.70
13	1	0.87	61.66	0.16	2.74	0.94	97.10	0.39	164.77
14	1	0.30	-25.38	0.66	111.64	1.40	-76.33	0.69	-35.44
15	1	0.96	-90.50	0.68	-87.74	0.76	96.60	0.47	130.62

Appendix B

Table B.1:
Cut-Off Frequency for Unknown Force Determination at Points 1-8

Point	1	2	3	4	5	6	7	8
Cut-Off Frequency (Hz)	451.17	435.55	442.87	505.37	505.37	518.55	538.57	445.80

Table B.2:
Cut-Off Frequency for Unknown Force Determination at Points 9-15

Point	9	10	11	12	13	14	15
Cut-Off Frequency (Hz)	516.60	435.55	402.34	445.31	514.16	435.55	462.89

Publication List

ISI Ranking Paper

1. Khoo, S. Y., Ismail, Z., Kong, K. K., Ong, Z. C., Noroozi, S., Chong, W. T., & Rahman, A. G. A. (2014). Impact force identification with pseudo-inverse method on a lightweight structure for under-determined, even-determined and over-determined cases. *International Journal of Impact Engineering, 63*(0), 52-62. doi: http://dx.doi.org/10.1016/j.ijimpeng.2013.08.005

2. Noroozi, S., Rahman, A. G. A., Khoo, S. Y., Zahedi, S., Sewell, P., Dyer, B., & Ong, Z. C. (2013). The dynamic elastic response to impulse synchronisation of composite prosthetic energy storing and returning feet. *Proceedings of the Institution of Mechanical Engineers, Part P: Journal of Sports Engineering and Technology*. doi: 10.1177/1754337113501491

3. Ong, Z. C., Khoo, S. Y., Rahman, A. G. A., Ismail, Z., & Noroozi, S. *Effect of cyclic force in performing Impact-Synchronous Modal Analysis (ISMA)*. Manuscript submitted for publication.

4. Rahman, A. G. A. , Khoo, S. Y., Ismail, Z., Chong, W. T., & Noroozi, S. *Accuracy improvement of impact force identification procedure with modal transformation method by using power spectral density tool.* Manuscript submitted for publication.

5. Rahman, A. G. A. , Khoo, S. Y., Ismail, Z., Chong, W. T., & Noroozi, S. *Effectiveness of different types of responses in impact force identification with modal transformation method.* Manuscript submitted for publication.

6. Rahman, A. G. A., Noroozi, S., Khoo, S. Y., Ismail, Z., & Chong, W. T. *Impact force identification from known acceleration responses using gaussian elimination with partial pivoting inverse technique*. Manuscript submitted for publication.

Conference Paper

1. Rahman, A. G. A., Khoo, S. Y., Ismail, Z., Chong, W. T., & Noroozi, S. (2012). Impact force identification by using modal transformation method for automobile test rig. In *Advances in Noise, Vibration and Comfort for Sustainable Environment: Proceedings of the 4th International Conference on Noise, Vibration and Comfort (NVC), Kuala Lumpur, Malaysia* (pp. 33). Kuala Lumpur: Faculty of Engineering and Built Environment, University Kebangsaan Malaysia.

2. Rahman, A. G. A., Khoo, S. Y., Ismail, Z., Chong, W. T., & Noroozi, S. *Impact force identification in collocated and non-collocated cases by using modal transformation method.* In *Proceedings of the 2th International Conference on Mechanical Engineering Research (ICMER), Bukit Gambang Resort City, Kuantan, Pahang, Malaysia.* (Computer Disk)

3. Noroozi, S., Rahman, A. G. A., Vinney, J., Ong, Z. C., Khoo, S. Y. Simulation of performance enhancement of bi-lateral lower-limb amputees through impulse synchronisation with self selected running step frequency. In *Proceedings of the 2th International Conference on Mechanical Engineering Research (ICMER), Pahang, Malaysia*. (Computer Disk)

4. Khoo, S. Y., Ong, Z. C., Kong, K. K., Ismail, Z., Chong, W. T., Noroozi, S., & Rahman, A. G. A. (2013). Importance of selecting a suitable analysis frequency range in impact force identification for automobile test rig. In *Proceedings of the 2h International Conference on Recent Advances in Automotive Engineering & Mobility Research (ReCAR), Kuala Lumpur, Malaysia.* Manuscript submitted for publication.